

Emerging consequences of regional-scale aquifer depletion: data-driven and numerical models of well failure, basin salinization, and contaminant transport

By

Richard Augustus Pauloo III

DISSERTATION

Submitted in partial satisfaction of the requirements for the degree of

DOCTOR OF PHILOSOPHY

in

Hydrologic Science

in the

OFFICE OF GRADUATE STUDIES

of the

UNIVERSITY OF CALIFORNIA

DAVIS

Approved:

Graham E Fogg, Chair

Thomas Harter

Jonathan Herman

Committee in charge

2020

Emerging consequences of regional-scale aquifer depletion: data-driven and numerical models of well failure, basin salinization, and contaminant transport

Copyright 2020
by
Richard Augustus Pauloo III

Contents

List of Figures	vi
List of Tables	xii
Abstract	xiv
Acknowledgments	xvi
Preface	xix
1 Introductory Remarks.	1
1.1 Background and Motivation	1
1.2 Objectives	3
1.3 References	4
2 Domestic Well Vulnerability to Drought Duration and Unsustainable Groundwater Management in California's Central Valley.	6
2.1 Abstract	6
2.2 Introduction	7
2.3 Study area	9
2.3.1 Data	11
2.3.2 Classification of failing and vulnerable wells	12
2.3.3 Groundwater level interpolation	12
2.3.4 Pump intake depth estimation	13
2.3.5 Model calibration based on 2012-2016 drought data	14
2.3.6 Simulation of drought duration scenarios	14
2.3.7 Projected groundwater management regimes	15
2.4 Results	17
2.4.1 Well failure prediction during the 2012-2016 drought	17
2.4.2 Failing and vulnerable wells in drought duration scenarios	19
2.4.3 Failing wells in projected groundwater management regimes	22
2.5 Discussion	24
2.5.1 Impact of drought duration on well failure and vulnerability	24
2.5.2 Implications for groundwater management and policy	25

2.5.3	Applicability to other areas	27
2.5.4	Implications for adaptation to climate change	28
2.5.5	Additional perspective on the data and model	29
2.6	Conclusions	30
2.7	Supporting Information Appendix	32
2.7.1	Study Area	32
2.7.2	Data	32
2.7.3	Formal evaluation of well failure	33
2.7.4	Vulnerable wells	35
2.7.5	Groundwater level interpolation	36
2.7.6	Impact of drought on seasonal groundwater levels	37
2.7.7	Pump intake depth estimation	38
2.7.8	Model calibration and performance	41
2.8	Acknowledgments	49
2.9	Data availability	49
2.10	References	50
3	Anthropogenic Basin Closure and Groundwater Salinization (ABCSAL)	55
3.1	Abstract	55
3.2	Introduction	56
3.3	Methods	62
3.3.1	Study area	62
3.3.2	Mixing Cell Model Development	67
3.3.3	Boundary conditions, model parameters, and stochastic simulation	71
3.4	Results	77
3.4.1	Groundwater and salt budget	77
3.4.2	Progression of groundwater salinization	80
3.4.3	Additional perspective on the model	82
3.5	Discussion	83
3.5.1	ABCSAL threatens regional groundwater quality and sustainable yield	83
3.5.2	Key features of ABCSAL	85
3.5.3	Implications for groundwater management	86
3.6	Conclusions	89
3.7	Supporting Information Appendix	92
3.7.1	C2VSim average annual land surface and rootzone water budget (1961-10-31 to 2001-09-30)	92
3.7.2	TDS of natural waters measured at NWIS stations in Kern, Kings, Tulare, and Fresno counties	93
3.7.3	Spatial distribution of pre-1960 groundwater quality in the TLB	97
3.7.4	Vertical groundwater velocity in the TLB	98
3.7.5	Porosity of sediments in the TLB	99
3.7.6	Mixing cell model geologic and hydrologic parameters and mass balance error	101
3.8	Acknowledgments	105
3.9	References	106

4 Mean flow direction modulates non-Fickian transport in a heterogeneous alluvial aquifer-aquitard system	113
4.1 Abstract	113
4.2 Introduction	114
4.3 Methods	118
4.3.1 Heterogeneous hydrofacies model and study site	118
4.3.2 Groundwater flow and transport simulation	120
4.3.3 Hydraulic gradient scenarios	122
4.3.4 Metrics of non-Fickian transport	124
4.4 Results	126
4.4.1 Tailing in breakthrough	126
4.4.2 Temporal evolution of the plume spatial variance	128
4.4.3 Influence of geology on preferential flow and tailing	132
4.5 Discussion	135
4.5.1 Mean flow direction modulates the degree of non-Fickian transport	135
4.5.2 Hydrogeologic heterogeneity underpins non-Fickian transport	136
4.5.3 Implications for upscaled transport models	140
4.5.4 Study limitations and additional considerations	141
4.6 Conclusions	142
4.7 Supporting Information Appendix	144
4.7.1 Simulated groundwater head for VHGR scenarios	144
4.7.2 Particle trajectory coordinate rotation and travel time normalization via the characteristic travel time	144
4.7.3 RW3D parameters	146
4.7.4 Hydrofacies proportions over time	147
4.8 Acknowledgments	148
4.9 References	149
5 Concluding Remarks.	155
5.1 References	159

List of Figures

2.1	California's Central Valley is a major agricultural hub in the Western US, approximately 720 km long and 64 to 97 km wide. (A) The 2,027 reported domestic well failures during the 2012-2016 drought (red dots) cluster in the southeast. 67,011 domestic wells (blue dots) reported in OSWCR and constructed after 1976 were used to define the study area (SI Appendix 2.7.1 for details). (B) Average groundwater level change from 2012-2016 in unconfined to semi-confined aquifers. Areas of large groundwater level decline correspond to areas of high reported well failure.	10
2.2	Conceptual model of well failure in an unconfined to semi-confined alluvial aquifer (details provided in SI Appendix, 2.7.3). (A) Groundwater level is above all pump intakes, and all wells are active. (B) Groundwater level falls below the pump intake of the shallow well, causing it to fail. The deep well remains active. In our study site, shallow wells tend to be domestic, and deep wells tend to be agricultural and public supply wells.	13
2.3	Projected groundwater management regimes using actual groundwater elevation change for a point in Tulare County as an example. Groundwater level change is approximated by three linear trends, based on different time periods. In this figure, we show the different projected groundwater management regimes using the linear approximation based on the 1998-2017 period. In the analysis, we calculate groundwater levels across the entire CV, using all three trends, and all three regimes.	16
2.4	Model performance in predicting the spatial intensity of observed domestic well failures during the 2012-2016 drought. (A) Observed well failure point pattern and kernel density estimate. (B) Predicted well failure mean estimate ($n = 2,513$) and kernel density of the mean prediction. The 5 and 95% confidence intervals of predicted well failures span the interval from 2,144 - 2,868. (C) Residual (predicted minus observed) error. Red areas indicate areas of over-prediction, and blue areas indicate under-prediction.	18
2.5	Simulated domestic well failure point patterns and associated kernel density estimates for 5 to 8 year drought duration scenarios beginning in Fall 2016 (maps show mean prediction). n is the 5 and 95% confidence interval of cumulative well failure count in each scenario, including the 2,027 failing wells in the 2012-2016 drought.	19

2.6	Left: Cumulative domestic well failures from 2012-2016. Right: Cumulative domestic well failures resulting from simulated drought durations 5 to 8 years in length. The continuous drought duration scenario (blue) leads to more well failure compared to the intervening wet winter scenario (green). Points represent the mean well failure estimate, and shaded regions represent the 5 and 95% confidence intervals.	20
2.7	Top row: kernel density estimates of low vulnerability (white) and high vulnerability (red) regions in extended drought duration scenarios and in Fall 2018. Bottom row: histograms of failing wells (grey), vulnerable wells (red), and active wells (blue) for the extended drought scenarios and Fall 2018 scenario. The black dotted line at 3 meters is the threshold at which wells are at risk of decreased efficiency. All numbers reported are the mean estimate of dry, vulnerable, and failing wells.	21
2.8	Domestic well failures projected for three groundwater management regimes (columns) based on three different time periods of linear groundwater level change (rows). The left plot of each pair is the mean projected groundwater level change from 2017-2040. Groundwater level decline (red) is more common than groundwater level increase (blue). The right plot of each pair shows the mean predicted well failure point pattern for that combination of groundwater management regime and groundwater level change approximation. See SI Appendix Table 2.2 for confidence intervals.	23
2.9	Decision tree representing the steps taken to evaluate active and retired wells, initially active and well failures, and finally, active wells and well failures given the following boundary conditions: retirement age, initial groundwater level, and final groundwater level.	34
2.10	Groundwater levels during the most intense 4-year period of the 2012-2016 drought in (A) spring 2011, and (B) fall 2015. (C) Box plots showing the median and 25% and 75% percentiles of depth to groundwater. Compared to spring groundwater levels, fall levels tend to be deeper. The schematic assumes that groundwater levels do not decrease with depth, which is not a concern for most of the domestic wells because they tend not to be very deep.	38
2.11	Density distributions of estimated pump intake depth for a subset of 16 Bulletin 118 subbasins. The red vertical line indicates the mean pump depth.	40
2.12	Relationship between the logarithm of pump depth (z), and logarithm of the bottom of the screened interval (z_b) for a subset of 16 Bulletin 118 subbasins.	41
2.13	(A) Count of wells per Bulletin 118 subbasin with recorded screen bottom and directly estimable pump depth, further classified into northern and southern subbasins. (B) & (C) Northern and Southern subbasins used to construct the linear relationships between pump depth and screened interval bottom; the wells within are shown as black points. (D) & (E) Northern and Southern linear models used to impute pump depth for northern and southern basins with fewer than 75 samples.	42

2.14 (A) Retirement age of domestic wells and associated SSE in the calibration spatial units. Low retirement ages remove too many wells from the model, resulting in unrealistically low SSE compared to a validation set. (B) Retirement age of domestic wells and associated count of failing wells during the 2012-2016 drought. The horizontal dashed black line shows the number of observed failing wells during the drought, constraining the feasible solution space to retirement ages of 25 years or greater. The red dot indicates the most reasonable model that balances low SSE, acceptable retirement age (28 years), and a compensation for well failure under-reporting. Error bars show the 5 and 95% confidence intervals of predicted well failures, computed by propagating uncertainty in pump location estimation and groundwater level estimation through the model.	44
2.15 Predicted vs. observed log failure ratio for the 11 calibration spatial units.	46
3.1 Conceptual model of ABCSAL. (A) Open basin, pre-groundwater development: surface and groundwater systems connect. Groundwater discharges dissolved solids into surface water which exits the basin. Groundwater at this stage is predominantly fresh (e.g., < 1,000 mg/L). (B) Closed basin: groundwater pumping causes elimination of baseflow to streams. Lower groundwater levels cause subsurface inflow to drain adjacent basins. Pumped groundwater is concentrated by evapotranspiration (ET) when applied for irrigation. Salts migrate into the production zone of the aquifer, driven by vertical hydraulic gradients from recharge and pumping. Although these figures show two extremes (open and closed), partially-closed basins also exist.	60
3.2 The TLB overlies an agriculturally intensive sedimentary aquifer in California's southern Central Valley. Significant changes are observed in selected decadal hydrologic year water budget terms derived from C2VSim at (A) early-groundwater-development (not to be confused with pre-groundwater-development) and (B) post-groundwater-development timescales in the TLB. Notably, gaining streams transition to losing streams, and increases are observed in pumping, evapotranspiration (ET), and recharge (from diversions and natural sources, like streams, lakes, and watersheds). All terms are aggregated at the scale of the TLB, except for subsurface inflow, which is calculated at the northern TLB boundary. Note that this is not the TLB groundwater budget (Table 3.1) nor the land surface and rootzone budget (SI Appendix Table 3.2), but rather, a combination of ground and surface water budget terms that illustrate hydrologic change and show the main inputs (recharge) and outputs (pumping and evapotranspiration). Major rivers (shown in blue) from north to south include the San Joaquin, Kings, Kaweah, Tule, and Kern. Minor streams and tributaries are not shown.	63

3.3	Conceptual land-rootzone model and groundwater mixing cell model with surface area A , porosity η , aquifer fraction f , rock-water interaction coefficient ρ , and m cells. The cell thickness Δz_j is given per equation (3.4), where average linear velocity $v_j = q_j/f\eta$. The cell volume V_j is the total bulk volume of the rock including aquifer and non-aquifer material. The TDS in cell j is calculated by equation (3.3). The land and root budget (SI Appendix Table 3.2) accounts for pumping (P), surface water diversions (D), precipitation (P_t), evapotranspiration (E), runoff (Ro), return flow (R_f), and net deep percolation (N). N enters the top of the groundwater mixing cell model along with recharge from streams, lakes, and watersheds (R), boundary inflow from mountain front recharge (B), and managed aquifer recharge (M). Internal flows from subsurface inflow from the north (I), subsidence flow (C), and pumping (P) are distributed proportional to cell volume, e.g., equation (3.12). The average annual groundwater and salt budget is reported in Table 3.1.	70
3.4	Pre-1960 groundwater quality generally decreases with depth, reaching an average concentration of 1,000 mg/L at 526 m deep. The initial TDS-depth concentration at $t = 0$ is approximated by a linear model, shown as a black line. The transparent, grey rectangle shows the depth of the mixing cell model (212 m).	76
3.5	Annual mass flux and TDS of selected budget terms. The height of each column is the ensemble median result, and the width of error bars, if present, is the interquartile range of the ensemble distribution. (A) Pumped groundwater contributes more mass than surface water diversions and all other water budget terms combined (represented by their symbol: I, W, R, B). (B) TDS of <i>pumped groundwater</i> is diluted when mixed with imported surface water, which forms <i>total applied water</i> . However, evapotranspiration concentrates total applied water, which enters the groundwater system as <i>net deep percolation</i> . Over time in a closed basin system, the groundwater salinates, which in turn increases the concentration of total applied water and net deep percolation.	79
3.6	Progression of groundwater salinization ensemble results for two scenarios (with and without rock-water interactions). RWI stands for rock-water interactions. The blue and purple lines show the ensemble median concentration for the two scenarios, and the interquartile range (IQR) of the ensemble simulations is shown as a grey shaded area. Complete statistics are provided in SI Appendix Table 3.8.	81
3.7	Median TDS of natural waters measured at NWIS stations in Kern, Kings, Tulare, and Fresno counties*.	93
3.8	Spatial distribution of pre-1960 groundwater quality (Figure 3.4) at 4 depth quartiles from land surface to 762 m in depth (near the base of fresh water). The mixing model (depth = 212 m) is contained within depth quartiles 1 and 2. Quartile 1 = 0.00 to -160.93 m, Quartile 2 = -160.94 to -256.03 m, Quartile 3 = -256.04 m to -454.15, Quartile 4 = -454.16 to -762.00 m.	97

3.9	Sampling distribution of the porosity sample means from Johnson (1968), Table 3.5. The bootstrapped distribution of 100,000 samples of size $n = 5$ taken with replacement are approximately normal in distribution. Via the Central Limit Theorem, this indicates that the sampling distribution mean is approximately equal to the population mean. Thus, the sampling distribution mean (0.40) is used as the upscaled porosity in the mixing model. A single value is used because the interquartile range, bounded by 0.39 and 0.41, does not vary appreciably.	100
4.1	The Kings River alluvial fan hydrofacies model in California's Central Valley (USA) with a section cut away to reveal the geologic heterogeneity and four representative particle trajectories from the four VHGR scenarios in this study (section 4.3.3). The location of the instantaneous nonpoint source term (10 000 particles, 10 m below the water table) is represented by a horizontal pink line. Particle trajectories are increasingly horizontal and non-Fickian with decreasing VHGR. Note that the vectors representing flow in z , y , (and their geometric sum in the mean flow direction, y') are illustrative, and not drawn to scale.	119
4.2	(a-d) RW3D breakthrough curves (colored points) and fitted TFADE models (black line) measured at the bottom face of the domain (Figure 4.1) for the four VHGR scenarios. Note the difference in x-axis travel times. (e) Breakthrough curves are normalized by the characteristic travel time (see SI Appendix Table 4.3 for details). Measured slopes of tails (denoted as m) increase as VHGR decreases, corresponding to increasingly anomalous transport.	128
4.3	Temporal evolution of the centered second spatial moments (Equation 4.6) calculated from the distribution of particle trajectories along the (a) longitudinal, (b) transverse vertical, and (c) transverse horizontal directions indicate superdiffusive early time scaling that reduces to less superdiffusive or Fickian scaling in late times, depending on the VHGR and direction of scaling. Triangles at early and late times show the slope of MSD temporal scaling, ϕ (Section 4.3.4.2).	130
4.4	(a) Transparent hydrofacies domain highlighting a lateral, interconnected sand and gravel incised valley fill; (b) The down-gradient side of the domain. A black oval marks the incised valley fill exit, and black outlines mark prominent interconnecting sands and gravel bodies that promote preferential flow. These same regions are marked in black in all other subplots; (c,e,g,i) The final z and x position of particles, colored by the time they exit the domain (residence time); (d,f,h,j) the final z and x position of particles, colored by the length (y) into the page, where yellow is the up-gradient side and purple is the down-gradient side. Particle clusters at $z = 0$ m indicate trajectories that exit the bottom face (Figure 4.5).	133
4.5	(a) The 3D hydrofacies domain; (b) the bottom of the domain with prominent sand and gravel bodies outlined in black; (c,e,g,i) the final x and y position of particles, colored by the time they exit the domain (residence time); (d,f,h,j) the final x and y position of particles, colored by the length (z) into the page, where yellow is the bottom face and purple is the top face. Particle clusters at $y = 15\,000$ m indicate trajectories that exit the down-gradient side of the domain (Figure 4.4).	134
4.6	(a-d) Simulated steady state groundwater head across the 4 VHGR scenarios tested in this study.	144

List of Tables

2.1	Linear regression model coefficients, goodness of fit, and sample size for the subset of wells with 75 or more samples.	43
2.2	Domestic well failure counts under different groundwater management regimes (Sustainable, Glide path, and Business as usual).	48
3.1	Average annual groundwater and salt budget for the TLB (equation 3.5) from C2VSim (1961-10-31 to 2001-09-30), and the modified no-overdraft budget used in this analysis (equation 3.7).	64
3.2	C2VSim average annual land surface and rootzone water budget (1961-10-31 to 2001-09-30).	92
3.3	TDS of natural waters (derived from NWIS samples, see Figure 3.7) and agricultural diversions (derived from Central Valley Project and State Water Project water and salt budgets). C is the concentration of TDS. From C2VSim, total applied water is 45.1% agricultural diversions and 54.9% groundwater pumping. Natural waters are the TDS of R , B , C , I , and M in Table 1. Agricultural diversions are D in Table 3.2.	96
3.4	Linear model coefficients for Equation (3.8). The Darcy velocity (m/yr) at the top of cell $j = 1$ is β_0 , and decreases by β_1 with every vertical meter of depth. To account for groundwater velocity change in the alternate groundwater budget, groundwater velocity is scaled proportional to the decrease in vertical flow, $P_{alt}/(P - C)$, a 15 % reduction. This is equivalent to the ratio of net downward flow in the alternate budget to the historical budget (Table 1).	98
3.5	Sample mean porosities from Johnson (1968) Table 10.	99
3.6	Mixing cell model geologic and hydrologic parameters: η is the porosity, f is the aquifer fraction, ρ is the rock-water interaction coefficient, and E_a is the application efficiency. Ranges are provided for parameters used in the Monte Carlo simulation.	101
3.7	Cell by cell budget and mass balance error, per equations (9) and (10).	102
3.8	Mixing model TDS-depth profile over time. Median and IQR refer to the median and interquartile range of TDS (mg/L) at the depth (d) of the cell bottom.	103
3.9	Mixing model TDS-depth profile over time when the TDS of $M = 0 mg/L$. Median and IQR refer to the median and interquartile range of TDS (mg/L) at the depth (d) of the cell bottom.	104

4.1	Hydrofacies properties including mean lengths l in xyz directions (strike, dip, and vertical in Figure 4.1), hydraulic conductivity K (m/s), and average Peclet number across the VHGR scenarios.	120
4.2	Fitted TFADE model parameters indicate an increasingly small tempering parameter as VHGR decreases, consistent with the observation of increased tailing in low VHGR scenarios.	127
4.3	Mean velocity \bar{v} along the longitudinal direction (y'), the angle of mean flow, relative to the horizontal direction in the un-rotated Cartesian coordinate system Φ , the characteristic hydrofacies length c along the longitudinal direction, and the characteristic time t_c along the longitudinal direction ($t_c = l_c/\bar{v}$).	145
4.4	RW3D parameters for each VHGR scenario including the number of injected particles (particle count), the maximum simulation time (max time), and the number of snapshots saved (snapshot count). Note that the snapshot count = max time · 10 000, meaning that for each scenario, 100 snapshots were taken per year of simulation time.	146

Richard Augustus Pauloo III
September 2020
Hydrologic Science

Emerging consequences of regional-scale aquifer depletion: data-driven and numerical models of well failure, basin salinization, and contaminant transport

Abstract

In the past century, global groundwater extraction has transformed arid and semi-arid regions worldwide into areas of significant food production, and provided water for drinking and basic needs to billions of people. However, despite its critical role in irrigated agriculture and drinking water supply, negative consequences of excessive groundwater development threaten the long-term sustainability of major aquifer systems. The numerous consequences of groundwater over-extraction include land subsidence, leaching of contaminants, chronic decline of groundwater level and aquifer storage, surface water depletion, loss of groundwater dependent ecosystems, and seawater intrusion. Emerging challenges of aquifer depletion that have received much less attention include well failure and closed basin salinization. These topics are understudied not because they are unimportant, but rather, because the data and models to describe them have only recently become available, or have not yet been developed. Three case studies using the Central Valley as a study site are presented herein, and these studies advance novel models and conceptual frameworks to address the emerging challenges of well failure and closed basin salinization. First a data-driven model of well failure forecasts the magnitude and spatial distribution of domestic well failure resulting from extended (5 to 8 years in length) drought scenarios, and show that groundwater management regimes (business as usual, glide path, strict sustainability), and wet winter recharge events substantially influence the occurrence of well failure. Next a conceptual model and first-order estimates of the timescales and depth scales of groundwater salinization due to basin closure in California's Tulare Basin are presented. Results suggest that shallow aquifer salinization proceeds at similar rates to groundwater lifespan in the study area and point towards an alternate groundwater management paradigm in which greater emphasis is placed on subsurface storage in order to keep

groundwater basins open, and hence, fresh. Finally, a study in groundwater flow and contaminant transport in the Kings River Fan shows that varying the mean flow direction in a 3D hydrofacies model can lead to differing degrees of non-Fickian transport, with implications for efforts to upscale transport modeling of nonpoint source plumes, and the conceptualization of transport in highly heterogeneous alluvial aquifer-aquitard systems.

Acknowledgments

The Chinese philosopher Chuang Tzu wrote, “Your life has a limit, but knowledge has none. If you use what is limited to pursue what has no limit, you will be in danger.”

This work therefore, is the product of living dangerously. I’ve spent many years of my life–time I will never get back–in pursuit of knowledge. Some of my most cherished moments have been precisely when I’ve grasped a sense of how infinite knowledge can feel, where a mind is a drop in an ocean, how the currents of knowledge expand like an inflationary universe, how knowledge accretes from the collective effort of people buried in books, clamoring over computers, laboring in labs, exploring the environment, studying social structures. This small dissertation are three drops of water in an ever-growing ocean of knowledge, three drops of water that I’ve been honored and humbled to document, three drops of water that I could not have described or understood were it not for a community of people lifting me up, a community of people that have my most sincere and heartfelt appreciation.

I am deeply grateful for my adviser Graham Fogg. Graham gave me the freedom to make mistakes, to learn how to think independently, and to develop scientific and intellectual curiosity. I also want to thank my dissertation and qualifying exam committee members Thomas Harter, Laura Foglia, Jon Herman, Randy Dahlgren, and Robert Hijmans for sharing their ideas with me and steering me in the right direction. I especially want to thank Jon Herman and Robert Hijmans for instilling a love of programming through their obstinate proselytization of Python and R–those courses forever changed how I approach scientific problems and I’m fully converted. Thank you to close collaborators who have helped me along the way, in particular Zhilin Guo, Christopher Henri, Alvar Escriva-Bou, Helen Dahlke, Andrew Calderwood, Darcy Bostic, Herve Guillon, and Amanda Fencl. Aakash Ahmed, Corey Scher, and Kyra Kim have been a tremendous source of inspiration for me–meeting them reassured me that I was on the right path in life. Each of these scientists has selflessly taken the time to educate me, share their ideas and refine mine, and contribute to my work. I have nothing but gratitude, admiration, and respect for these mentors, collaborators, and friends–my scientific community.

I'm also very thankful for the support of the Guardian Professions Program, specifically the indefatigable and generous Sylvia Sensiper who coached me more than once on the mysteries of graduate school, helped fund my education, and encouraged me to think bigger about my ambitions long before I believed in myself by saying, "I meet a lot of prospective students, and you seem like PhD material to me". Carole Hom deserves special thanks for her dedication to training an interdisciplinary group of scientists, which I was fortunate to be a part of and learn from. Shila Ruiz is a saint: she always had an open door, an open mind, and a smile to share. Sam Sandoval has been a warm and supportive academic advisor and co-conspirator.

Many groups have funded my research, travel, and training, including the National Science Foundation Climate Change Water and Society (CCWAS) IGERT, the University of California Water (UC Water) Security and Sustainability Research Initiative, the US Department of Energy's US-China Center for Energy and Clean Energy Research Center for Water-Energy Technologies (CERC-WET), the American Geophysical Union, the West Big Data Hub, NASA, Microsoft, and RStudio.

My labmates, the HSGG community, and the greater UC Davis graduate student cohort have been a source of friendship, strength, and inspiration throughout the years. Students in the program have enriched my academic and personal life and transformed this quiet college town into a supportive backdrop for intellectual exploration and growth. In particular I want to thank Jason Wiener, Steve Maples, Gus Tolley, Gaby Castrellon, Amy Yoder, Katie Markovich, Noelle Patterson, Kim Miles, Tara Seely, Bal Sah, Sam Sharp, Lisa Rosenthal, Ernst Bo, Ali Hill, Angadh Nanjangud, and Marina Mautner for our conversations and camaraderie. Looking forward, the newer HSGG students continue to inspire me and teach me new things, and I'm glad to have overlapped with many, including Bill Rice, Claire Kouba, Nusrat Molla, Bradley Simms, and Sam Winter.

Exchanges with water policy experts over the years have also transformed how I think about the role of science in society, and I want to thank Jeff Mount, Ellen Hanak, Meredith Lee, Debbie Franco, Greg Gearheart, and Brent Vanderburgh for our energizing dialogues.

There are hundreds, perhaps thousands of anonymous people who have directly or indi-

rectly helped me solve coding problems on Stack Overflow, at the UC Davis Data Lab, and within the UC Davis geospatial and R-users group forums. These communities of practice have sustained me when I've hit walls, and selflessly shared their time to help me grow and tackle increasingly challenging problems.

To Natalie Popovich and Julia Michaels, my first friends in Davis and housemates of nearly 3 years, thank you for your friendship and humor, for celebrating achievements with me, and for routinely turning our house in a classical music concert hall. These are among my most cherished memories of this sleepy college town. To Ben Dawson, Lillie Mansfield, Bree DeRobbio, and Grace Woodmansee thank you for keeping me grounded, for group meals, and for sharing your perspectives and pace of life. To Gabe Patterson, Meghan Jones, John Mitchell, Jess Gold, Jake Stahl, and Jenn Nill thank you for being my COVID-19 pod, for trips to the mountains, and for getting me through the final days of my dissertation.

Three powerful women deserve special recognition, and those women are my mother, sister, and partner. If this dissertation is dedicated to anyone, it's to them. I'm often humbled by the sacrifices my mother made to create opportunity for me. I wouldn't be here today if my she had not decided to immigrate from Thailand to the United States, and then, as a single mother, work two jobs to support her children. She is the meaning of resilience. My sister's love, iron-will, and belief in me has helped me persist in the toughest times. Thank you so much for everything Jen. And finally, I could not have done this without the unconditional love and support of my partner Marisa. Thank you for being my rock, my sanity, and my best friend.

Preface

About this dissertation

Groundwater resources are found in diverse settings worldwide, and like groundwater, the work herein is the product of many conversations and collaborations between researchers from the US, China, and Europe. It is also the synthesis of ideas shared by academic colleagues, as well as colleagues in government, industry, and the nonprofit sector.

Notes on Chapter 2

Chapter 2 presents a data-driven methodology for estimating well failure applied to California's Central Valley. It was coauthored with Graham Fogg, Alvar Escriva-Bou, Helen Dahlke, Herve Guillon, and Amanda Fencl. The topic of statewide domestic well failure analysis arose after nearly one million digitized well completion reports detailing over 100 years of groundwater development in California were released to the public, permitting the first domestic well failure models. The initial kernel of this chapter won an award at the 2018 California Water Data Challenge, then grew to encompass a wider body of work that was published in *Environmental Research Letters* (doi: 10.1088/1748-9326/ab6f10).

Notes on Chapter 3

Chapter 3 explores another consequence of aquifer depletion, and that is basin closure and subsequent salinization. Graham Fogg, Zhilin Guo, and Thomas Harter were co-authors. This work was submitted on 2020-07-07 to *Journal of Hydrology* (preprint doi: 10.1002/essoar.10502733.1) and will likely appear in that journal by late 2020 or early 2021.

Notes on Chapter 4

Chapter 4 builds on Chapter 3 by exploring the physical and hydrogeologic controls on subsurface contaminant transport that challenge the development of regional, upscaled transport models. It was coauthored with Graham Fogg, Zhilin Guo, and Christopher Henri. This work is in preparation for submission to *Water Resources Research*.

Chapter 1

Introductory Remarks

1.1 Background and Motivation

In 1798 the economist Thomas Malthus speculated that world food demand would outstrip population and lead to the collapse of civilization (Malthus, Winch, & James, 1992). The so-called “Malthusian curse” was famously averted by mid-twentieth century scientific innovations that have come to be known as the “Green Revolution,” and comprised developments in plant genetics, nitrogen fixation, and the development of groundwater resources for irrigation. Importantly, the development of drilling technology in the past century has allowed humans to access ever-deeper aquifers that, coupled with surface water diversions, have transformed arid and semi-arid regions worldwide into productive bread baskets. Today, groundwater provides part of the drinking water supply for at least 50% of the global population, and accounts for 43% of all water used for irrigation (Siebert et al., 2010). It is estimated that 2.5 Billion people—about one in three people on Earth—depend solely on groundwater resources to satisfy their basic daily water needs (UNESCO, 2015). However, despite its critical role in sustaining food production regions of the world and providing basic drinking water needs to a substantial fraction of the human population, groundwater resources are imperiled. Numerous studies have documented the long-term unsustainable extraction of groundwater (Famiglietti, 2014; Wada et al., 2010; Döll et al., 2012; Gleeson, Wada, Bierkens, & van Beek, 2012; de Graaf, Gleeson, van Beek, Sutanudjaja, & Bierkens,

2019), and numerous others have documented the negative consequences of groundwater pumping, including land subsidence (Brush, Dogrul, & Kadir, 2013), leaching of contaminants and other impacts to subsurface contaminant migration (Smith, Knight, & Fendorf, 2018), chronic decline of groundwater level and storage (Scanlon et al., 2012), surface water depletion and loss of groundwater dependent ecosystems (TNC, 2014), and seawater intrusion (Bear, Cheng, Sorek, Ouazar, & Herrera, 1999). These challenges have been met by the development of groundwater flow and contaminant transport models (Domenico, Schwartz, et al., 1998; Fetter, 2001), remote sensing and GPS methods that measure gravimetric fluctuations (Ramillien, Famiglietti, & Wahr, 2008) and land surface deformation (Galloway et al., 1998), and geophysical methods (Goebel, Knight, & Halkjær, 2019). Nonetheless, ongoing groundwater depletion has created new and emerging consequences of regional scale aquifer depletion, including well failure and regional-scale groundwater basin salinization, and these understudied challenges require the development of methods and models to adequately describe, understand, and forecast the severity of their impact to groundwater supplies.

In California alone, more than half of all pumped groundwater is used for irrigation (Faunt et al., 2009), about 85% of Californians depend on groundwater for some portion of their water supply (Chappelle, Hanak, & Harter, 2017), and 1.5 million residents rely solely on domestic wells for drinking water (Dieter et al., 2018). Groundwater development in the past century has transformed California's Central Valley into one of the most heavily irrigated and economically productive agricultural regions in the world, and also made it a case study in chronic historical overdraft (Hanak, Lund, Dinar, Gray, & Howitt, 2011). In the backdrop of these groundwater challenges in California (which are emblematic of global groundwater challenges) is a warming climate, and it is in this increasingly drier and warmer climate (Diffenbaugh, Swain, & Touma, 2015; Cook, Ault, & Smerdon, 2015) characterized by more frequent, more spatially extensive heat waves and extended droughts (Tebaldi, Hayhoe, Arblaster, & Meehl, 2006; Lobell, Torney, & Field, 2011), that California will implement a statewide policy of sustainable groundwater management ("Sustainable Groundwater Management Act, California Water Code sec. 10720-10737.8," 2014). These policies aim to prevent chronic groundwater overdraft and other undesirable results, but fail

to anticipate two critical challenges: domestic well failure and regional groundwater salinization due to basin closure induced and then sustained by pumping. Presently, we lack conceptual models and methodological approaches to describe and anticipate these critical challenges, and thus, inform the implementation of policy and mitigative actions aimed minimizing the harm caused by them. It is the aim of this dissertation to address the knowledge gaps surrounding well failure and closed basin salinization.

1.2 Objectives

In this dissertation, data-driven and numerical models of well failure, basin salinization, and contaminant transport are developed in order to address exigent and emerging threats to fresh groundwater resources in a typical alluvial aquifer-aquitard system, using California's Central Valley as a case study. The specific objectives of this dissertation are:

- Develop a data-driven, regional-scale model of well failure of California's Central Valley that *(i)* reproduces the well failure impacts of the historical severe 2012-2016 drought, and forecasts the impact of: *(ii)* extended (5 to 8 year long) drought duration scenarios, *(iii)* three different groundwater management regimes (sustainability, glide path, business as usual), and *(iv)* the impact of wet winter recharge events. (Chapter 2)
- Develop a conceptual framework and simple mixing tank model to estimate the approximate timescales and depth scales associated with regional aquifer salinization in California's Tulare Basin. (Chapter 3)
- Extend the work presented in Chapter 3 by using numerical groundwater flow and contaminant transport modeling to investigate how mean flow direction and hydraulic boundary condition transience modulate the degree of non-Fickian transport in a typical alluvial aquifer-aquitard system. This study aims to improve our understanding of the various methods to upscale transport, and inform the development of new upscaling methods. (Chapter 4)

1.3 References

- Bear, J., Cheng, A. H.-D., Sorek, S., Ouazar, D., & Herrera, I. (1999). *Seawater intrusion in coastal aquifers: Concepts, methods and practices*. Springer Science & Business Media.
- Brush, C. F., Dogrul, E. C., & Kadir, T. N. (2013). *Development and calibration of the California central valley groundwater-surface water simulation model (c2vsim), version 3.02-cg*. Sacramento, CA: Bay-Delta Office, California Department of Water Resources.
- Chappelle, C., Hanak, E., & Harter, T. (2017). *Groundwater in California*. Public Policy Institute of California Water Policy Center. San Francisco, California.
- Cook, B. I., Ault, T. R., & Smerdon, J. E. (2015). Unprecedented 21st century drought risk in the American Southwest and Central Plains. *Science Advances*, 1(1), e1400082.
- de Graaf, I. E., Gleeson, T., van Beek, L. R., Sutanudjaja, E. H., & Bierkens, M. F. (2019). Environmental flow limits to global groundwater pumping. *Nature*, 574(7776), 90–94.
- Dieter, C., Linsey, K., Caldwell, R., Harris, M., Ivahnenko, T., Lovelace, J., ... Barber, N. (2018). Estimated use of water in the United States county-level data for 2015 (ver. 2.0, June 2018): US Geological Survey data release. Available at: <https://www.sciencebase.gov/catalog/item/get/5af3311be4b0da30c1b245d8> [Accessed July 1, 2019]. doi:[10.3133/cir1441](https://doi.org/10.3133/cir1441)
- Diffenbaugh, N. S., Swain, D. L., & Touma, D. (2015). Anthropogenic warming has increased drought risk in California. *Proceedings of the National Academy of Sciences*, 112(13), 3931–3936.
- Döll, P., Hoffmann-Dobrev, H., Portmann, F. T., Siebert, S., Eicker, A., Rodell, M., ... Scanlon, B. R. (2012). Impact of water withdrawals from groundwater and surface water on continental water storage variations. *Journal of Geodynamics*, 59, 143–156.
- Domenico, P. A., Schwartz, F. W. et al. (1998). *Physical and chemical hydrogeology*. Wiley New York.
- Famiglietti, J. S. (2014). The global groundwater crisis. *Nature Climate Change*, 4(11), 945–948.
- Faunt, C., Hanson, R. T., Belitz, K., Schmid, W., Predmore, S. P., Rewis, D. L., & McPherson, K. (2009). *Groundwater availability of the Central Valley Aquifer, California*, US Geological Survey Professional Paper (tech. rep. No. 1766). USGS. doi:[10.3133/pp1766](https://doi.org/10.3133/pp1766)
- Fetter, C. W. (2001). *Applied Hydrogeology* (4th). Upper Saddle River, NJ: Prentice Hall.
- Galloway, D. L., Hudnut, K. W., Ingebritsen, S., Phillips, S. P., Peltzer, G., Rogez, F., & Rosen, P. (1998). Detection of aquifer system compaction and land subsidence using interferometric synthetic aperture radar, Antelope Valley, Mojave Desert, California. *Water Resources Research*, 34(10), 2573–2585.
- Gleeson, T., Wada, Y., Bierkens, M. F., & van Beek, L. P. (2012). Water balance of global aquifers revealed by groundwater footprint. *Nature*, 488(7410), 197–200.
- Goebel, M., Knight, R., & Halkjær, M. (2019). Mapping saltwater intrusion with an airborne electromagnetic method in the offshore coastal environment, Monterey Bay, California. *Journal of Hydrology: Regional Studies*, 23, 100602.
- Hanak, E., Lund, J., Dinar, A., Gray, B., & Howitt, R. (2011). *Managing California's Water: From Conflict to Reconciliation*. San Francisco, CA: Public Policy Institute of California.
- Lobell, D. B., Torney, A., & Field, C. B. (2011). Climate extremes in California agriculture. *Climatic Change*, 109(1), 355–363. doi:[10.1007/s10584-011-0304-5](https://doi.org/10.1007/s10584-011-0304-5)
- Malthus, T. R., Winch, D., & James, P. (1992). *Malthus: 'an essay on the principle of population'*. Cambridge University Press.

- Ramillien, G., Famiglietti, J. S., & Wahr, J. (2008). Detection of continental hydrology and glaciology signals from grace: A review. *Surveys in geophysics*, 29(4-5), 361–374.
- Scanlon, B. R., Faunt, C. C., Longuevergne, L., Reedy, R. C., Alley, W. M., McGuire, V. L., & McMahon, P. B. (2012). Groundwater depletion and sustainability of irrigation in the US High Plains and Central Valley. *Proceedings of the national academy of sciences*, 109(24), 9320–9325.
- Siebert, S., Burke, J., Faures, J.-M., Frenken, K., Hoogeveen, J., Döll, P., & Portmann, F. T. (2010). Groundwater use for irrigation—a global inventory. *Hydrology and earth system sciences*, 14(10), 1863–1880.
- Smith, R. G., Knight, R., & Fendorf, S. (2018). Overpumping leads to california groundwater arsenic threat. *Nature communications*, 9(1), 2089.
- Sustainable Groundwater Management Act, California Water Code sec. 10720-10737.8. (2014). California State Water Resources Control Board.
- Tebaldi, C., Hayhoe, K., Arblaster, J. M., & Meehl, G. A. (2006). Going to the extremes. *Climatic Change*, 79(3-4), 185–211. doi:[10.1007/s10584-006-9051-4](https://doi.org/10.1007/s10584-006-9051-4)
- TNC. (2014). *Groundwater and Stream Interaction in California's Central Valley: Insights for Sustainable Groundwater Management*. (tech. rep. No. February). The Nature Conservancy.
- UNESCO. (2015). *The United Nations World Water Development Report*. United Nations World Water Assessment Programme. Perugia, Italy.
- Wada, Y., Van Beek, L. P., Van Kempen, C. M., Reckman, J. W., Vasak, S., & Bierkens, M. F. (2010). Global depletion of groundwater resources. *Geophysical research letters*, 37(20).

Chapter 2

Domestic Well Vulnerability to Drought Duration and Unsustainable Groundwater Management in California’s Central Valley.¹

2.1 Abstract

Millions of Californians access drinking water via domestic wells, which are vulnerable to drought and unsustainable groundwater management. Groundwater overdraft and the possibility of longer drought duration under climate change threatens domestic well reliability, yet we lack tools to assess the impact of such events. Here, we leverage 943,469 well completion reports and 20 years of groundwater elevation data to develop a spatially-explicit domestic well failure model covering California’s Central Valley. Our model successfully reproduces the spatial distribution of observed domestic well failures during the severe 2012-2016 drought ($n = 2,027$). Next, the impact of longer

¹This chapter has been published: Pauloo, R. A., Escriva-Bou, A., Dahlke, H., Fencl, A., Guillon, H., & Fogg, G. E. (2020). “Domestic well vulnerability to drought duration and unsustainable groundwater management in California’s Central Valley”. *Environmental Research Letters*, 15(4), 044010.

drought duration (5 to 8 years) on domestic well failure is evaluated, indicating that if the 2012-2016 drought would have continued into a 6- to 8-year long drought, a total of 4,037 - 5,460 to 6,538- 8,056 wells would fail. The same drought duration scenarios with an intervening wet winter in 2017 lead to an average of 498 and 738 fewer well failures. Additionally, we map vulnerable wells at high failure risk and find that they align with clusters of predicted well failures. Lastly, we evaluate how the timing and implementation of different projected groundwater management regimes impact groundwater levels and thus domestic well failure. When historic overdraft persists until 2040, domestic well failures range from 5,966 - 10,466 (depending on the historic period considered). When sustainability is achieved progressively between 2020 and 2040, well failures range from 3,677 - 6,943, and from 1,516 - 2,513 when groundwater is not allowed to decline after 2020.

2.2 Introduction

Presently, more than 13 million households rely on private domestic wells for drinking water in the United States (“US Census American Housing Survey,” [2017](#)). In the State of California alone, around 1.5 million residents rely on domestic wells for drinking water, around one third of which live in the Central Valley (CV) (Dieter et al., [2018](#)). Domestic wells in the CV are greater in number than agricultural or public supply wells, yet tend to be more shallow and have much smaller pumping capacities (e.g., 0.25 - 1.0 m^3/hr compared to 100.0 - 900.0 m^3/hr (Harter, [2003](#))). Well completion report data (CA-DWR, [2018](#)) suggest that between 1900 and 2018 in the CV, 96,299 domestic wells with an interquartile (IQR) depth range of 36.6 - 75.6 m were drilled, compared to 43,861 agricultural wells (IQR: 57.9 - 152.0 m) and 3,649 public supply wells (IQR: 76.2 - 159.0 m). Hence, a large number of shallow domestic wells in the CV are vulnerable to both lowering of the groundwater table (Theis, [1935](#), [1940](#); Sophocleous, [2000](#); Greene, [2018](#); Debra Perrone & Jasechko, [2019](#)) and contamination by pollutants such as total dissolved solids (Cismowski et al., [2006](#); Bertoldi, Johnston, & Evenson, [1991](#)), nitrates (Harter & Lund, [2012](#); Balazs, Morello-Frosch, Hubbard, & Ray, [2011](#); Ransom et al., [2017](#)), arsenic (Welch, Westjohn,

Helsel, & Wanty, 2000; Ahuja, 2008), uranium (Jurgens, Burow, Dalgish, & Shelton, 2008; Fujii & Swain, 1995), and hexavalent chromium (Robertson, 1991; Ellis, Johnson, & Bullen, 2002), among others.

Past droughts in California have encouraged both additional well drilling and groundwater pumping to supplement dwindling surface water supplies (Hanak, Lund, Dinar, Gray, & Howitt, 2011; Medellin-Azuara et al., 2016). During the 2012-2016 drought, 2,027 private domestic drinking water wells were reported dry in California's CV (CA-OPR, 2018); because reporting was voluntary, actual well failure counts are possibly greater. To date, limited long-term data and solutions exist to address the vulnerability of rural community drinking water supply wells to severe droughts (Mitchell et al., 2017; Feinstein, Phurisamban, Ford, Tyler, & Crawford, 2017).

The paucity of well failure research, particularly in California, is partially due to privately-held records on well location and construction. In 2017, the public release of over one hundred years of digitized domestic Well Completion Reports (WCR) enabled the first spatial distribution and count estimates of domestic wells in California (Johnson & Belitz, 2015, 2017). The California Online State Well Completion Report Database (OSCWR) (CA-DWR, 2018) and similar well construction databases across the U.S. have allowed near-continental scale estimation of failing wells (Perrone & Jasechko, 2017) and well depths (Debra Perrone & Jasechko, 2019). A recent study in the Tulare County, California (around $5,000 \text{ km}^2$) estimated domestic well supply interruptions from groundwater level decline during the 2012-2016 drought, and the associated costs of maintaining domestic water well supplies (Gailey, Lund, & Medellin-Azuara, 2019). However, to our knowledge, no studies have developed models at the regional aquifer scale (around $50,000 \text{ km}^2$ or greater) that simulate the impact of drought and sustainable groundwater management regimes on domestic well failure. Such a model can help evaluate the consequences of future droughts and statewide groundwater management options.

Groundwater overdraft in California is part of a larger global trend in aquifer depletion (Famiglietti, 2014; Wada et al., 2010; Döll et al., 2012; Siebert et al., 2010). Like many other semi-arid, agriculturally intensive regions worldwide, in the decades to come, California will grapple with the impacts of climate change and policy on its overdrafted aquifers. By the end of the

21st century, California’s snowpack is projected to decline by as much as 79.3% (Rhoades, Jones, & Ullrich, 2018), and drought frequency in the southern CV may increase by upwards of 100% (Swain, Langenbrunner, Neelin, & Hall, 2018). It is in this increasingly drier and warmer climate (Diffenbaugh, Swain, & Touma, 2015; Cook, Ault, & Smerdon, 2015) characterized by more frequent, more spatially extensive heat waves and extended droughts (Tebaldi, Hayhoe, Arblaster, & Meehl, 2006; Lobell, Torney, & Field, 2011), that California will implement a statewide policy of sustainable groundwater management (“Sustainable Groundwater Management Act, California Water Code sec. 10720-10737.8,” 2014). These policies aim to prevent chronic groundwater overdraft and other undesirable results, including domestic well failure. However, we lack both methodological approaches to forecasting well failure, and a basic understanding of how climate change (i.e., drought) and policy (i.e., groundwater management regimes) will impact well failure.

In this paper, we present a regional aquifer scale model covering California’s CV that predicts domestic well failure in response to groundwater level decline from extended drought and different groundwater management regimes. The model was developed using reported domestic well failures from the severe 2012-2016 California drought. The goal of this study is to evaluate the risk of domestic well failure in response to 1) extended (5 to 8 year) drought duration scenarios and 2) three different groundwater management regimes (sustainability, glide path, business as usual) in California’s CV.

2.3 Study area

The domestic well failure model was developed for the California CV alluvial groundwater basin (Figure 2.1). We chose this area for its geologic continuity, data availability, social and economic significance, and high rates of domestic well failure reported during the recent 2012-2016 drought. The study area was further pared down to only include areas with domestic wells completed on or after 1976 (SI Appendix 2.7.1).

The CV is heavily dependent on winter snowpack and groundwater for agriculture (Scanlon et al., 2012; Faunt et al., 2009; Hanak et al., 2011). In an average year, groundwater provides

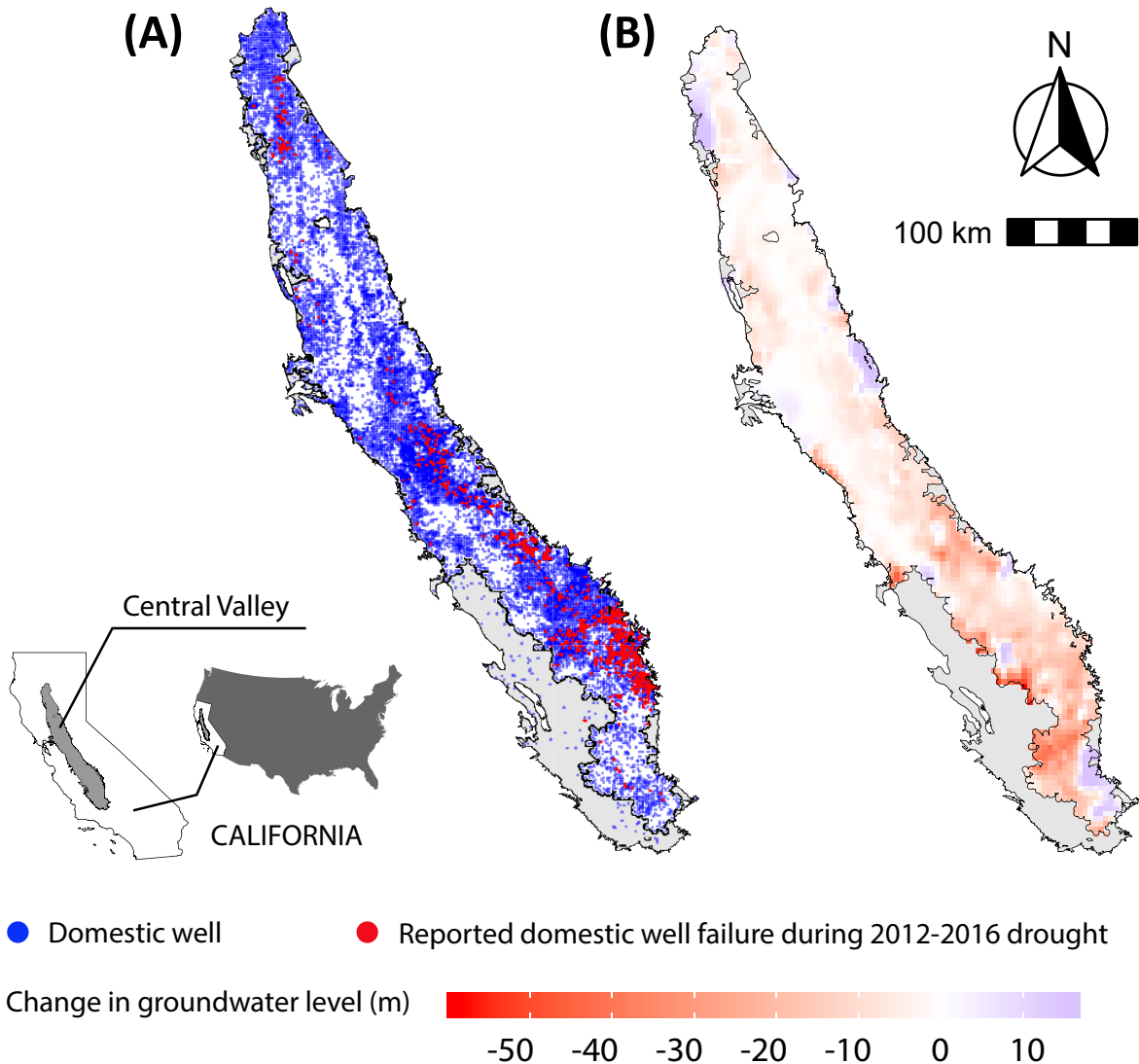


Figure 2.1: California's Central Valley is a major agricultural hub in the Western US, approximately 720 km long and 64 to 97 km wide. (A) The 2,027 reported domestic well failures during the 2012-2016 drought (red dots) cluster in the southeast. 67,011 domestic wells (blue dots) reported in OSWCR and constructed after 1976 were used to define the study area (SI Appendix 2.7.1 for details). (B) Average groundwater level change from 2012-2016 in unconfined to semi-confined aquifers. Areas of large groundwater level decline correspond to areas of high reported well failure.

about 30% of the water demand, but in drought years, groundwater can account for upwards of 60% of water consumed in some parts of the CV (Brush, Dogru, & Kadir, 2013). Nearly all of this water is consumed by agriculture (Brush et al., 2013; Faunt et al., 2009). It is well established that scarce surface water supply during drought encourages groundwater pumping (Lund, Medellin-Azuara, Durand, & Stone, 2018; Feinstein et al., 2017; Mount et al., 2018). The United States Geologic Survey estimated that during periods of drought, groundwater pumping in the CV increased upwards of 180% compared to the long-term mean (1962-2003) (Faunt et al., 2009). Estimated annual baseline groundwater depletion in the San Joaquin Valley (southern CV) is $2.3 \text{ km}^3/\text{yr}$, but during drought, the groundwater depletion rate may be up to 5 times greater (Hanak et al., 2019). Modeled CV groundwater depletion during the 1976-1977, 1987-1992, 2012-2016 droughts is estimated at 24.6 km^3 , 49.3 km^3 , and $40.0 \pm 0.8 \text{ km}^3$ respectively (Scanlon et al., 2012; Xiao et al., 2017). Thus, four- and five-year long historical droughts in California's CV have led to groundwater storage losses roughly equivalent to the combined storage capacity of California's surface water reservoirs (51.8 km^3) (Hanak et al., 2011).

Groundwater storage change leads to groundwater level change. Data from 506 monitoring wells in the Tulare Lake hydrologic region indicate that between fall 2011 and fall 2017, around 90 % of wells experienced a decline in groundwater level, and 58.9 % of wells experienced more than 7.5 m of groundwater level decline (CA-DWR, 2017a).

2.3.1 Data

The study used well completion reports from 943,469 wells from the California Department of Water Resources (data.ca.gov/dataset/well-completion-reports) (CA-DWR, 2018). Further, the study used seasonal groundwater level measurements (CA-DWR, 2019) spanning the period 1998-2017 and well failures reported during the 2012-2016 drought. The well failure dataset was obtained via an agreement with the California Department of Water Resources and the California Governor's Office of Planning and Research (CA-OPR, 2018). A limitation of the reported well failure data is that data was neither collected nor verified consistently by counties, and reporting was voluntary (and usually happens only when a well owner could not self-solve their issues). Hence, the reported

data under-counts the domestic wells impacted during the drought. All data are accessible online (Pauloo et al., 2019), with the exception of observed well failure data, which are confidential and may be obtained by contacting the California Department of Water Resources. Further information on data sources is provided in SI Appendix 2.7.2.

2.3.2 Classification of failing and vulnerable wells

We distinguish between three classes of well status: *active*, *failing*, and *vulnerable*. A well is classified as *active* when the groundwater level at the location of the well is above the level of the pump intake. If the groundwater level falls at or below the pump intake, the well is classified as *failing* (Figure 2.2). The well failure data collected during the 2012-2016 drought did not distinguish between failing wells and wells experiencing a decrease in pump efficiency, thus for the model calibration, wells are considered as either failing or active. Further detail is provided in SI Appendix 2.7.3.

Wells are classified as *vulnerable* to well failure when the groundwater level in a well falls within 3 m of the pump intake. As the distance between a well's pump intake and the groundwater level decreases, the fluid pressure (i.e. the net positive suction head) declines, causing cavitation, which may physically damage the pump and decrease its efficiency (Tullis, 1989; Helweg, Scott, & Scalmanini, 1983). In this study, we estimate the minimum separation distance required to avoid decreases in well function as 3 m (see SI Appendix 2.7.4).

2.3.3 Groundwater level interpolation

Seasonal (spring and fall) groundwater level data for each year between 1998 and 2017 (CA-DWR, 2019) were used to determine groundwater level changes in the unconfined to semi-confined shallow aquifer, which domestic wells draw from. For each set of seasonal groundwater levels, we applied ordinary kriging to the log-transformed groundwater levels to normalize the data distribution, suppress outliers, and improve data stationarity (Deutsch & Journel, 1998; Varouchakis, Hristopulos, & Karatzas, 2012). Because the expected value of back-transformed log-normal kriging estimates is biased (i.e. not equal to the sample mean), we applied the cor-

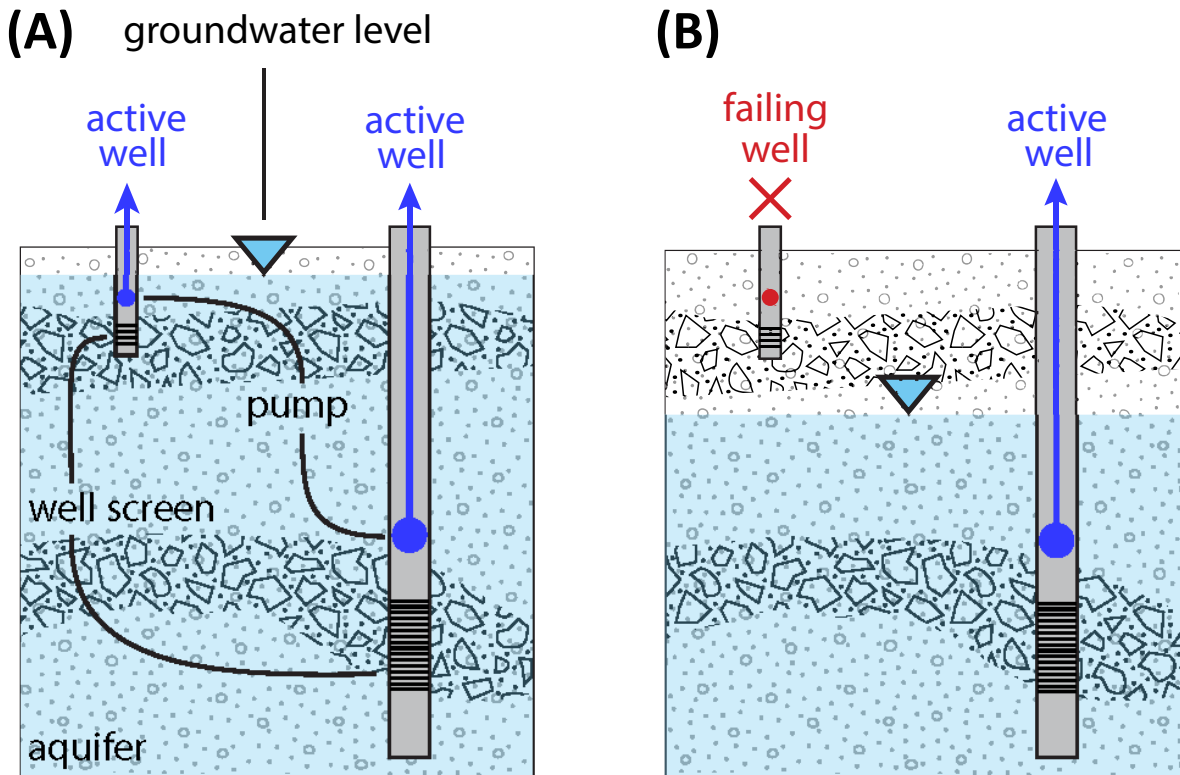


Figure 2.2: Conceptual model of well failure in an unconfined to semi-confined alluvial aquifer (details provided in SI Appendix, 2.7.3). (A) Groundwater level is above all pump intakes, and all wells are active. (B) Groundwater level falls below the pump intake of the shallow well, causing it to fail. The deep well remains active. In our study site, shallow wells tend to be domestic, and deep wells tend to be agricultural and public supply wells.

rection of Laurent (Laurent, 1963; Journel & Huijbregts, 1978) to recover unbiased groundwater level estimates (SI Appendix 2.7.5). We further calculated the 5% and 95% confidence intervals of the kriging estimates to propagate kriging uncertainty through the model and into the well failure estimates.

2.3.4 Pump intake depth estimation

Pump intake depth is not explicitly recorded on WCRs, thus for each well, it was estimated as the mean of the static water level at the time of well completion, and the top of the screened

interval (SI Appendix 2.7.7). When pump depth could not be directly calculated (i.e. - a WCRs is missing static water level or the top of the screened interval information), we imputed pump depths with simple linear models to regress known pump depths onto the bottom of the screened interval, which is known for nearly all wells (SI Appendix Figure 2.12). Pump depth exhibits spatial variance due to geologic heterogeneity and historical groundwater level, hence imputation was conducted at the Bulletin 118 subbasin level (SI Appendix Figure 2.11) to ensure hydrogeologic similarity. As with the kriging estimates, we calculated the 5 and 95% confidence intervals of the estimated pump locations to propagate this uncertainty into the well failure estimates.

2.3.5 Model calibration based on 2012-2016 drought data

The well failure model was calibrated with observed 2012-2016 well failures by relating groundwater level changes to estimated pump intake locations of wells in OSWCR, and minimizing error between the observed and predicted well failures during the 2012-2016 drought (SI Appendix 2.7.8). Well failures tend to form clusters, thus we calculated Gaussian kernel density estimates for the observed and predicted point patterns and calculated residual error as their difference. We use a kernel bandwidth of 433 m , calculated as $0.15/\sqrt{5 \cdot \lambda}$ where λ is the point intensity—the number of observations divided by the study site area (Stoyan & Stoyan, 1994). Calibration results are depicted at the Public Land Survey System (USDOI, 2009) township resolution (roughly 10 km) to improve mapping.

2.3.6 Simulation of drought duration scenarios

Climate change may cause severe and extended droughts exceeding 4 years in duration, yet the impact of such drought durations on domestic well failure remains unknown. Thus, we simulate drought durations of 5 to 8 years in length by extending the observed 2012-2016 drought with an additional 1 to 4 years using two scenarios:

1. *Continuous drought*: 1 to 4 years of drought immediately following the 2012-2016 drought.
2. *Intervening wet winter*: identical to the continuous drought scenario, but groundwater levels

are allowed to recover after 4 years, due to one intervening wet winter.

Groundwater level change in each drought duration scenario was determined by assuming that the impact of future droughts is proportional to the historical 2012-2016 drought. In other words, the groundwater level change associated with 1 to 4 additional years of drought is computed by scaling the change in the groundwater level field observed during the 2012-2016 drought by 0.25, 0.50, 0.75, and 1 respectively.

In the “continuous drought” scenario, groundwater levels are already low from the 2012-2016 drought, and increased well failure is expected. Hence, the “intervening wet winter” scenario examines how much a wet winter event, such as the one observed in 2017, may buffer against well failure over a longer drought duration.

2.3.7 Projected groundwater management regimes

In California, the Sustainable Groundwater Management Act (SGMA) enacted in 2014, requires the development and implementation of local groundwater management plans by 2020. These plans aim to prevent undesirable results, including the chronic lowering of groundwater levels, to achieve groundwater sustainability by 2040 for critically overdrafted basins. Overlying landowners of overdrafted basins may deploy different groundwater management regimes, which will impact groundwater level change in the coming decades to various degrees.

To analyze how different groundwater management regimes might impact groundwater level change and hence domestic well failure, we simulate three simplified regimes for the period 2017 – 2040 (Figure 2.3):

1. *Strict sustainability*: water levels do not decline after 2020. This represents a theoretical (and idealized) best case management regime for domestic wells.
2. *Glide path*: groundwater level decline is gradually reduced over the implementation period until 2040.

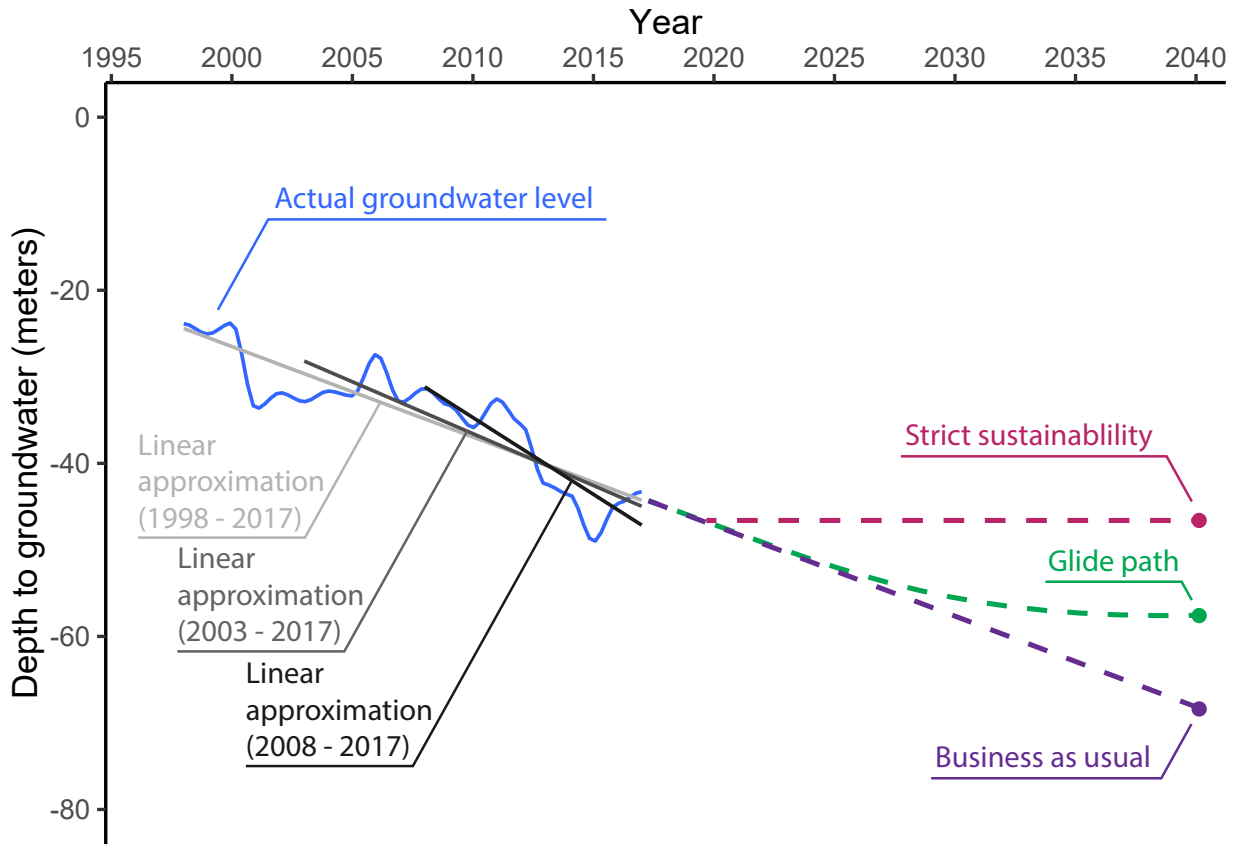


Figure 2.3: Projected groundwater management regimes using actual groundwater elevation change for a point in Tulare County as an example. Groundwater level change is approximated by three linear trends, based on different time periods. In this figure, we show the different projected groundwater management regimes using the linear approximation based on the 1998-2017 period. In the analysis, we calculate groundwater levels across the entire CV, using all three trends, and all three regimes.

3. *Business as usual*: groundwater level decline continues at the historic rate. This regime is used for comparison.

To project the number of failing wells for each groundwater management regime, we extend past groundwater level trends through 2040. For this, we first determined past groundwater level trends using data for the period from 1998-2017 and estimated annual groundwater levels at each point of the CV via ordinary kriging as discussed above and in SI Appendix section 2.7.5. To estimate declining groundwater level trends consistently over time, we only use fall measurements

following the growing season. We then obtain linear approximations of groundwater level for each cell using a $5 \times 5 \text{ km}^2$ raster. We use three different approximations of groundwater level based on changes observed from 1998-2017, 2003-2017, and 2008-2017 to account for differences in initial groundwater level and thus, uncertainty introduced by the period over which the linear models are built. Finally, to project the “Strict sustainability” regime we extend these three approximations into 2020, then eliminate further overdraft. In contrast, the “Business as usual” regime projects the linear trends into 2040 before ending overdraft, and the “Glide path” regime gradually reduces the slope of the linear trend between 2020 to 2040, representing a middle path between the “Strict sustainability” and the “Business as usual” regimes.

2.4 Results

2.4.1 Well failure prediction during the 2012-2016 drought

The calibrated model reproduced both the magnitude and spatial distribution of the 2,027 well failures observed in the study area during the 2012-2016 drought (Figure 2.4A). The model predicts a slightly higher mean number of well failures ($n = 2,513$) (Figure 2.4B), which is expected, as observed well failures are most probably under-reported due to the voluntary nature of data collection, and a well-owner’s perceived consequence of reporting a failed well to their county or state.

The normally distributed residual error (Figure 2.4C) indicates the unbiasedness and strength of the model: well failure predictions for the observed 2012-2016 drought were within 20% of the actual value for around 68.2% of the study area, between 20% and 55% of the actual value for around 27.2% of the study area, and greater than 55% of the actual value for less than 5% of the study area.

Unsurprisingly, both observed and predicted failures tend to cluster in the southeastern CV, where agricultural groundwater use is comparatively higher than elsewhere in the state (Brush et al., 2013; Faunt et al., 2009); households reliant on domestic wells in this region are particularly susceptible to failure.

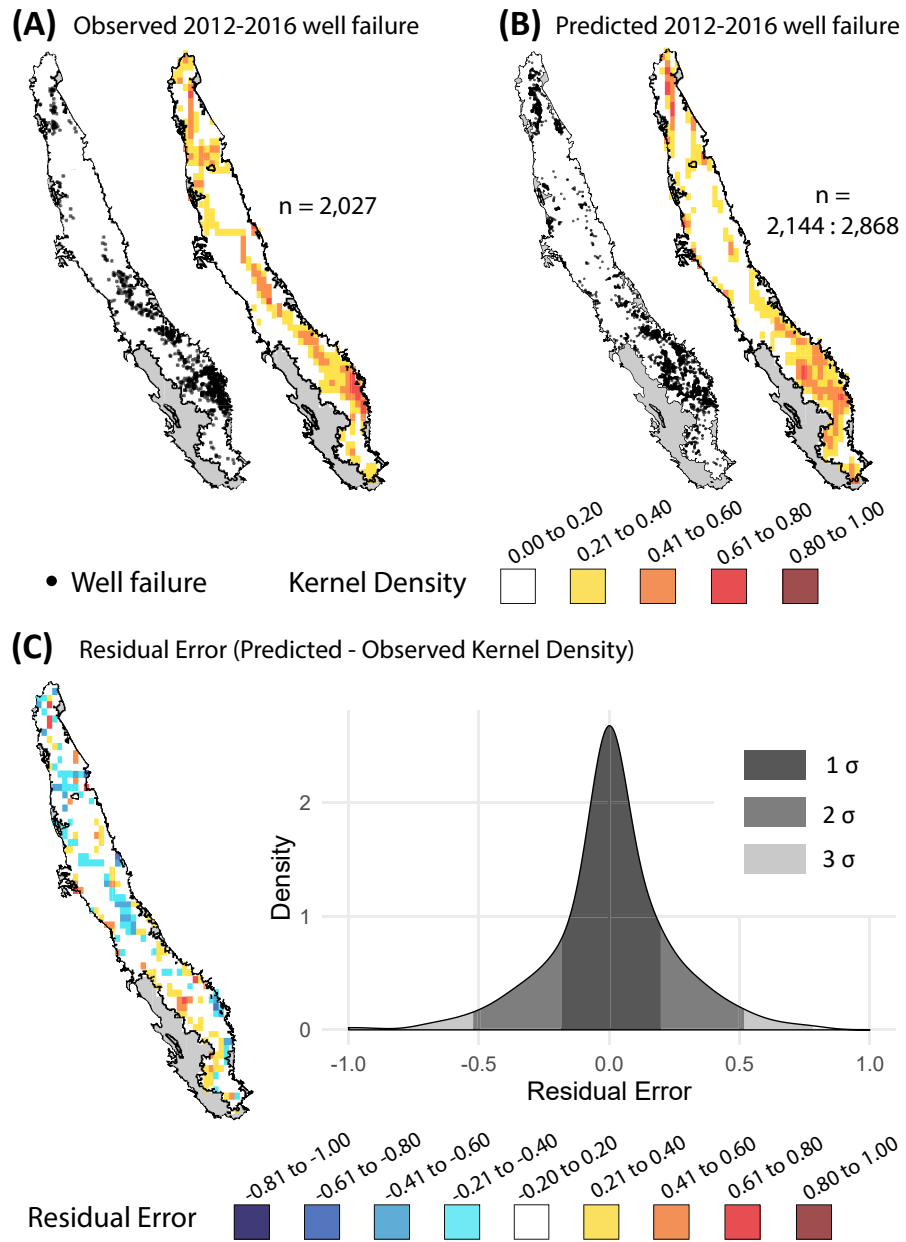


Figure 2.4: Model performance in predicting the spatial intensity of observed domestic well failures during the 2012-2016 drought. (A) Observed well failure point pattern and kernel density estimate. (B) Predicted well failure mean estimate ($n = 2,513$) and kernel density of the mean prediction. The 5 and 95% confidence intervals of predicted well failures span the interval from 2,144 - 2,868. (C) Residual (predicted minus observed) error. Red areas indicate areas of over-prediction, and blue areas indicate under-prediction.

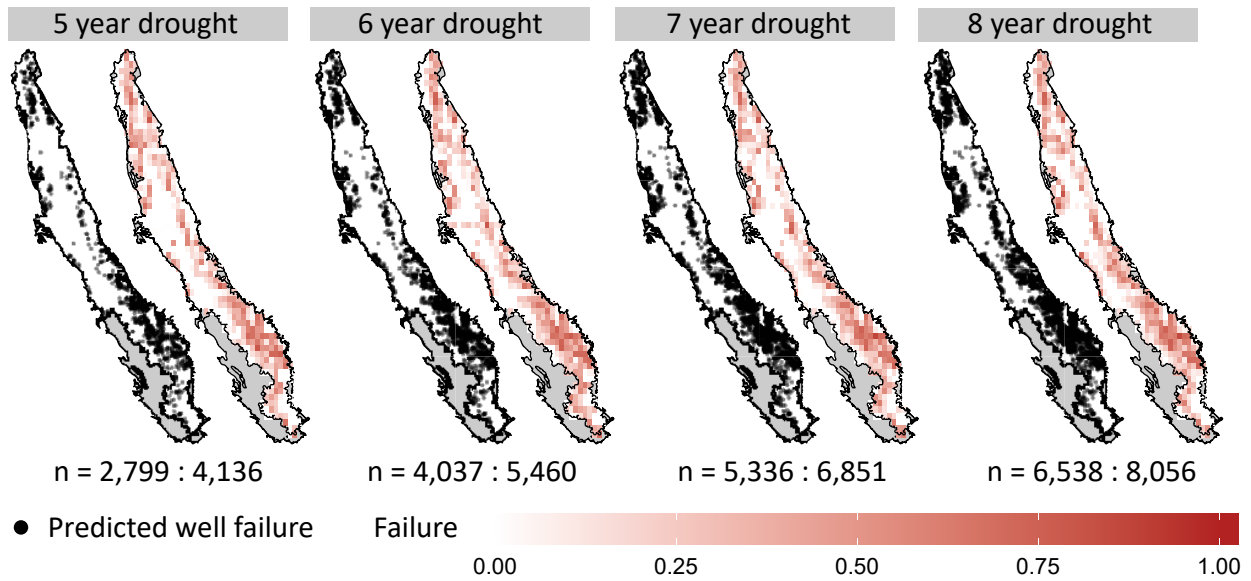


Figure 2.5: Simulated domestic well failure point patterns and associated kernel density estimates for 5 to 8 year drought duration scenarios beginning in Fall 2016 (maps show mean prediction). n is the 5 and 95% confidence interval of cumulative well failure count in each scenario, including the 2,027 failing wells in the 2012-2016 drought.

2.4.2 Failing and vulnerable wells in drought duration scenarios

Longer drought duration results in widespread well failure episodes concentrated primarily in the southeastern CV (Figure 2.5). Consistent with domestic well failure patterns observed during the 2012-2016 drought, well failure density is highest in Madera, Kings, Kaweah, Tule, Tulare Lake, and Kern subbasins.

In the “continuous drought” simulation, two- and four-year long droughts immediately following the 2012-2016 drought (6 and 8 years total without an intervening wet winter) result in 4,037 to 5,460 and 6,538 to 8,056 cumulative well failures, respectively. Thus, a two-year drought duration following the 2012-2016 drought results in more well failures than the 2012-2016 drought alone, and a combined 8 year drought duration results in nearly twice the failures observed from 2012-2016 (Figure 2.6). Intensified well failure during extended drought reinforces the interdependence of well failure on groundwater level: when groundwater levels cannot recover to pre-drought levels and pump depths are fixed, wells are more vulnerable to failure.

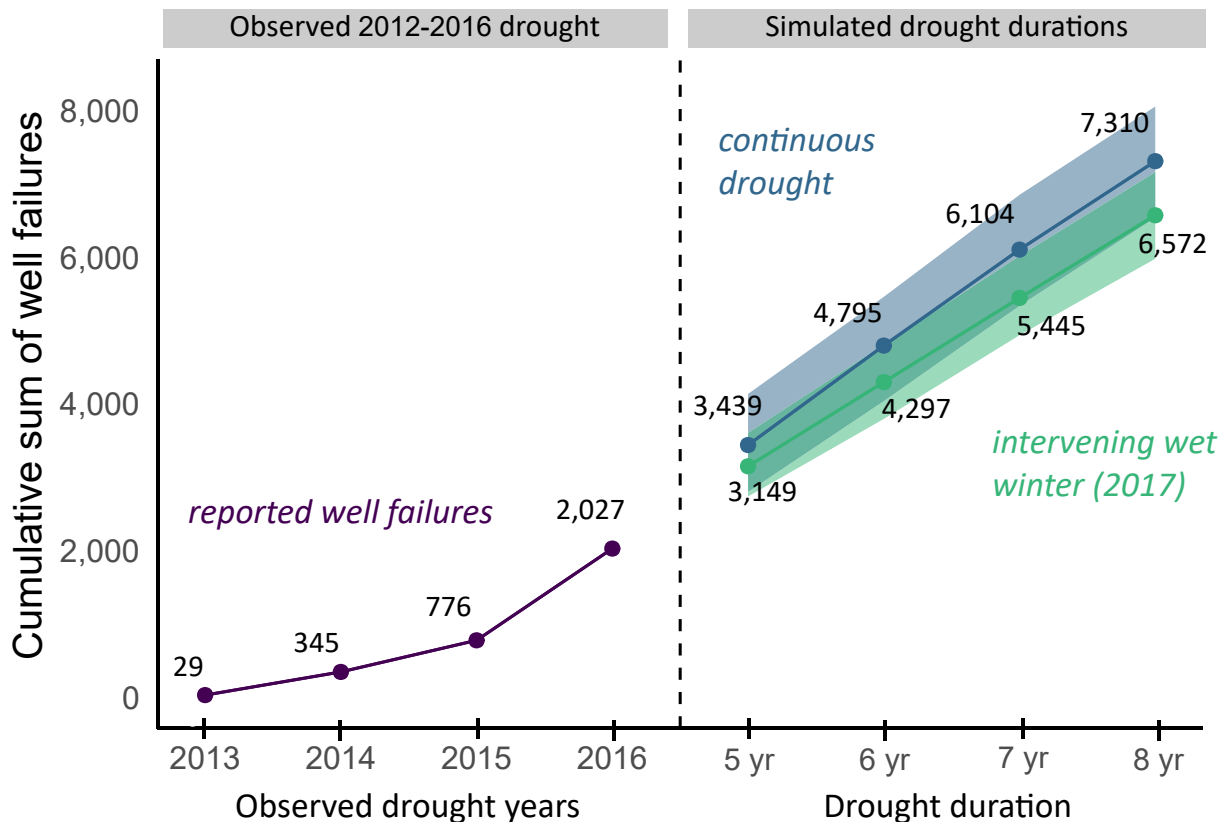


Figure 2.6: Left: Cumulative domestic well failures from 2012-2016. Right: Cumulative domestic well failures resulting from simulated drought durations 5 to 8 years in length. The continuous drought duration scenario (blue) leads to more well failure compared to the intervening wet winter scenario (green). Points represent the mean well failure estimate, and shaded regions represent the 5 and 95% confidence intervals.

In the “intervening wet winter” scenario, groundwater levels are allowed to recover during 2017, and well failure slightly abates: 498 and 738 fewer wells fail in the 6 and 8 year drought scenarios, indicating that an increase in median groundwater level of only a few meters across the Central Valley can prevent hundreds of domestic well failures during extended drought.

The cumulative sum of annual well failures observed in the evaluated drought duration scenarios follows a linear trend (Figure 2.6). If the drought were to continue past the simulated 8 years scenario, well failures likely would follow a sigmoidal trend: inflecting then leveling off, as failure progresses to increasingly infrequent and deeper wells until none are left.

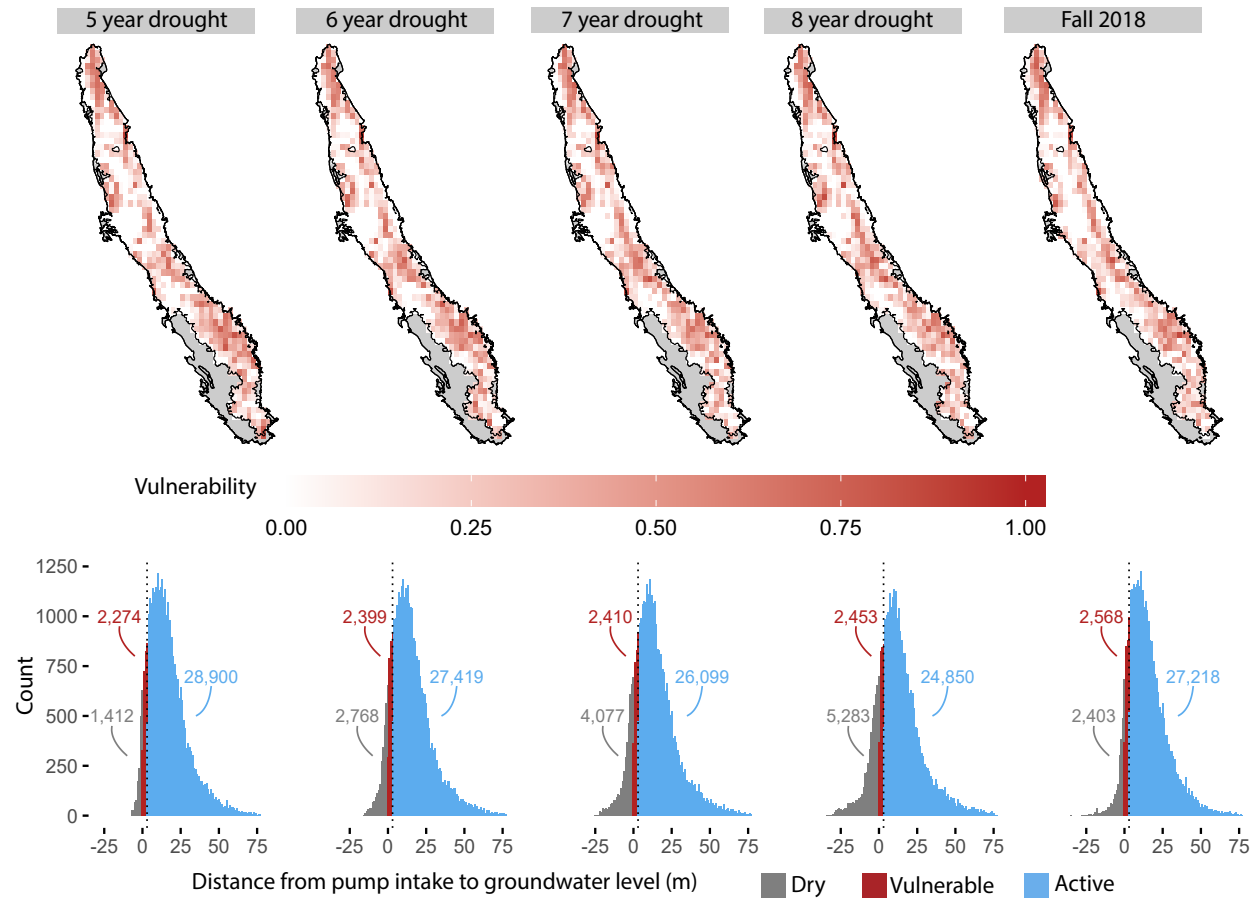


Figure 2.7: Top row: kernel density estimates of low vulnerability (white) and high vulnerability (red) regions in extended drought duration scenarios and in Fall 2018. Bottom row: histograms of failing wells (grey), vulnerable wells (red), and active wells (blue) for the extended drought scenarios and Fall 2018 scenario. The black dotted line at 3 meters is the threshold at which wells are at risk of decreased efficiency. All numbers reported are the mean estimate of dry, vulnerable, and failing wells.

Vulnerable wells (Figure 2.7) are those with estimated pump intakes within 3 m of the groundwater level, and are at heightened risk of experiencing a reduction in pump efficiency, or a failure episode. Since this 3 m window is fixed in our analysis, the spatial distribution and count of vulnerable wells is relatively constant across the drought duration scenarios (2,274 to 2,453 wells), and the present day scenario of Fall 2018 (mean estimate = 2,568). Moreover, the spatial distribution of vulnerable wells mirrors those of well failures.

2.4.3 Failing wells in projected groundwater management regimes

Projecting groundwater depths into 2040 under three different management regimes results in significant differences in domestic well failures (Figure 2.8). The “Business as usual” regime, with no change in the historical trend of groundwater level decline, would lower the groundwater level by up to 100 m in parts of the southern CV, but significant groundwater level declines are widespread. Scenarios aimed at achieving sustainability would reduce these declines, hence the differences between the ambitious “Strict sustainability”, “Glide path” and “Business as usual” pathways might be quite important for water resources managers and policy makers.

The groundwater depth changes and associated well failures are sensitive to the period used for the linear approximation of groundwater level declines. The period from 2008-2017 leads to significantly worse groundwater depletion than both periods 2003-2017 and 1998-2017, particularly because of the effects of the 2012-2016 drought. Average well failures for the “Business as usual” regime range from 5,966 to 10,466 (depending on the period used for the linear interpolation), while under the “Glide Path” regime they range from 3,677 to 6,943, and from 1,516 to 2,513 under the “Strict sustainability” regime (confidence intervals are reported in SI Appendix Table 2.2).

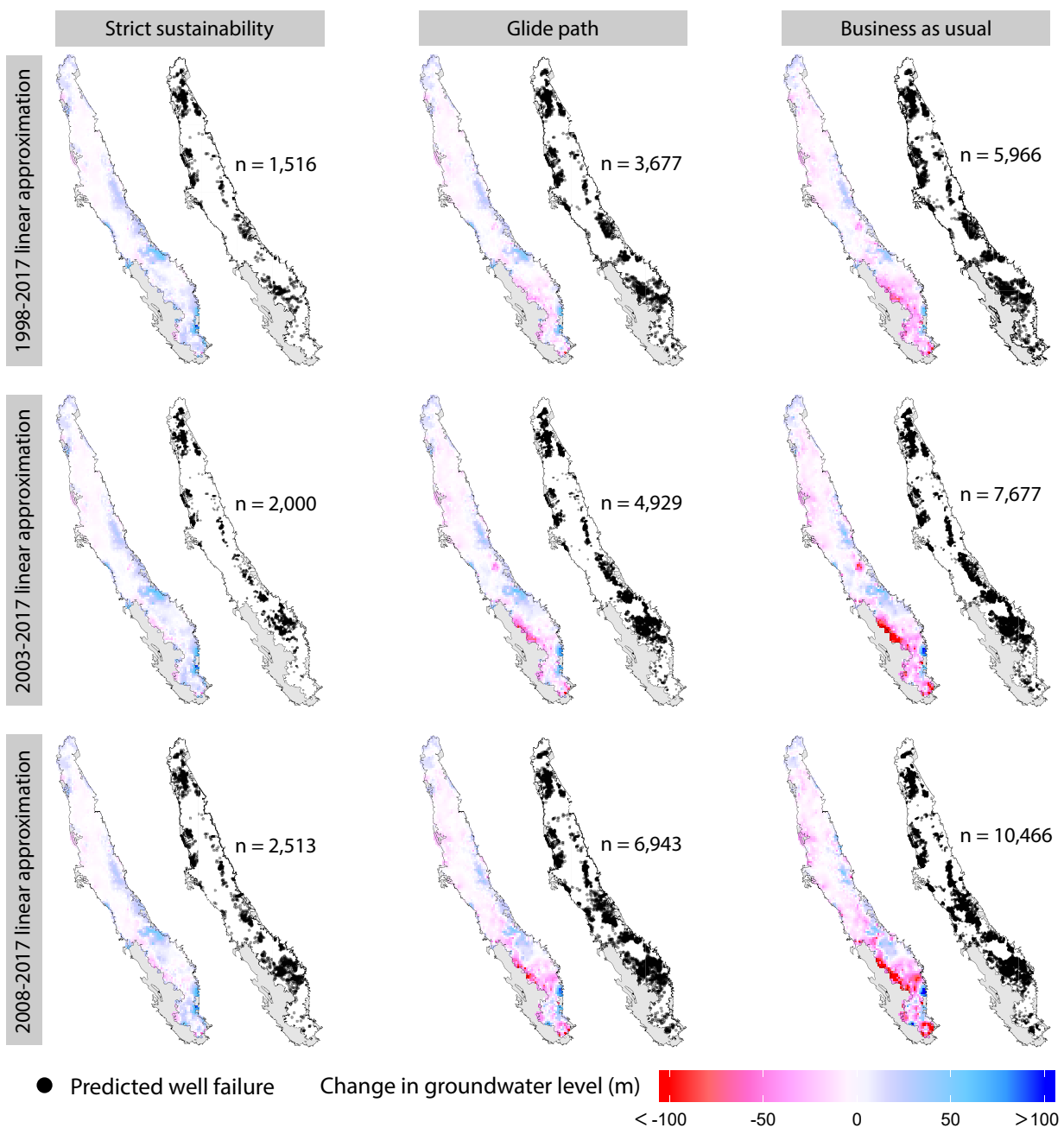


Figure 2.8: Domestic well failures projected for three groundwater management regimes (columns) based on three different time periods of linear groundwater level change (rows). The left plot of each pair is the mean projected groundwater level change from 2017-2040. Groundwater level decline (red) is more common than groundwater level increase (blue). The right plot of each pair shows the mean predicted well failure point pattern for that combination of groundwater management regime and groundwater level change approximation. See SI Appendix Table 2.2 for confidence intervals.

Most of the estimated domestic well failures are still concentrated in the southeastern CV, but the central and northern CV are also affected, presumably due to the ubiquity of relatively shallow wells in these regions. The “Business as usual” regime leads to especially severe well failure in all three projected groundwater level trends.

2.5 Discussion

2.5.1 Impact of drought duration on well failure and vulnerability

It is well understood that drought duration leads to increased groundwater extraction (Hanak et al., 2011; Medellin-Azuara et al., 2016), and hence domestic well failure (Perrone & Jasechko, 2017; Feinstein et al., 2017). Thus, we tested the impact of previously unseen drought durations ranging 5 to 8 years in length, by simulating an additional 2 to 4 years of severe drought immediately following the 2012-2016 drought, calculating the change in groundwater level, and determining failing and vulnerable wells.

A previous study estimated that 4 years of drought in the Tulare County, California immediately following the 2017 wet winter would result in about 200 - 850 domestic well failures (Gailey et al., 2019). Our model’s equivalent scenario (intervening wet winter with an 8 year drought duration) results in a similar range of 585 - 715 domestic well failures in Tulare County. Additional comparisons are not possible given the lack of research on this topic.

At the level of California’s CV, our results suggest that drought durations of 6 to 8 years result in 4,037 to 5,460 and 6,538 to 8,056 cumulative well failures, respectively. However, an intervening wet winter during the 6- and 8-year long drought duration simulations buffers against well failure: when groundwater is allowed to recover after 4 years of drought (as happened during the 2017 wet winter), an average of 498 and 738 less domestic wells fail. These findings support research indicating that limiting groundwater pumping during drought may reduce well failure (Hanak et al., 2019; Gailey et al., 2019), and a general understanding that groundwater pumping can lower proximal groundwater levels (Theis, 1935).

During the 2012-2016 drought, the median groundwater level in the CV fell to progressively

new historic lows each fall after the summer growing season (SI Appendix 2.7.6) (CA-DWR, 2017a). Our results indicate that between fall of 2014 and 2015, the median groundwater level across the entire CV fell by nearly 5 m , and in some areas (i.e. - Tulare, Kings, and Kern counties), by tens of meters. In fall of 2016, the median groundwater level in the CV was 27.0 m below land surface. Moreover, our results indicate that the interquartile range of domestic well pump locations in the CV is 24.5 to 52.3 m below land surface. The proximity of pump intake depths to groundwater levels explains why domestic wells are sensitive to even slight declines in groundwater level: 5 to 10 m of groundwater level decline may easily impact thousands of domestic well pump intakes and cause failure.

In the four drought duration scenarios evaluated, an average of 2,274 to 2,453 domestic well pumps reside within 3 m of the groundwater level. We classified these wells as vulnerable, because they are likely to fail first under persistent groundwater level decline. The spatial distribution of well vulnerability mirrors that of well failures. Mapping clusters of predicted failing and vulnerable wells is essential for sustainable water management and disaster response.

2.5.2 Implications for groundwater management and policy

The strong dependence of domestic well failure on groundwater pumping to support irrigated agriculture raises serious questions concerning the role of sustainable groundwater policy in mitigating well failure (Hanak et al., 2019). We evaluated three different projected groundwater management regimes to curb groundwater level declines in the coming years: a “Strict sustainability” theoretical best-case regime wherein declining trends in groundwater level stop in 2020, a “Business as usual” regime that continues groundwater decline until 2040, and a final “Glide path” moderate regime that slows the rate of groundwater level decline to the midway point between the former two regimes.

Our results suggest that choices embedded within each of the groundwater management regimes vastly impact the amount of expected well failures. For instance, the “Glide path” regime predicts 3,677 to 6,943 domestic well failures by 2040, and the “Business as usual” regime predicts 5,966 to 10,466 domestic well failures by 2040. Both groundwater management regimes would result

in twice to almost three times as many well failures than the “Strict Sustainability” regime (1,516 to 2,513 failures). All three scenarios are sensitive to the period of record used to approximate the linear groundwater level decline, however they underpin the vulnerability of domestic wells to historic rates of groundwater level decline, and demonstrate the impact of management on well failure.

Refilling overdrafted aquifers via managed aquifer recharge might meet the dual objectives of increasing groundwater storage, and bolstering domestic well dependent households’ drought resilience. In California, high-magnitude flood flows are likely the most accessible and largest sources of water to replenish groundwater aquifers through managed aquifer recharge (Kocis & Dahlke, 2017), which might considerably slow or reverse trends in groundwater depletion. The emerging research in the strategic siting of managed aquifer recharge considers impacts on crop health (Dahlke, Brown, Orloff, Putnam, O’Geen, et al., 2018), human health (Ayuso-Gabella et al., 2011), the mobilization of contaminants into groundwater (Xanke et al., 2017), and hydrogeologic suitability (i.e. - highly conductive flowpaths and geologic formations capable of accommodating large volumes of water, such as incised valley fills) (Maples, Fogg, & Maxwell, 2019). In the San Joaquin Valley where domestic well failures peak, managed aquifer recharge alone may not be enough to offset groundwater overdraft, but coupled with a reduction in agricultural water use (Hanak et al., 2019), groundwater levels may stabilize enough to prevent widespread future failure events.

This study assumes that no interim well construction takes place to prepare for falling groundwater levels, such as the practice of pump lowering or well deepening. Pump lowering typically takes place in 6 m intervals (the length of standard discharge piping), and costs around \$2,000 USD per lowering event (Gailey et al., 2019). If we consider the cost of pump lowering in all failing wells in the 6- and 8-year drought duration scenarios (in reality some wells will not have room to be lowered) and assuming every failing well’s pump is lowered once (some will require more than one lowering), at \$2,000 USD per 6 m unit of discharge piping, 4,037 - 5,460 and 6,538- 8,056 failures correspond to \$8.7 - \$10.4 and \$13.8 - \$15.5 million USD.

During the recent drought, it is likely that some households also deepened their wells.

In California and nationwide, drilling deeper wells is a common practice to adapt to declining groundwater levels (Debra Perrone & Jasechko, 2019), but is a costly and unsustainable solution that may furthermore result in cross-contamination due to interconnection of confined aquifers by well construction (Gailey, 2017). Moreover, the financial burden of pump lowering or well deepening might disproportionately impact disadvantaged populations (Famiglietti, 2014) unable to afford chasing after declining groundwater levels. Since many of these disadvantaged groups may not own their land and thus wells, well construction decisions may be made by landowners rather than the affected groups.

Sustainable long-term solutions for drinking water access might include connecting vulnerable households to nearby centralized water provisions. Recent research indicates that many rural communities, assumed to be on domestic wells, are actually quite close (less than 2 km) to a potable water supply system (London et al., 2018). However, as annexation and consolidation is financially and physically impractical for all domestic-well dependent households, many will remain too remote and isolated to connect to a nearby water system.

Short- and long-term solutions to domestic well failure remain largely unexplored. What role can managed aquifer recharge play in mitigating well failure? Given the strong dependence of groundwater level decline on extraction for irrigated agriculture, could agri-business proximal to centers of high well failure collectively fund safety nets that internalize the cost of well failure during periods of increased groundwater pumping? Should vulnerable domestic well reliant populations connect to nearby municipal water systems with more reliable water supply? What is the appropriate solution for those that are too remote or isolated to connect to a community system?

2.5.3 Applicability to other areas

The well failure model presented in this study is extensible to other areas outside of California where sufficient data or groundwater flow models are available. It relies on two inputs: (1) a time series of spatially-explicit groundwater level surfaces reflecting typical groundwater level changes (specifically, the maximum drawdown), and (2) well construction information (i.e. - geographic location and pump intake depth).

Approaches for interpolating groundwater levels and estimating pump intake depths are demonstrated in this study, though others exist (Gailey et al., 2019; Perrone & Jasechko, 2017; O’sullivan & Unwin, 2010; Journel & Huijbregts, 1978). Groundwater levels provided by a groundwater flow model such as MODFLOW (Harbaugh, Banta, Hill, & McDonald, 2000) would easily couple to a well failure model, enabling the simulation of water management regimes and the impact of the resulting groundwater level on domestic well failure at arbitrary temporal scales. In California, existing regional-scale groundwater flow models such as C2VSim (Brush et al., 2013) and CVHM (Faunt et al., 2009) can be used to plan for the impact of future failure episodes under different water management regimes involving changes in both pumping and recharge in space and time.

This study aimed for regional prediction of failing, vulnerable, and active wells, but more nuanced impact analyses can be made. For instance, variable losses in well efficiency may be quantified as groundwater levels fall (Medellin-Azuara et al., 2016). This in turn enables the cost estimation of repairing failing and vulnerable wells (e.g. - pump lowering, well deepening), compared to water management actions (e.g. - fallowing fields, reduced groundwater pumping).

Where resources exist to survey households, detailed domestic well information such as geographic location, pump intake depth, and retirement age may be obtained, and would further constrain the uncertainty inherent in the estimation of these parameters. Additionally, well failure observations are essential for model calibration. Though this study benefited from failure data, efforts to anticipate domestic well failures as proactive hazard mitigation should not wait for the existence of observational data. It does, however, suggest the benefit of having such a system in place as part of local and state-level drought preparedness.

2.5.4 Implications for adaptation to climate change

Our results demonstrate that the mechanisms leading to domestic well failure are heavily dependent on groundwater level declines due to pumping for irrigated agriculture and increased pumping during drought. A historical lack of groundwater management in California (Hanak et al., 2011) has led to widespread groundwater level decline. Climate change compounds the impact of

water management decision-making. Warming will increase the frequency and duration of drought in California and other parts of the world (Diffenbaugh et al., 2015; Cook et al., 2015; Swain et al., 2018; Rhoades et al., 2018; Van Loon et al., 2016), and if left unchecked, groundwater withdrawal will likely intensify as surface water becomes more scarce, as it has in the past (Hanak et al., 2011). As we demonstrate in this study, groundwater replacement of lost surface water during extended drought intensifies well failure due to already low groundwater levels. Thus, managing for low to no domestic well failure requires a consideration of the complex interaction between land use change, water resources management, human decision-making, and climate change. Unless adaptation strategies become integral to sustainable groundwater management policy, the extended droughts anticipated under climate change and resulting changes in groundwater levels will put thousands of domestic wells in California's CV at risk of failure, and hence, thousands of Californians at risk of losing access to water.

2.5.5 Additional perspective on the data and model

There is generally good agreement between the observed and predicted well failure at the 10 km resolution of the residual error maps (Figure 2.4A-B), and better agreement (Figure 2.4C) is achieved at larger spatial scales (i.e. - Bulletin 118 groundwater subbasins, entire CV). Thus, the results presented in this study should not be taken as *de facto* predictions of the exact locations of well failure, but rather, as *regional-scale* well failure estimates. Local-scale errors introduced by uncertainty in well failure reporting, well completion reporting, groundwater level, and model formulation are overcome at regional scales.

We acknowledge that spatial and temporal variability in monitoring well data introduces uncertainty in the interpolated groundwater level. Ambient monitoring wells measured each season (i.e. - spring and fall) are not the same across seasons, and each season's measurements are sampled over a roughly three month time frame (January-March in the spring, and October-December in the fall). However, because most of the groundwater level change observed in a year takes place as the result of the summer growing season, and the fall measurements take place after the summer, spring and fall measurements still reflect ambient conditions. Moreover, both scaling

the 2012-2016 groundwater level change to create future drought scenarios, and calculating 2040 groundwater levels with linear trends are simple approaches to estimate future groundwater level decline, but the accuracy of any method to forecast unseen future events are also questionable. Additionally, we do not account for any emergency response measures in response to drought such as groundwater pumping curtailments. In California, some households were able to drill deeper wells, lower their pumps, or connect to a nearby surface water supply system during the drought. Because these corrective actions are cost-prohibitive and highly unlikely to be widespread, our modeling assumptions (no corrective action) and hence results, still agree with observed well failure rates from 2012-2016.

2.6 Conclusions

In this study, we developed a data-driven well failure model and applied it to California's CV to make regional-scale estimates of domestic well failure, and assess future well failure under different groundwater level scenarios.

Our model reproduces reported domestic well failures during the 2012-2016 drought in California's CV ($n = 2,027$), and furthermore, simulates the impact of different drought duration scenarios up to 8 years in length. We show that small declines in groundwater level are sufficient to cause thousands of wells failures when groundwater levels are already low, and that wet winters, and hence groundwater recharge or reduced pumping, may buffer against well failure. A simulated drought duration of 6 years (2012-2018) results in 4,037 - 5,460 total well failures. Similarly, an 8-year long drought (2012-2020), corresponds to a median groundwater level change of less than 10 m across the CV, but results in 6,538- 8,056 total well failures. The same 6 and 8 year long drought duration scenarios with an intervening wet winter in 2017 lead to an average of 498 and 738 fewer well failures. Lastly, wells that do not fail may still be vulnerable to failure. Our model estimates that in Fall 2018, an average of 2,568 well pump intakes were within 3 m of the groundwater level, and 10,544 well pump intakes were within 10 m of the groundwater level.

Our model further shows that early adoption of sustainable groundwater management

regimes aimed at halting declining trends in groundwater level will lessen the magnitude of domestic well failure. A “Business as usual” linear groundwater level decline would result in an average of 5,966 - 10,466 domestic well failures by 2040. In contrast, a more gradual “Glide path” decline would result in 3,677 - 6,943 domestic well failures by the same date. A “Strict sustainability” regime that allows groundwater levels to decline until 2020 before halting would result in 1,516 - 2,513 well failures.

Together, these results demonstrate that access to domestic water supply for large rural populations may be imperiled by a relatively small number of agricultural users, posing challenges for equitable and sustainable groundwater management which may not adequately represent domestic well users.

Models like the one developed in this study may be updated over time to accommodate additional wells, refine existing well construction information, and evaluate the impact of potential water management strategies on groundwater level changes, and hence well failure. This study’s approach to well failure modeling may be applied in other arid regions worldwide to facilitate drought preparedness planning. We anticipate that the model developed herein may be used by local and state agencies developing groundwater management plans in accordance with California’s Sustainable Groundwater Management Act.

2.7 Supporting Information Appendix

2.7.1 Study Area

The study area was pared down from the Central Valley (CV) to only the area where more recently completed domestic wells (1976 and younger) were present. This cutoff was chosen because the model period in this study ends in 2016, thus wells completed on or after 1976 ($n = 67,011$) assumes a conservatively high well retirement age of 40 years. Circular, 5 km buffers were drawn around each well, then joined to create a unified study area polygon. Some isolated circles that were not connected to any other buffers (< 1% of the buffered area) were removed in order to constrain the study site to one contiguous spatial extent in the CV corresponding to the areas of greatest domestic well density. The small removed areas principally occur in the western San Joaquin Valley. Low rates of domestic well completion in the west side of the San Joaquin Valley compared to the CV as a whole are explained by a relatively deep water table, poor shallow groundwater quality, and perhaps missing well completion records in places where there are actually households on unregistered or non-permitted domestic wells.

2.7.2 Data

The California DWR keeps paper records of wells drilled in California that contain well construction information, such as the depth of the well, perforated interval dimensions, location, and well type (e.g. - irrigation, domestic, monitoring, etc.) among other data. These records are submitted by the well-drilling company to the state in the form of a Well Completion Report (WCR). Nearly all WCRs in the state have been digitally scanned, and key fields in the reports have been digitized. Until recently, WCR information was confidential under state law, and they were unavailable to the general public, limiting researchers' abilities to answer questions like those set forth in this study.

The State's Household Water Supply Shortage Reporting System (HWSSRS) was established in late 2014 as a tool to capture information on water supplies running dry due to worsening drought conditions across California. The data gathered by the system was used for coordinating

the State's drought emergency response efforts. The system was set up as a voluntary, self-reporting system and, as such, only represents some fraction of the actual water supply shortages occurring. Most of the reported shortages were dry wells, but some were streams. Most of the reports were actually received by county health officials who entered the data into the system. Some counties were very active in reporting, while some were not. A download of the reported HWSSRS data has been made available to researchers with redaction of some data fields and a reduction in the accuracy of geospatial data to protect personal identification. The precision of the geospatial data is 36 arc seconds, corresponding to approximately 1 km in the study area. The coordinate reference system used in this study is EPSG 4326.

The great majority of well locations in OSCWR ($> 95\%$) are rounded to the nearest centroid of the Public Land Survey System (PLSS) section. The PLSS is composed of a nested series of cadastral surveyed lands (e.g. townships, range and sections). Townships measure 6x6 square miles (93.24 km^2 each) in size and are made up of thirty-six one-square mile sections (2.56 km^2). As the distance between the cell centroid and a corner of each section is the half-diagonal $0.5 \cdot \sqrt{2} \cdot 1.6 = 1.14 \text{ km}$, the reported location (x, y) of each well is always $0 \leq (x, y) \leq 1.14 \text{ km}$ from the true location. Determining the exact location of a well from the scanned well completion reports is intractable as well coordinates are rarely provided on the scanned forms, and the listed street address typically corresponds to the well owner's residence, not necessarily where the well is located, thus hampering efforts at geocoding. Due to these limitations, the reported PLSS section centroid was taken as the approximate well location, with a maximum error of 1.14 km .

2.7.3 Formal evaluation of well failure

Classification into active wells and failing wells proceeds through several steps (Figure 2.9). Consider a well i . It has a set of spatial coordinates and an associated estimated pump depth (x_i, y_i, z_i) , where x_i and y_i are the Cartesian coordinates, and z_i is the estimated depth of the pump within the well casing that draws water from the surrounding aquifer. The groundwater level g is a scalar field which varies by location; the groundwater level at a well is thus a scalar defined by its coordinates: $g_i = f(x_i, y_i)$. We determine the groundwater level for some initial time $g(t_0)$ and

final time $g(t_f)$ at each location in the study area by ordinary kriging.

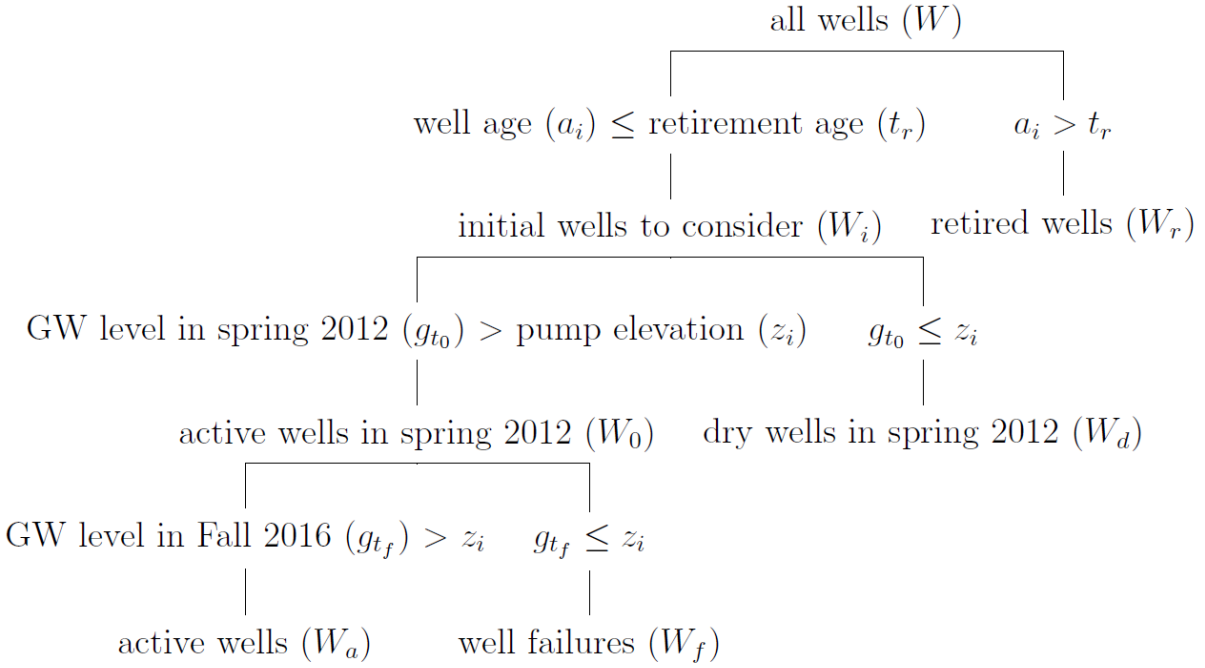


Figure 2.9: Decision tree representing the steps taken to evaluate active and retired wells, initially active and well failures, and finally, active wells and well failures given the following boundary conditions: retirement age, initial groundwater level, and final groundwater level.

Classification into active and failing wells proceeds as follows. Let the set of all domestic WCRs be called W . First, wells with age a greater than or equal to the calibrated retirement age t_r (Section 2.7.8) are removed from the simulation. This yields two sets: the initial wells to consider (W_i), and the retired wells (W_r).

$$W_i \subseteq W : a_i \leq t_r$$

$$W_r \subseteq W : a_i > t_r$$

The remaining active wells at this point are the initial wells to consider, W_i . However a well may not be active at t_0 frame if its pump is above the groundwater level at t_0 . Next, wells with

pumps above the groundwater level at the start of the simulation were removed, yielding another two sets: the active wells at time zero $W_a(t_0)$, and the failing wells at time zero $W_d(t_0)$.

The active wells at time zero are the subset of initial wells to consider where the groundwater level at time zero $g(t_0)$ at the location of the well exceeds the pump depth z , and the failing wells at time zero are the wells where the groundwater level at time zero at the location of the well falls at or below the pump depth.

$$W_a(t_0) \subseteq W_i : g(t_0) > z$$

$$W_d(t_0) \subseteq W_i : g(t_0) \leq z$$

Lastly, the groundwater level field at the final time $g(t_f)$ is applied, yielding the final two sets of wells: well failures $W_d(t_f)$ and active wells $W_a(t_f)$. Well failures are the subset of wells where the final groundwater level at the location of the well falls at or below the level of the pump, and active wells are the subset of wells where the final groundwater level at the location of the well does not fall below the level of the pump.

$$W_a(t_f) \subseteq W_0 : g(t_f) > z$$

$$W_d(t_f) \subseteq W_0 : g(t_f) \leq z$$

$W_d(t_f)$ and $W_a(t_f)$ combined form the set of all active wells at time zero $W_a(t_0)$.

Taken together, the three steps taken to classify wells into active and failing wells are visualized as a decision tree in Figure 2.9.

2.7.4 Vulnerable wells

Vulnerable wells are defined as wells that may experience a loss in function due to sufficiently low water levels above the estimated pump intake depth. We estimate that 3 m is the threshold at which a well may experience losses in function, based on a pumping rate of 1 m^3/hr , a

required net positive suction head of 5 m, a barometric pressure head of 10 m (at 25 degrees C and 0 m above mean sea level), a vapor pressure (at 25 degrees C) of 0.3 m, and friction head losses of 1 m Tullis, 1989.

2.7.5 Groundwater level interpolation

The groundwater level interpolation consists of five steps: (i) data collection; (ii) log transformation; (iii) ordinary kriging; and (iv) back-transformation and correction of the interpolated groundwater levels. Groundwater level data covering fall and spring measurements between 1998 and 2017 were obtained from DWR CA-DWR, 2019. Seasons are defined as either spring (January - March) or fall (August - October). Groundwater levels in a season reflect the ambient signal of the unconfined to semi-confined aquifer. Groundwater levels are measured in reference to the land surface at the measurement locations.

Many environmental data follow a log-normal distribution Stedinger, 1980, including the ambient groundwater levels used in this study. Depths to groundwater at each monitoring well were log transformed ($\ln(x)$) prior to interpolation to normalize the data distribution, suppress outliers, and improve data stationarity Deutsch and Journel, 1998; Varouchakis et al., 2012.

Ordinary kriging was then used to interpolate groundwater levels for each season. Inverse distance weighting and thin plate splines were also considered, but discarded because they produced unrealistic groundwater levels near the study area's boundaries, where conditioning data was sparse, and unlike kriging, are susceptible to bulls-eye patterns (concentric areas of equal value around known data points). Ordinary kriging parameters were determined by fitting an exponential semi-variogram model.

Since the expected value of back-transformed log-normal kriging estimates is biased (i.e. - not equal to the sample mean), we apply a correction Laurent, 1963; Journel and Huijbregts, 1978:

$$g = k_0 \cdot \exp \left[\ln(\hat{g}_{OK}) + \frac{\sigma_{OK}^2}{2} \right] \quad (2.1)$$

Where g is the corrected and back-transformed groundwater level, \hat{g}_{OK} is the ordinary

kriging estimate, σ_{OK}^2 is the kriging variance, and k_0 is the correction factor, proportional to the ratio of the mean of the sample values to the mean of the back-transformed kriging estimates.

Lastly, the the 5 and 95% confidence intervals of the kriging estimate was determined via: $\hat{g}_{OK} \pm (1.96 \cdot \sqrt{(\sigma_{OK}^2)})$. These confidence intervals are propagated through the model to account for uncertainty in the estimated groundwater level.

2.7.6 Impact of drought on seasonal groundwater levels

Interpolated seasonal groundwater levels in the study area during the 2012-2016 drought exhibit oscillating seasonal variation between spring and fall, a downward trend as the drought progresses from spring 2012 to fall 2015, and an upward trend beginning in spring 2016 and continuing into 2017. Seasonal groundwater level oscillation is a byproduct of agricultural groundwater demand, which peaks during summer and fall months.

The median groundwater level oscillates with the growing season (Figure 2.10C) and is generally higher in spring than in fall of the same year. Between spring and fall of 2015 alone, the median groundwater level across the CV fell by nearly 5 m. In that same water year, Sierra snowpack measured at an all time low of 5% of the average snowpack CA-DWR, 2017b, implying that low snowpack leads to more groundwater pumping and hence a seasonal lowering of groundwater levels.

Median groundwater levels decline between spring 2012 and fall 2015, the four driest consecutive years on California's record (Figure 2.10C). These groundwater level declines coincide with more pumping, which is due to less surface water delivered, which is due to less snowpack. In 2015, California set state records for high temperature, low precipitation, and low snowpack CA-DWR, 2017b. Median groundwater levels start trending upwards in spring 2016 and into 2017, indicating the easing of groundwater pumping. This inflection coincides with the relative return of the Sierra snowpack: in the 2016 and 2017 water years, Sierra snowpack was 85% and 159% of normal California Department of Water Resources, 2016; CA-DWR, 2017b.

Over the course of the drought, groundwater levels decline most evidently in the southern CV (i.e. - Madera, Kings, Kaweah, Tule, Tulare Lake, and Kern Bulletin 118 subbasins). These

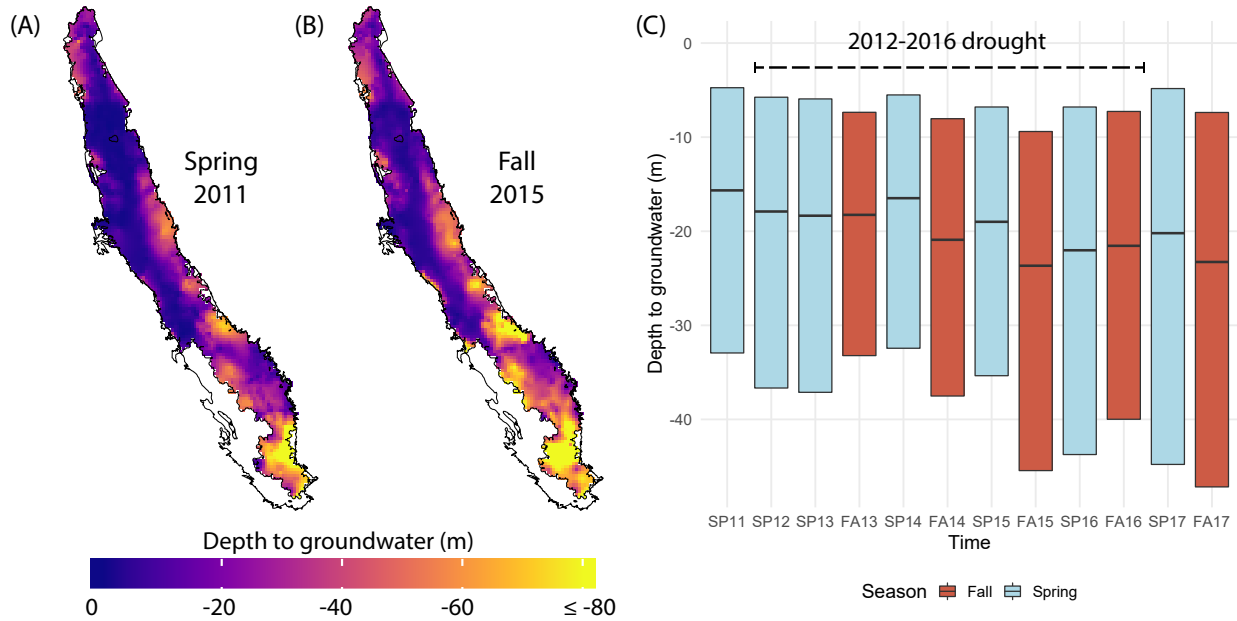


Figure 2.10: Groundwater levels during the most intense 4-year period of the 2012-2016 drought in (A) spring 2011, and (B) fall 2015. (C) Box plots showing the median and 25% and 75% percentiles of depth to groundwater. Compared to spring groundwater levels, fall levels tend to be deeper. The schematic assumes that groundwater levels do not decrease with depth, which is not a concern for most of the domestic wells because they tend not to be very deep.

findings are consistent with former research indicating that the central and southern CV experienced the largest surface water loss and groundwater replacement in 2016 [Medellin-Azuara et al., 2016](#), and estimates that California replaced more than 70% of lost surface water supply with groundwater during the 2012-2016 drought [Lund et al., 2018](#).

2.7.7 Pump intake depth estimation

The depth of the pump intake in each domestic well, henceforth called the pump depth (z), was estimated for all wells (W) as the mean of the static water level at the time of well completion, and the top of the screened interval. This assumption is based on the fact that well pumps are submerged upon installation, and the mean of the static water level at the time of well completion and top of the screened interval represents an unbiased best estimate of where the pump was likely

to be placed. Pump depth could not be directly calculated for wells missing either the static water level or the top of the screened interval. Moreover, pump depth exhibits spatial variance due to geologic heterogeneity and historical groundwater use (Figure 2.11), which suggests the need for imputation as a function of spatial location. Thus, simple linear models were developed for all wells located within a Bulletin 118 subbasin relating the logarithm of pump depth z to the logarithm of screen bottom, z_b (Figures 2.12-2.13).

$$\log(z) = \beta_0 + \beta_1 \log(z_b) + \epsilon \quad (2.2)$$

Conveniently, z_b is known for nearly all wells in the study area. Where it was unknown, it was taken as the total completed depth. Linear models for each subbasin were used to impute the pump depth for wells missing either static water level, top of screened interval, or both.

Pump depth estimates were generally poor in Bulletin 118 subbasins with fewer than 75 wells, such as in the western San Joaquin Valley, and in various subbasins from the Sacramento Valley to the northernmost CV (Figure 2.13A). To improve pump depth estimates in these regions, we used observations from adjacent subbasins (Figures 2.13B & 2.13C) to construct linear models relating pump depth and screen depth as described above (Figures 2.13D & 2.13E).

The 5 and 95% confidence intervals for each linear model were calculated via the standard approach James, Witten, Hastie, and Tibshirani, 2013, and propagated through the model to account for uncertainty in the estimated pump location.

Distributions of estimated pump intake depth at the DWR Bulletin 118 subbasin level tend to be either normal or left-skewed (Figure 2.11), indicating that most pumps are shallow and close to the land surface. The mean estimated pump depth across subbasins ranges from 25.44 m in the North American subbasin to 68.84 m in the Madera subbasin, suggesting that many pumps are, within tens of meters of the land surface. Considering that most groundwater levels are also tens of meters below land surface, the distance between a particular well's pump and the upper groundwater level may be only a few meters. Consequently, small groundwater level declines of only a few meters during a drought can lead to considerable domestic well failures.

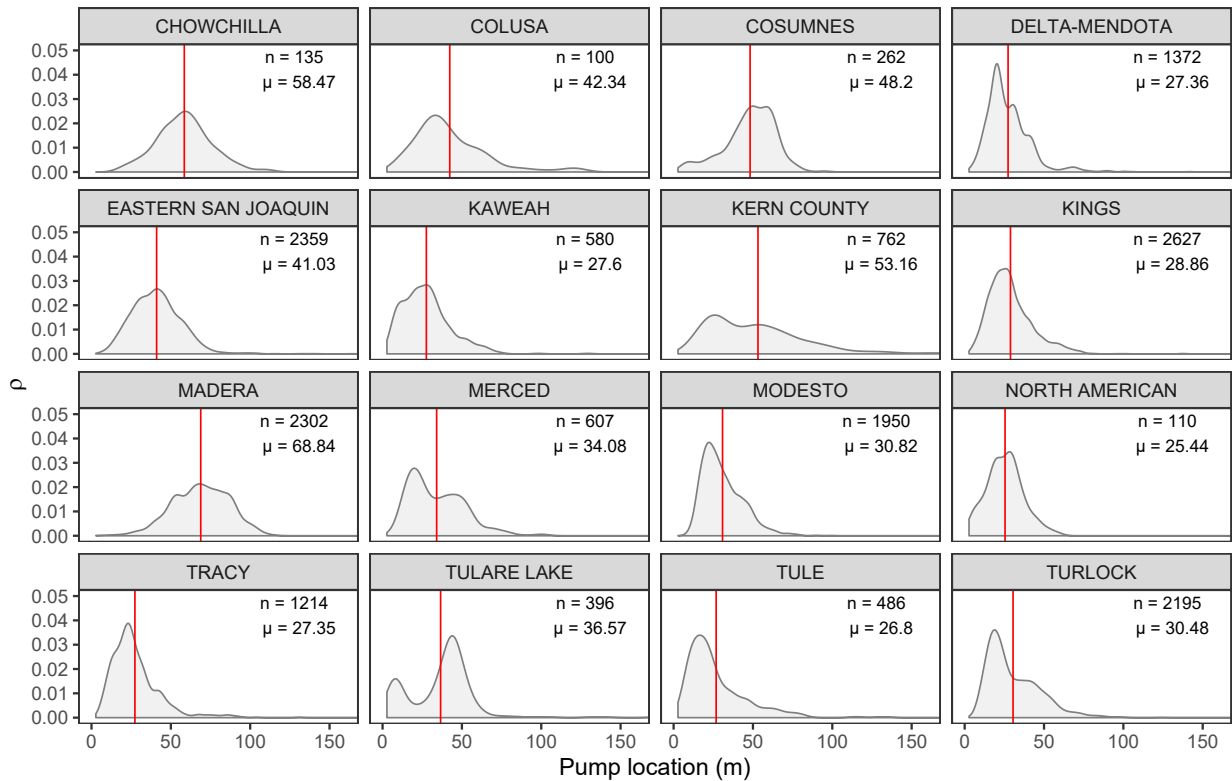


Figure 2.11: Density distributions of estimated pump intake depth for a subset of 16 Bulletin 118 subbasins. The red vertical line indicates the mean pump depth.

The strong relationship between the bottom of the screened interval and the estimated pump depth (Figure 2.12) was a useful approach for imputing missing pump depths. Goodness of fit (r^2) for subbasins have a median of 0.84, and range from 0.93 to 0.41. Residual plots were examined and do not exhibit non-constant variance in the error terms or heteroscedasticity, partially because log-transformation dampens the leverage of the few particularly deep wells. Model β_1 coefficients vary around 1, indicating that in most subbasins, an increase of 1 unit in the screened interval depth corresponds to an increase of 1 unit in the estimated pump depth. As expected, most intercepts (β_0) are negative, because the bottom of the screened interval is always deeper than the pump depth. Those with positive intercepts (Yolo and Chowchilla) have poor r^2 scores compared to other subbasins, attributable partly to a relatively low number of wells.

Northern basins are smaller in area than southern basins, and also tend to be more sparse

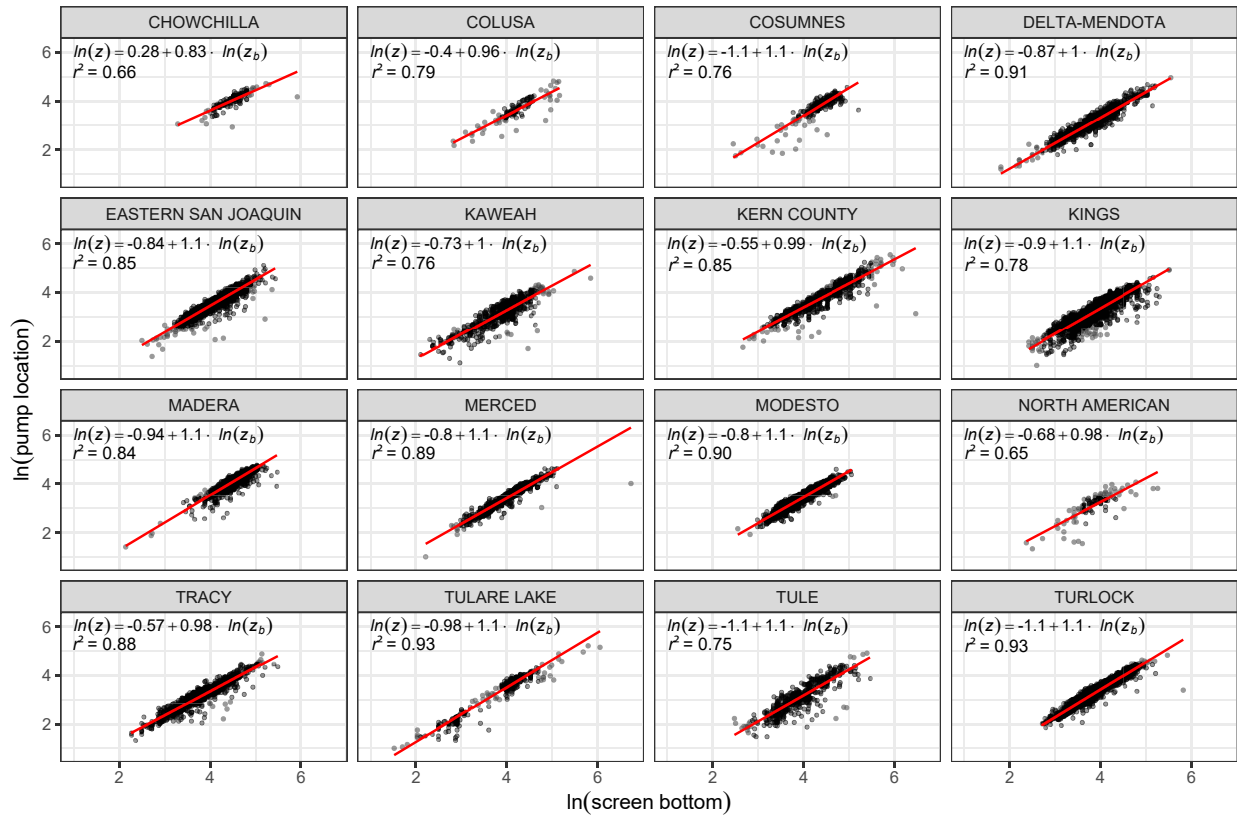


Figure 2.12: Relationship between the logarithm of pump depth (z), and logarithm of the bottom of the screened interval (z_b) for a subset of 16 Bulletin 118 subbasins.

in terms of screened interval information. The sparsity of data in some basins motivated the creation of north and south aggregate models (Figures 2.13A-E) to supplement data-poor basins with fewer than 75 samples. The south and north aggregate models show an r^2 of 0.90 and 0.71 respectively.

Model coefficients, goodness of fit scores, and sample sizes are reported in Table 2.1.

2.7.8 Model calibration and performance

We seek a well failure model that reproduces the observed well failures during 2012-2016 by relating changes in groundwater level to estimated pump locations of wells in the OSWCR database. The developed model may then be used to simulate the impact of future droughts. We perform calibration to minimize error between the observed ($n=2,027$) and predicted well failures

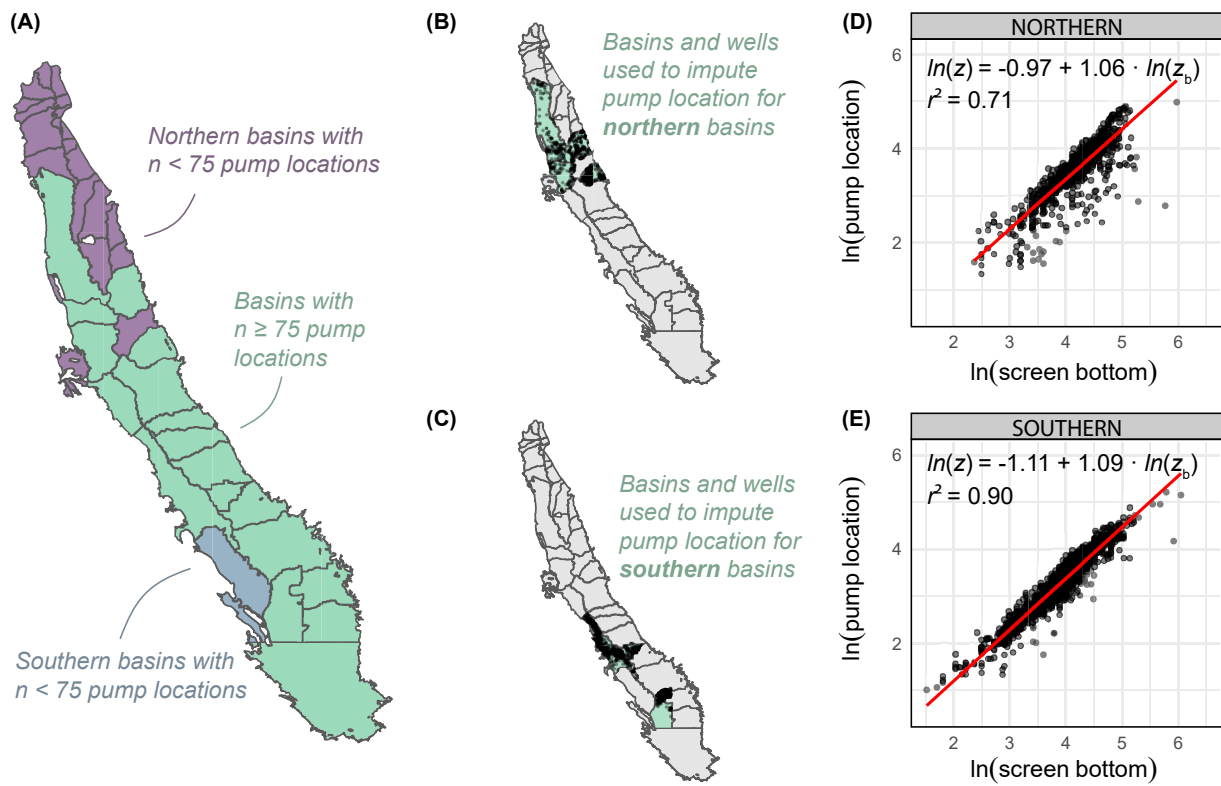


Figure 2.13: (A) Count of wells per Bulletin 118 subbasin with recorded screen bottom and directly estimable pump depth, further classified into northern and southern subbasins. (B) & (C) Northern and Southern subbasins used to construct the linear relationships between pump depth and screened interval bottom; the wells within are shown as black points. (D) & (E) Northern and Southern linear models used to impute pump depth for northern and southern basins with fewer than 75 samples.

during the 2012-2016 drought. Model calibration proceeded in three steps. First, groundwater levels across the CV during the 2012-2016 drought were mapped. Second, the spatial units at which the model was calibrated were selected (discussed below). Third, the optimum value of the well retirement age (t_r) was determined.

Groundwater levels across the CV were mapped by the interpolation approach described above and in the methods of the paper. In order to calculate groundwater level change over the drought, we set initial and final conditions, and take their difference. Because the observations are not spatially consistent across seasons, we take the mean groundwater level of adjacent sea-

Table 2.1: Linear regression model coefficients, goodness of fit, and sample size for the subset of wells with 75 or more samples.

<i>Subbasin Name</i>	β_0	β_1	r^2	<i>n</i>
Chowchilla	0.28	0.83	0.66	133
Colusa	-0.40	0.96	0.79	98
Cosumnes	-1.06	1.12	0.76	260
Delta-Mendota	-0.87	1.05	0.91	1370
Eastern San Joaquin	-0.84	1.07	0.85	2357
Kaweah	-0.73	1.00	0.76	578
Kern	-0.55	0.99	0.85	760
Kings	-0.90	1.06	0.78	2625
Madera	-0.94	1.12	0.84	2300
Merced	-0.80	1.06	0.89	605
Modesto	-0.80	1.07	0.90	1948
North American	-0.68	0.98	0.65	108
Solano	-0.47	0.89	0.66	75
Tracy	-0.57	0.98	0.88	1212
Tulare Lake	-0.98	1.12	0.93	394
Tule	-1.08	1.07	0.75	484
Turlock	-1.13	1.13	0.93	2193
Yolo	0.80	0.65	0.41	75
North aggregate	-0.97	1.06	0.71	866
South aggregate	-1.11	1.09	0.90	1920

Logarithm of pump depth z is regressed onto the logarithm of screen bottom elevation, z_b .

sons to reduce variance in the interpolated surface, and provide a more robust representation of groundwater levels during that time. The initial groundwater level (g_{t_0}) is the mean of spring 2011 and spring 2012 measurements, and the final groundwater level is the mean of spring and fall of 2016. The difference of the final and initial conditions defines the groundwater level change over four years of drought from 2012-2016. The upper and lower 2.5 percentiles of the raster (which incidentally coincide with areas of low to zero domestic well occurrence) were assigned to the 2.5

and 97.5 percentiles to control for outliers in the interpolation and improve mapping. The well failure model described in section 2.7.3 was then applied.

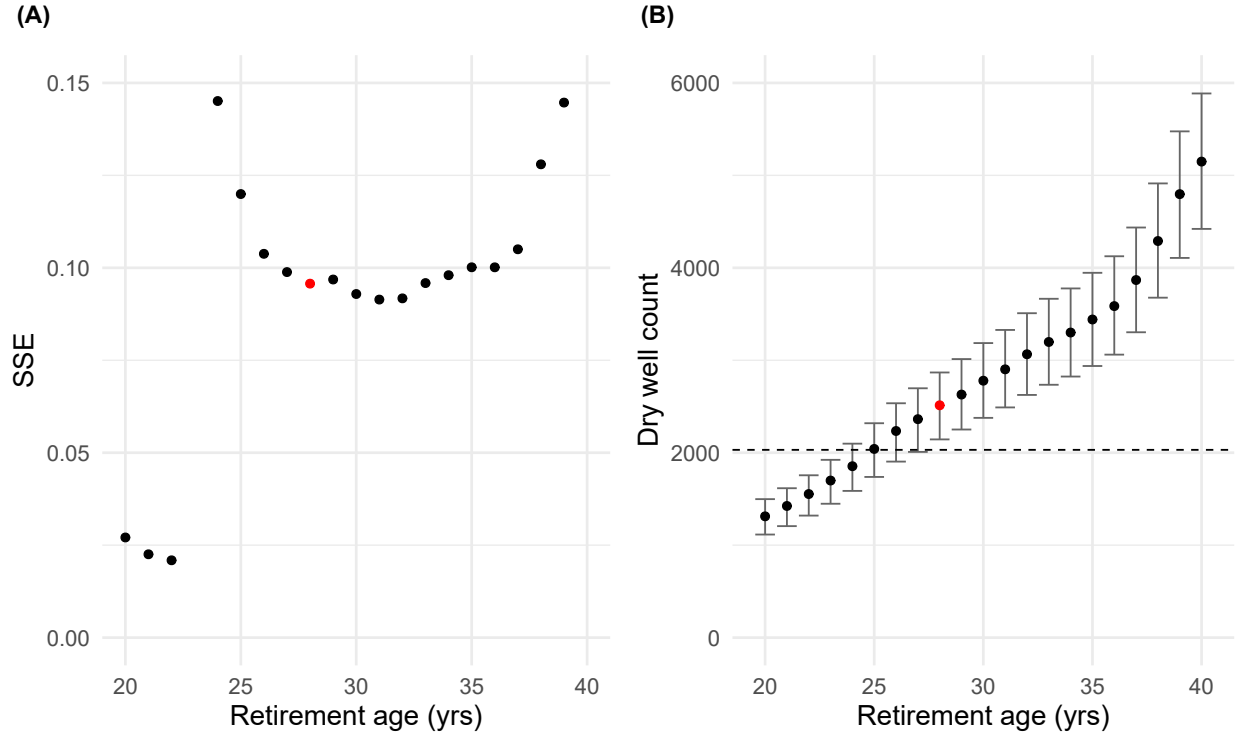


Figure 2.14: (A) Retirement age of domestic wells and associated SSE in the calibration spatial units. Low retirement ages remove too many wells from the model, resulting in unrealistically low SSE compared to a validation set. (B) Retirement age of domestic wells and associated count of failing wells during the 2012-2016 drought. The horizontal dashed black line shows the number of observed failing wells during the drought, constraining the feasible solution space to retirement ages of 25 years or greater. The red dot indicates the most reasonable model that balances low SSE, acceptable retirement age (28 years), and a compensation for well failure under-reporting. Error bars show the 5 and 95% confidence intervals of predicted well failures, computed by propagating uncertainty in pump location estimation and groundwater level estimation through the model.

One free parameter, the well retirement age (t_r) controls the number of wells active at time zero and thus the accuracy of the model. The optimum retirement age was determined by minimizing the sum of squared error (SSE) between the observed and predicted proportion of well

failure across all calibration units (Figure 2.14). Retirement ages from 20 to 40 years were tested, with the assumption that the true retirement age was within this range. SSE is calculated for the observed well failure *proportion* rather than the observed well failure *count*, because proportions are normalized by the total number of wells in each spatial unit. Thus, the error term weights all calibration units equally, and the calibration units with unusually low or high well counts do not exert excessive leverage.

Three-by-three blocks of PLSS townships (henceforth called aggregate-townships; length = 28.97 km , area = 839.16 km^2) were selected as the spatial units for calibration for two main reasons. First, since well failure reporting occurs at a county-level, calibration units must be at least this size, which the aggregate-township level achieves. Second, townships are meaningful units of spatial organization to planners and managers. We experimented with smaller calibration scales, such as the PLSS section (length = 1.61 km , area = 2.59 km^2), and PLSS township (length = 9.67 km , area = 93.24 km^2). However, small calibration spatial units suffer from high variance in prediction error: some spatial units show very low prediction error (e.g.- zero observed and zero predicted failures), while others show very high prediction error (e.g. - when a large difference between observed and predicted well failures exists). These differences are attributable to uncertainty in well failure reporting, well completion reporting, and groundwater level. A coarser calibration resolution at the aggregate-township (length = 28.97 km , area = 839.16 km^2) is less likely to contain spatial units with zero observations, and also averages the variance of observed failures at a larger scale, thus permitting spatially-explicit model validation at a coarser resolution. Small spatial units along the alluvial boundary edge less than 600 km^2 were removed in order to focus the calibration in regions representative of high well density.

To further control for uncertainty in the voluntary well failure reporting data, which we expect is more likely to be under-reported than not, only calibration units with observed failure ratios between the 25% and 95% percentiles were considered. Like well failure reporting, OSWCR reporting is also likely to under-count total domestic wells, thus only calibration units with well counts between the 25% and 95% percentiles were considered. Lastly, only aggregate-townships with at least 20 observed well failures were considered in the calibration. We select this threshold

because it represents approximately 1% of the roughly 2,000 observed well failures during the 2012-2016 drought. Eleven final aggregate-townships were selected to perform the calibration.

The well retirement age parameter ($t_r = 28$ years) led to the most reasonable model that balanced low SSE, and agreed with the mean retirement age for domestic wells in the CV found by Gailey et al., 2019. The 2,027 observed failures during the 2012-2016 drought imposes a hard constraint on feasible retirement ages equal to or greater than 25 years, because under this value, the predicted well failure count is less than the observed well failure count (Figure 2.14B). Low retirement ages (20-22 yrs) removed too many wells from the model, resulting in unrealistically low well failure count, (Figure 2.14A), and high retirement ages (37-40 yrs) left too many wells in the model, which led to high SSE and an unrealistically large number of well failures (greater than observed during the 2012-2016 drought).

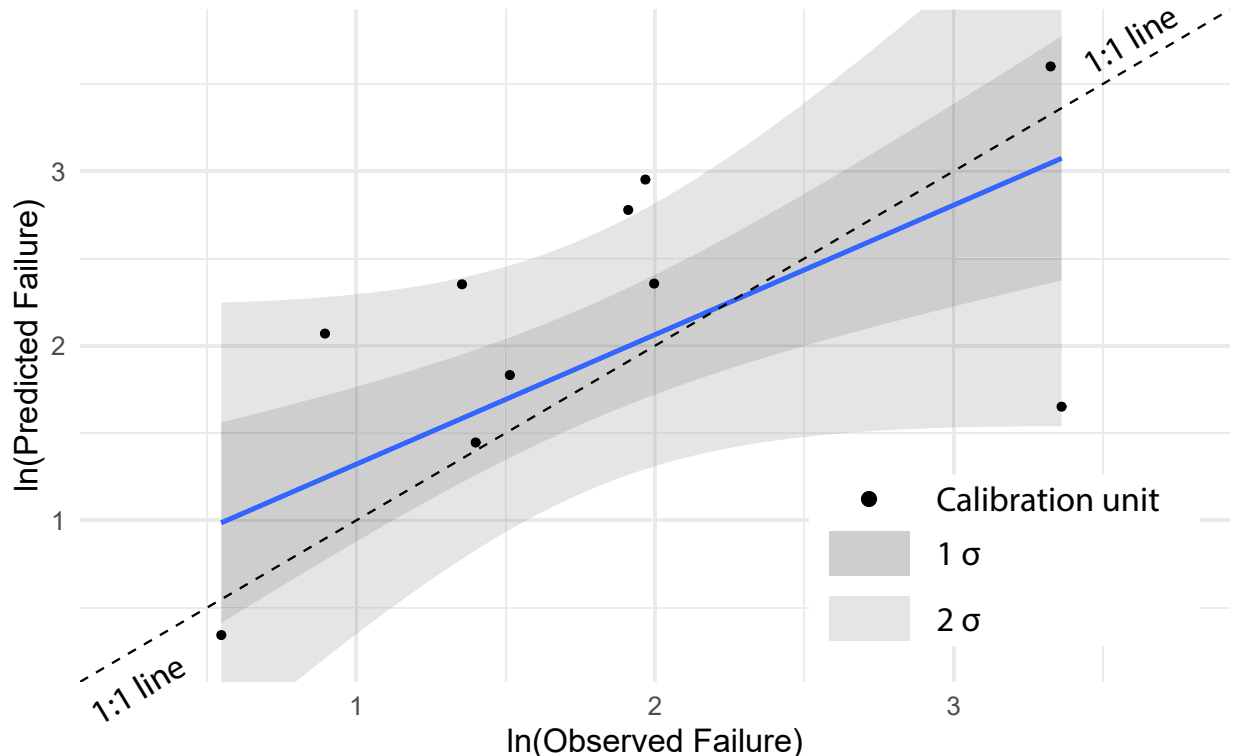


Figure 2.15: Predicted vs. observed log failure ratio for the 11 calibration spatial units.

The fit between observed and predicted calibration units suggests relatively high local-scale

error, with four calibration units falling more than 2 standard deviations from the least squares line through the observed and predicted scatter plot (Figure 2.15). These discrepancies are the product of uncertainty in well failure reporting, well completion reporting, groundwater level, and model formulation. As the failure model is subject to local error it is best interpreted as a regional-scale domestic well failure estimate.

Table 2.2: Domestic well failure counts under different groundwater management regimes (Sustainable, Glide path, and Business as usual).

scenario	mean failure count	5% CI failure count	95% CI failure count
<i>Sustainable</i>			
1998-2017	1516	1248	1809
2003-2017	2000	1619	2412
2008-2017	2513	2200	2914
<i>Glide path</i>			
1998-2017	3677	3359	4039
2003-2017	4929	4509	5361
2008-2017	6943	6501	7417
<i>Business as usual</i>			
1998-2017	5966	5650	6293
2003-2017	7677	7239	8092
2008-2017	10466	10087	10885

The mean failure count corresponds to the number of wells failing when the mean pump depth is used. Well failures at the 5% confidence interval (CI) and 95% CI correspond to uncertainty in the estimated pump location. Hydrologic uncertainty in groundwater level is accounted for by considering three different linear approximations of groundwater level decline, beginning in 1998, 2003, and 2008.

2.8 Acknowledgments

We thank the Governor’s Office of Planning and Research and the California Department of Water Resources for their assistance in acquiring domestic well failure, and well completion report data. Thomas Harter, Darcy Bostic, and Nisha Marwaha provided modeling advice and assistance. The West Big Data Hub has helped disseminate this research. Financial support was provided by the National Science Foundation (NSF) Climate Change, Water, and Society (CCWAS) Integrated Graduate Education and Research Traineeship (IGERT) program at the University of California, Davis (<http://ccwas.ucdavis.edu>, DGE-10693333), and the University of California Water (UC Water) Security and Sustainability Research Initiative.

2.9 Data availability

The data that support the findings of this study are openly available. These data(Pauloo et al., 2019) do not include observed well failure data (CA-OPR, 2018), which are confidential and must be obtained by contacting the California Department of Water Resources.

2.10 References

- Ahuja, S. (2008). *Arsenic Contamination of Groundwater: Mechanism, Analysis, and Remediation*. John Wiley & Sons, Inc.
- Ayuso-Gabella, N., Page, D., Masciopinto, C., Aharoni, A., Salgot, M., & Wintgens, T. (2011). Quantifying the effect of managed aquifer recharge on the microbiological human health risks of irrigating crops with recycled water. *Agricultural Water Management*, 99(1), 93–102. doi:10.1016/j.agwat.2011.07.014
- Balazs, C., Morello-Frosch, R., Hubbard, A., & Ray, I. (2011). Social disparities in nitrate-contaminated drinking water in California's San Joaquin Valley. *Environmental Health Perspectives*, 119(9), 1272–1278.
- Bertoldi, G. L., Johnston, R. H., & Evenson, K. D. (1991). *Ground water in the Central Valley, California; a summary report* (tech. rep. No. 1401-A). USGS. USGS.
- Brush, C. F., Dogrul, E. C., & Kadir, T. N. (2013). *Development and calibration of the California central valley groundwater-surface water simulation model (c2vsim), version 3.02-cg*. Sacramento, CA: Bay-Delta Office, California Department of Water Resources.
- California Department of Water Resources. (2016). *Hydroclimate Report Water Year 2016*. Office of the State Climatologist.
- Cismowski, G., Cooley, W., Grober, L. S., Martin, J., McCarthy, M., Schnagl, R. S., & Toto, A. (2006). *Salinity in the Central Valley: An Overview. Report of the Regional Water Quality Control Board, Central Valley Region, California Environmental Protection Agency* (tech. rep. No. 206). Central Valley Regional Water Quality Control Board. Rancho Cordova, California.
- Cook, B. I., Ault, T. R., & Smerdon, J. E. (2015). Unprecedented 21st century drought risk in the American Southwest and Central Plains. *Science Advances*, 1(1), e1400082.
- Dahlke, H., Brown, A., Orloff, S., Putnam, D., O'Geen, T., et al. (2018). Managed winter flooding of alfalfa recharges groundwater with minimal crop damage. *California Agriculture*, 72(1), 65–75.
- Deutsch, C. V. & Journel, A. G. (1998). *GSLIB: Geostatistical software library and user's guide (2nd ed)*. Oxford Univ. Press, New York.
- Dieter, C., Linsey, K., Caldwell, R., Harris, M., Ivahnenko, T., Lovelace, J., ... Barber, N. (2018). Estimated use of water in the United States county-level data for 2015 (ver. 2.0, June 2018): US Geological Survey data release. Available at: <https://www.sciencebase.gov/catalog/item/get/5af3311be4b0da30c1b245d8> [Accessed July 1, 2019]. doi:10.3133/cir1441
- Diffenbaugh, N. S., Swain, D. L., & Touma, D. (2015). Anthropogenic warming has increased drought risk in California. *Proceedings of the National Academy of Sciences*, 112(13), 3931–3936.
- Döll, P., Hoffmann-Dobrev, H., Portmann, F. T., Siebert, S., Eicker, A., Rodell, M., ... Scanlon, B. R. (2012). Impact of water withdrawals from groundwater and surface water on continental water storage variations. *Journal of Geodynamics*, 59, 143–156.
- CA-DWR. (2017a). *Fall 2017 Groundwater Level Data Summary*. Department of Water Resources. Retrieved from <https://water.ca.gov/-/media/DWR-Website/Web-Pages/Programs/Groundwater-Management/Data-and-Tools/Files/Statewide-Reports/Fall-2017-Groundwater-Level-Data-Summary.pdf>
- CA-DWR. (2017b). *Hydroclimate Report Water Year 2017*. Office of the State Climatologist.

- CA-DWR. (2018). California Online State Well Completion Report Database. Available at: <https://data.cnra.ca.gov/dataset/well-completion-reports> [Accessed January 1, 2018].
- CA-DWR. (2019). Groundwater Information Center. Available at: <https://gis.water.ca.gov/app/gicima/> [Accessed May 8, 2018].
- Ellis, A. S., Johnson, T. M., & Bullen, T. D. (2002). Chromium isotopes and the fate of hexavalent chromium in the environment. *Science*, 295(5562), 2060–2062.
- Famiglietti, J. S. (2014). The global groundwater crisis. *Nature Climate Change*, 4(11), 945–948.
- Faunt, C., Hanson, R. T., Belitz, K., Schmid, W., Predmore, S. P., Rewis, D. L., & McPherson, K. (2009). *Groundwater availability of the Central Valley Aquifer, California, US Geological Survey Professional Paper* (tech. rep. No. 1766). USGS. doi:[10.3133/pp1766](https://doi.org/10.3133/pp1766)
- Feinstein, L., Phurisamban, R., Ford, A., Tyler, C., & Crawford, A. (2017). *Drought and Equity in California Drought and Equity in California*. Pacific Institute.
- Fujii, R. & Swain, W. C. (1995). *Areal distribution of selected trace elements, salinity, and major ions in shallow ground water, Tulare Basin, southern San Joaquin Valley, California*. Water-Resour. Investig. Rep. 95-4048. USGS.
- Gailey, R. M. (2017). Inactive supply wells as conduits for flow and contaminant migration: Conditions of occurrence and suggestions for management. *Hydrogeology Journal*, 25(7), 2163–2183.
- Gailey, R. M., Lund, J. R., & Medellin-Azuara, J. (2019). Domestic well reliability: Evaluating supply interruptions from groundwater overdraft, estimating costs and managing economic externalities. *Hydrogeology Journal*, 27(4), 1159–1182.
- Greene, C. (2018). Broadening understandings of drought – The climate vulnerability of farm-workers and rural communities in California (USA). *Environmental Science and Policy*, 89(August), 283–291. doi:[10.1016/j.envsci.2018.08.002](https://doi.org/10.1016/j.envsci.2018.08.002)
- Hanak, E., Escriva-Bou, A., Gray, B., Green, S., Harter, T., Jezdimirovic, J., ... Seavy, N. (2019). *PPIC: Water and the Future of the San Joaquin Valley* (tech. rep. No. February). Public Policy Institute of California.
- Hanak, E., Lund, J., Dinar, A., Gray, B., & Howitt, R. (2011). *Managing California's Water: From Conflict to Reconciliation*. San Francisco, CA: Public Policy Institute of California.
- Harbaugh, A. W., Banta, E. R., Hill, M. C., & McDonald, M. G. (2000). *MODFLOW-2000, The U.S. Geological Survey Modular Ground-Water Model—User Guide to Modularization Concepts and the Ground-Water Flow Process, Open-file Report 00-92*. USGS. Reston, Virginia: USGS.
- Harter, T. (2003). *Water well design and construction* (tech. rep. No. 8086). University of California Division of Agriculture and Natural Resources. Oakland, CA.
- Harter, T. & Lund, J. R. (2012). *Addressing nitrate in California's drinking water: With a focus on tulare lake basin and salinas valley groundwater: Report for the state water resources control board report to the legislature*.
- Helweg, O., Scott, V., & Scalmanini, J. (1983). *Improving pump and well efficiency*. Denver, CO: American Water Works Association.
- James, G., Witten, D., Hastie, T., & Tibshirani, R. (2013). *An introduction to statistical learning*. Springer.
- Johnson, T. D. & Belitz, K. (2015). Identifying the location and population served by domestic wells in California. *Journal of Hydrology: Regional Studies*, 3, 31–86.

- Johnson, T. D. & Belitz, K. (2017). Domestic well locations and populations served in the contiguous US: 1990. *Science of The Total Environment*, 607, 658–668.
- Journel, A. G. & Huijbregts, C. J. (1978). *Mining geostatistics*. London: Academic press.
- Jurgens, B. C., Burow, K. R., Dalgish, B. A., & Shelton, J. L. (2008). *Hydrogeology, water chemistry, and factors affecting the transport of contaminants in the zone of contribution of a public-supply well in Modesto, eastern San Joaquin Valley, California* (tech. rep. No. 2008-5156). USGS. doi:[10.3133/sir20085156](https://doi.org/10.3133/sir20085156)
- Kocis, T. N. & Dahlke, H. E. (2017). Availability of high-magnitude streamflow for groundwater banking in the central valley, California. *Environmental Research Letters*, 12(8), 084009.
- Laurent, A. G. (1963). The lognormal distribution and the translation method: Description and estimation problems. *Journal of the American Statistical Association*, 58(301), 231–235.
- Lobell, D. B., Torney, A., & Field, C. B. (2011). Climate extremes in California agriculture. *Climatic Change*, 109(1), 355–363. doi:[10.1007/s10584-011-0304-5](https://doi.org/10.1007/s10584-011-0304-5)
- London, J., Fencl, A., Watt, S., Jarin, J., Aranda, A., King, A., ... Introduction, A. (2018). *The Struggle for Water Justice in California's San Joaquin Valley : A Focus on Disadvantaged Unincorporated Communities*. UC Davis Center for Regional Change.
- Lund, J., Medellin-Azuara, J., Durand, J., & Stone, K. (2018). Lessons from California's 2012–2016 drought. *Journal of Water Resources Planning and Management*, 144(10), 04018067.
- Maples, S., Fogg, G., & Maxwell, R. (2019). Modeling Managed Aquifer Recharge Processes in a Highly-Heterogeneous, Semi-Confining Aquifer System. *Hydrogeology Journal*, 27, 2869–2888. doi:[10.1007/s10040-019-02033-9](https://doi.org/10.1007/s10040-019-02033-9)
- Medellin-Azuara, J., MacEwan, D., Howitt, R. E., Sumner, D. A., Lund, J. R., Scheer, J., ... Arnold, B. (2016). *Economic Analysis of the 2016 California Drought on Agriculture: A report for the California Department of Food and Agriculture*. Center for Watershed Sciences, University of California Davis. Davis, CA.
- Mitchell, D., Hanak, E., Baerenklau, K., Escriva-Bou, A., Mccann, H., Pérez-Urdiales, M., & Schwabe, K. (2017). *Building Drought Resilience in California's Cities and Suburbs*. Public Policy Institute of California. doi:[10.13140/RG.2.2.12398.41288](https://doi.org/10.13140/RG.2.2.12398.41288)
- Mount, J., Hanak, E., Baerenklau, K., Butsic, V., Chappelle, C., Escriva-bou, A., ... Moyle, P. (2018). *Managing Drought in a Changing Climate: Four Essential Reforms*. Public Policy Institute of California.
- O'sullivan, D. & Unwin, D. (2010). *Geographic information analysis* (2nd). John Wiley & Sons.
- CA-OPR. (2018). Observed domestic well failures during 2012-2016 drought dataset. Obtained via an agreement with the California Governor's Office of Planning and Research. [Accessed May 6, 2018]. Department of Water Resources, the California Governor's Office of Planning, and Research.
- Pauloo, R., Dahlke, H., Escriva-Bou, A., Fencl, A., Fogg, G. E., & Guillon, H. (2019). Domestic Well Vulnerability to Drought Duration and Unsustainable Groundwater Management in California's Central Valley. UC Davis, Dataset, <https://doi.org/10.25338/B8Q31D>.
- Perrone, D. & Jasechko, S. (2017). Dry groundwater wells in the western United States. *Environmental Research Letters*, 12(10), 104002.
- Perrone, D. [Debra] & Jasechko, S. [Scott]. (2019). Deeper well drilling an unsustainable stopgap to groundwater depletion. *Nature Sustainability*, 2(8), 773–782.

- Ransom, K. M., Nolan, B. T., A. Traum, J., Faunt, C. C., Bell, A. M., Gronberg, J. A. M., ... Harter, T. (2017). A hybrid machine learning model to predict and visualize nitrate concentration throughout the Central Valley aquifer, California, USA. *Science of the Total Environment*, 601-602, 1160–1172. doi:[10.1016/j.scitotenv.2017.05.192](https://doi.org/10.1016/j.scitotenv.2017.05.192)
- Rhoades, A. M., Jones, A. D., & Ullrich, P. A. (2018). The Changing Character of the California Sierra Nevada as a Natural Reservoir. *Geophysical Research Letters*, 45(23), 13–008.
- Robertson, F. N. (1991). *Geochemistry of ground water in alluvial basins of Arizona and adjacent parts of Nevada, New Mexico, and California, USGS Professional Paper 1406-C*. USGS. USGS.
- Scanlon, B. R., Faunt, C. C., Longuevergne, L., Reedy, R. C., Alley, W. M., McGuire, V. L., & McMahon, P. B. (2012). Groundwater depletion and sustainability of irrigation in the US High Plains and Central Valley. *Proceedings of the national academy of sciences*, 109(24), 9320–9325.
- Siebert, S., Burke, J., Faures, J.-M., Frenken, K., Hoogeveen, J., Döll, P., & Portmann, F. T. (2010). Groundwater use for irrigation—a global inventory. *Hydrology and earth system sciences*, 14(10), 1863–1880.
- Sophocleous, M. (2000). From safe yield to sustainable development of water resources—the kansas experience. *Journal of Hydrology*, 235(1-2), 27–43.
- Stedinger, J. R. (1980). Fitting Log Normal Distributions to Hydrological Data. *Water Resources Research*, 16(3), 481–490. doi:[10.1029/WR016i003p00481](https://doi.org/10.1029/WR016i003p00481)
- Stoyan, D. & Stoyan, H. (1994). *Fractals, random shapes, and point fields: Methods of geometrical statistics*. John Wiley & Sons Inc.
- Sustainable Groundwater Management Act, California Water Code sec. 10720-10737.8. (2014). California State Water Resources Control Board.
- Swain, D. L., Langenbrunner, B., Neelin, J. D., & Hall, A. (2018). Increasing precipitation volatility in twenty-first-century California. *Nature Climate Change*, 8(5), 427.
- Tebaldi, C., Hayhoe, K., Arblaster, J. M., & Meehl, G. A. (2006). Going to the extremes. *Climatic Change*, 79(3-4), 185–211. doi:[10.1007/s10584-006-9051-4](https://doi.org/10.1007/s10584-006-9051-4)
- Theis, C. V. (1935). The relation between the lowering of the piezometric surface and the rate and duration of discharge of a well using ground-water storage. *Eos, Transactions American Geophysical Union*, 16(2), 519–524.
- Theis, C. V. (1940). The source of water derived from wells. *Civil Engineering*, 10(5), 277–280.
- Tullis, J. P. (1989). *Hydraulics of pipelines: Pumps, valves, cavitation, transients*. John Wiley & Sons.
- US Census American Housing Survey. (2017). Available at: <https://www.census.gov/programs-surveys/ahs/data.html> [Accessed May 8, 2018].
- USDOI. (2009). *Manual of surveying instructions: For the survey of the public lands of the united states*. US Department of the Interior. Denver, CO: Government Printing Office Bureau of Land Management.
- Van Loon, A. F., Gleeson, T., Clark, J., Van Dijk, A. I., Stahl, K., Hannaford, J., ... Uijlenhoet, R., et al. (2016). Drought in the Anthropocene. *Nature Geoscience*, 9(2), 89–91. doi:[10.1038/ngeo2646](https://doi.org/10.1038/ngeo2646), 2016.

- Varouchakis, E., Hristopulos, D., & Karatzas, G. (2012). Improving kriging of groundwater level data using nonlinear normalizing transformations—a field application. *Hydrological Sciences Journal*, 57(7), 1404–1419.
- Wada, Y., Van Beek, L. P., Van Kempen, C. M., Reckman, J. W., Vasak, S., & Bierkens, M. F. (2010). Global depletion of groundwater resources. *Geophysical research letters*, 37(20).
- Welch, A., Westjohn, D., Helsel, R., & Wanty, R. (2000). Arsenic in Ground Water of the United States: Occurrence and Geochemistry. *Ground Water*, 38, 589–604. doi:doi.org/10.1111/j.1745-6584.2000.tb00251.x
- Xanke, J., Liesch, T., Goeppert, N., Klinger, J., Gassen, N., & Goldscheider, N. (2017). Contamination risk and drinking water protection for a large-scale managed aquifer recharge site in a semi-arid karst region, Jordan. *Hydrogeology Journal*, 25(6), 1795–1809. doi:[10.1007/s10040-017-1586-0](https://doi.org/10.1007/s10040-017-1586-0)
- Xiao, M., Koppa, A., Mekonnen, Z., Pagán, B. R., Zhan, S., Cao, Q., ... Lettenmaier, D. P. (2017). How much groundwater did California's Central Valley lose during the 2012–2016 drought? *Geophysical Research Letters*, 44(10), 4872–4879.

Chapter 3

Anthropogenic Basin Closure and Groundwater Salinization (ABCSAL).¹

3.1 Abstract

Global food systems rely on irrigated agriculture, and most of these systems in turn depend on fresh sources of groundwater. In this study, we demonstrate that groundwater development, even without overdraft, can transform a fresh, open basin into an evaporation dominated, closed-basin system, such that most of the groundwater, rather than exiting via stream baseflow and lateral subsurface flow, exits predominantly by evapotranspiration from irrigated lands. In these newly closed hydrologic basins, just as in other closed basins, groundwater salinization is inevitable because dissolved solids cannot escape, and the basin is effectively converted into a salt sink. We first provide a conceptual model of this process, called “**A**nthropogenic **B**asin **C**losure and groundwater **S**ALinization” (ABCSAL). We examine the temporal dynamics of ABCSAL using the Tulare Lake Basin, California, as a case study for a large irrigated agricultural region with Mediterranean

¹This chapter has been submitted to *Journal of Hydrology*: Pauloo, R. A., Fogg, G. E., Guo, Z., & Harter, T. “Anthropogenic Basin Closure and Groundwater Salinization (ABCSAL)”. (Preprint 10.1002/essoar.10502733.1)

climate, overlying an unconsolidated sedimentary aquifer system. Even with modern water management practices that arrest historic overdraft, results indicate that shallow aquifers (36 m deep) exceed maximum contaminant levels for total dissolved solids on decadal timescales. Intermediate (132 m) and deep aquifers (187 m), essential for drinking water and irrigated crops, are impacted within two to three centuries. Hence, ABCSAL resulting from groundwater development constitutes a largely unrecognized constraint on groundwater sustainable yield on similar timescales to aquifer depletion in the Tulare Lake Basin, and poses a serious challenge to groundwater quality sustainability, even when water levels are stable. Results suggest that agriculturally intensive groundwater basins worldwide may be susceptible to ABCSAL.

3.2 Introduction

Groundwater from major aquifer systems supplies 43% of the world's irrigation water (Siebert et al., 2010). As a result of excessive groundwater development and land use change, groundwater quantity and quality in these agriculturally intensive groundwater basins has been significantly impacted. Numerous global and regional studies document aquifer depletion related to agricultural withdrawal (Brush, Dogrul, & Kadir, 2013; Döll et al., 2012; Famiglietti, 2014; Faunt et al., 2009; Gleeson, Wada, Bierkens, & van Beek, 2012; Russo & Lall, 2017; Bridget R Scanlon et al., 2012; Siebert et al., 2010; Vörösmarty, Green, Salisbury, & Lammers, 2000; Wada, Wisser, & Bierkens, 2014). Anthropogenic contaminants to groundwater include nitrates, which originate from agricultural fertilizers (Burow, Shelton, & Dubrovsky, 2008), pesticides (Burow et al., 2008; Burow, Stork, & Dubrovsky, 1998), and animal farming (Harter & Lund, 2012). Groundwater pumping may even mobilize naturally-occurring contaminants such as arsenic (Winkel et al., 2011; Smith, Knight, & Fendorf, 2018) and uranium (Jurgens, Burow, Dalgish, & Shelton, 2008; Jurgens, Fram, Belitz, Burow, & Landon, 2010).

Another class of groundwater contaminants are total dissolved solids (TDS), also referred to as salts or salinity. TDS are sourced both naturally (e.g., produced by rock-water interactions) and anthropogenically (e.g., imported by surface water for irrigation). Elevated TDS is an indicator

of human impact on freshwater systems (Ayers, Westcot, & W, 1985; Kaushal, McDowell, & Wollheim, 2014), and reduces agricultural productivity (Lopez-Berenguer, Martinez-Ballesta, Moreno, Carvajal, & Garcia-Viguera, 2009; Munns, 2002; Pessarakli, 2016), which has prompted states to set agricultural irrigation water quality goals, (e.g., 450 mg/L in California) (CSWRCB, 2019a). For drinking water, the United States Environmental Protection Agency and the state of California recommend a secondary maximum contaminant level of 500 mg/L TDS (CSWRCB, 2019b, 2019a). Water high in TDS may exhibit discoloration, unpleasant odor and taste, and may be unsuitable for human consumption or irrigation (Hem, 1985). Fresh water is defined as containing TDS less than 1,000 mg/L, brackish water ranges from 1,000 to 10,000 mg/L, and saline water ranges from 10,000 to 100,000 mg/L (Fetter, 2001).

Groundwater salinization is widely studied (Greene, Timms, Rengasamy, Arshad, & Cresswell, 2016) in terms of (1) seawater intrusion (Bear, Cheng, Sorek, Ouazar, & Herrera, 1999; Werner et al., 2013), (2) naturally-occurring salinization in closed surface-water basins (i.e., endorheic basins and playas) (Eugster & Hardie, 1978; Hardie & Eugster, 1970), (3) high water tables causing groundwater evaporation and soil salinization via capillary rise (Datta & De Jong, 2002; Barrett-Lennard, 2003; Chaudhuri & Ale, 2014; Hillel, 1992), and (4) soil salinization due to irrigation (Blaine Hanson, Grattan, & Fulton, 1999; Bernstein & Francois, 1973; Hillel, 2000). This study describes a fifth type of groundwater salinization that remains largely unexplored: salinization of an entire groundwater basin created by historically excessive pumping, then sustained by the inability of a closed groundwater system to discharge salts. Henceforth, we refer to this fifth type as “**Anthropogenic Basin Closure and groundwater SALinization**” (ABCSAL).

This fifth type of salinization, ABCSAL, is related to naturally-occurring closed basin salinization (case (2) above), but has significantly different phenomenology. It is therefore useful to first consider the difference between an open, fresh hydrologic basin, and a naturally closed, saline basin.

An open, fresh groundwater basin has sufficient natural outlets for TDS, such as baseflow to streams and lateral subsurface flow across basin boundaries, which maintains a balance between salinity that is naturally generated within the basin (i.e., mineral dissolution) and salinity that is

exported out of the basin. Basins containing fresh groundwater exist only because they have outlets for both the circulating groundwater and the dissolved salts therein, originating from intrabasin rocks and sediments (Domenico, Schwartz, et al., 1998).

In contrast, closed hydrologic basins – common in arid to semiarid regions worldwide – naturally form when (a) outflow by surface water or groundwater flows is absent or small, and (b) evaporation is the dominant mechanism by which water exits the basin (Hardie & Eugster, 1970; Eugster & Hardie, 1978; Jones & Deocampo, 2003). Because TDS concentrations in precipitation are low (around 10^1 mg/L), most TDS originates from rock-water reactions in surface runoff and in the subsurface. Salts may accumulate at the evaporative boundaries of the basin: at or immediately below the surface where discharging groundwater evaporates or at the bottom of a surface depression in terminal and sometimes ephemeral lakes that collect runoff, baseflow, and spring outflow (Wooding, Tyler, & White, 1997; Richter & Kreitler, 1986). Examples of naturally closed hydrologic basins with saline features at or near the land surface are found worldwide: playas and salt flats such as those in the Great Basin (USA) and Salar de Uyuni (Bolivia); saline lakes like the Great Salt Lake (USA) and the Dead Sea (Middle east); in extremely arid deserts such as the Arabian and Atacama; and in the unsaturated subsurface of semi-arid regions with insufficient precipitation to recharge groundwater (Bridget R. Scanlon, Tyler, & Wierenga, 1997; Kreitler, 1993).

In this paper, we argue that sufficient groundwater development can lower groundwater levels in an open to semi-open and relatively fresh basin, thus converting it into a closed basin, which then salinates in a distinctly different manner from those described in (1) - (4). First, moderate to large amounts of groundwater development may result in sufficient reduction of groundwater levels that reduce or eliminate natural baseflow to streams (Russo & Lall, 2017; Barlow & Leake, 2015; Hunt, 1999) and reverse existing groundwater gradients at subsurface outflow boundaries (Figure 3.1A). Progressively greater closed basin conditions diminish and eventually entirely eliminate natural TDS export from the groundwater basin (Figure 3.1B). Furthermore, if the basin is irrigated, crop evapotranspiration becomes the dominant water outflow from the basin, leaving behind salts that are returned to the groundwater basin via irrigation return flows and recharge

from precipitation. Across the globe, water level stabilization in such overdrafted basins is sometimes achieved by importing additional surface water. However, water imports can add significant salt to the basin. Moreover, even when balancing the water budget with imported water, this does not stop the ABCSAL process if groundwater does not have exits (e.g., baseflow to streams or lateral subsurface outflow), and if water continues to leave the basin predominantly through evapotranspiration, which leaves behind salts. Although these latter two conditions are similar to those in a naturally closed basin (2) (Hardie & Eugster, 1970; Jones & Deocampo, 2003), vertical groundwater fluxes under ABCSAL are in the opposite direction from natural basin salinization and thus, the location of salinization is different. In a naturally closed basin, salinization occurs at the land surface due to upward groundwater discharge. Under ABCSAL, pumping and recharge from irrigation lead to a net downward flux, then mobilize salts left behind by irrigated crops downward into the production zone of the groundwater basin, before they are recycled by pumping wells to the land surface and the process repeats.

Importantly, we point out that the long-term continuous decline of groundwater storage is not a necessary condition for ABCSAL. Rather, even in basins where groundwater levels are stable and hence assumed to be free of overdraft, as long as they remain physically closed, they will saline. Furthermore, although for simplicity we describe basins as either “open” or “closed”, in reality, closure ranges from 0-100 % (i.e., fully open to fully closed), and gradations of basin closure exist, which impact the rate of salinization and hence, the long-term temporal and vertical spatial salt distribution. Except for the most extremely exploited aquifers (one of which we explore in this study), many aquifers will fall somewhere between fully open to fully closed and not exactly at one extreme.

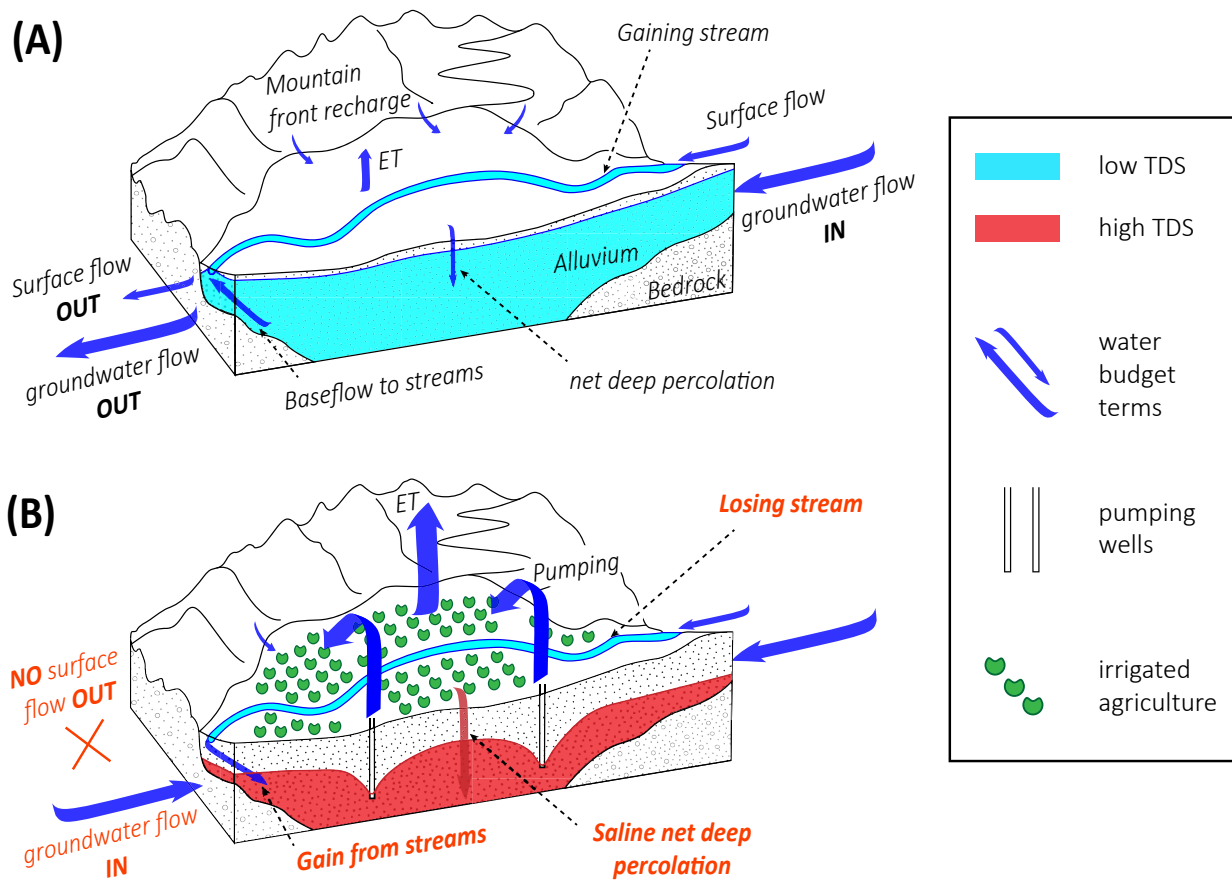


Figure 3.1: Conceptual model of ABCSAL. (A) Open basin, pre-groundwater development: surface and groundwater systems connect. Groundwater discharges dissolved solids into surface water which exits the basin. Groundwater at this stage is predominantly fresh (e.g., < 1,000 mg/L). (B) Closed basin: groundwater pumping causes elimination of baseflow to streams. Lower groundwater levels cause subsurface inflow to drain adjacent basins. Pumped groundwater is concentrated by evapotranspiration (ET) when applied for irrigation. Salts migrate into the production zone of the aquifer, driven by vertical hydraulic gradients from recharge and pumping. Although these figures show two extremes (open and closed), partially-closed basins also exist.

In this research, we illustrate the development of ABCSAL in a historically open, freshwater basin using the agriculturally intensive Tulare Lake Basin (TLB) in California's southern Central Valley as a case study. Previous research in the TLB has shown evidence of salt accumulation in groundwater via simple water and salt budgets (Schmidt, 1975), and shallow aquifer

salt accumulation from sediment dissolution processes in highly-soluble calcium and magnesium carbonates and sulfates (Schoups et al., 2005). Other studies have shown that TDS concentrations in TLB groundwater have increased over the last century (Hansen, Jurgens, & Fram, 2018; Lindsey & Johnson, 2018), and suggested this is the result of pumping for municipal and irrigation supply which has caused shallow, higher TDS groundwater to be driven downward into deeper aquifers. We are not aware of prior work that has placed these trends into the context of ABCSAL, or quantified potential rates of salinization across a range of aquifer depths and timescales.

Our aim in this study is to assess the first order salt balance and timescales over which the TLB as a large production aquifer system becomes regionally degraded over most of the vertical extent of its nearly 200 *m* thick main production zone. We conservatively assume that, under recent state regulation, groundwater overdraft is arrested, but not reversed. We compare timescales of ABCSAL degradation against the estimated lifespan of the greater Central Valley aquifer (i.e., 390 years at historical overdraft rates) (Faunt et al., 2009), challenge the notion that the depletion of groundwater storage is a more urgent issue than the degradation of groundwater quality in the TLB (and in other basins with ABCSAL conditions), and consider the water management implications and the steps required to reverse extensive basin-scale groundwater salinization. The management would likely involve both hydrologic opening of the basin to provide natural outlets for salt, a reduction of sources of salinity, and the development of regional groundwater quality management models (Fogg & LaBolle, 2006; CRWQCB, 2018). The adaptation might involve the eventual desalination of most groundwater pumped from the basin, producing a future economic burden that should be anticipated and evaluated, as it bears on the security of water, food, and energy resources.

This paper is organized as follows: first, we describe the hydrogeology, water budget, and water quality of the study site. Then we describe and justify our approach involving a simple 1D mixing cell solute transport model. Next, we present our results, and finally, we discuss the implications of the research, the limitations of our approach, and the extensibility of the study to other areas.

3.3 Methods

3.3.1 Study area

In selecting the TLB as our study site, we looked for (1) a history of intensive groundwater pumping and irrigation, (2) availability of historical water budget and water quality data, and (3) social and economic significance. The TLB (Figure 3.2) occupies the southern third of the Central Valley, California and is bounded by the Coast Ranges to the west, the Tehachapi Mountains to the south, and the southern Sierra Nevada to the east. Geology strongly influences dissolved solid concentrations in the clastic sedimentary aquifer system composed of fluvial and alluvial fan deposits. Calcium and magnesium sulfates and carbonates in Coast Range sediment in the western TLB are more soluble than sediments from the predominately crystalline rocks of the Sierra Nevada to the east, thus the groundwater in the western basin tends to have higher TDS (Fujii & Swain, 1995; K. R. Belitz & Heimes, 1990; Deverel & Millard, 1988). Fresh groundwater in the TLB spans depths from land surface to around 1,000 m where brackish water and marine deposits limit the development of groundwater resources (DeSimone, MacMahon, & Rosen, 2010; Kang & Jackson, 2016). Above this deep brackish zone is a major freshwater aquifer system. In combination with a natural endowment of significant, but intermittent runoff from surrounding uplands, abundant fresh groundwater has transformed the TLB into one of the most heavily irrigated and economically productive agricultural regions in the world (Hanak, Lund, Dinar, Gray, & Howitt, 2011). At its peak in the 1980s, approximately 14,164 km^2 of its 44,110 km^2 were irrigated (TNC, 2014). Today roughly 12,140 km^2 remain irrigated, with a total gross value of all agricultural crops and products at \$23.4 billion USD in 2017 (Fankhauser, 2018; Hook, 2018; L. Wright, 2018; M. Wright, 2018).

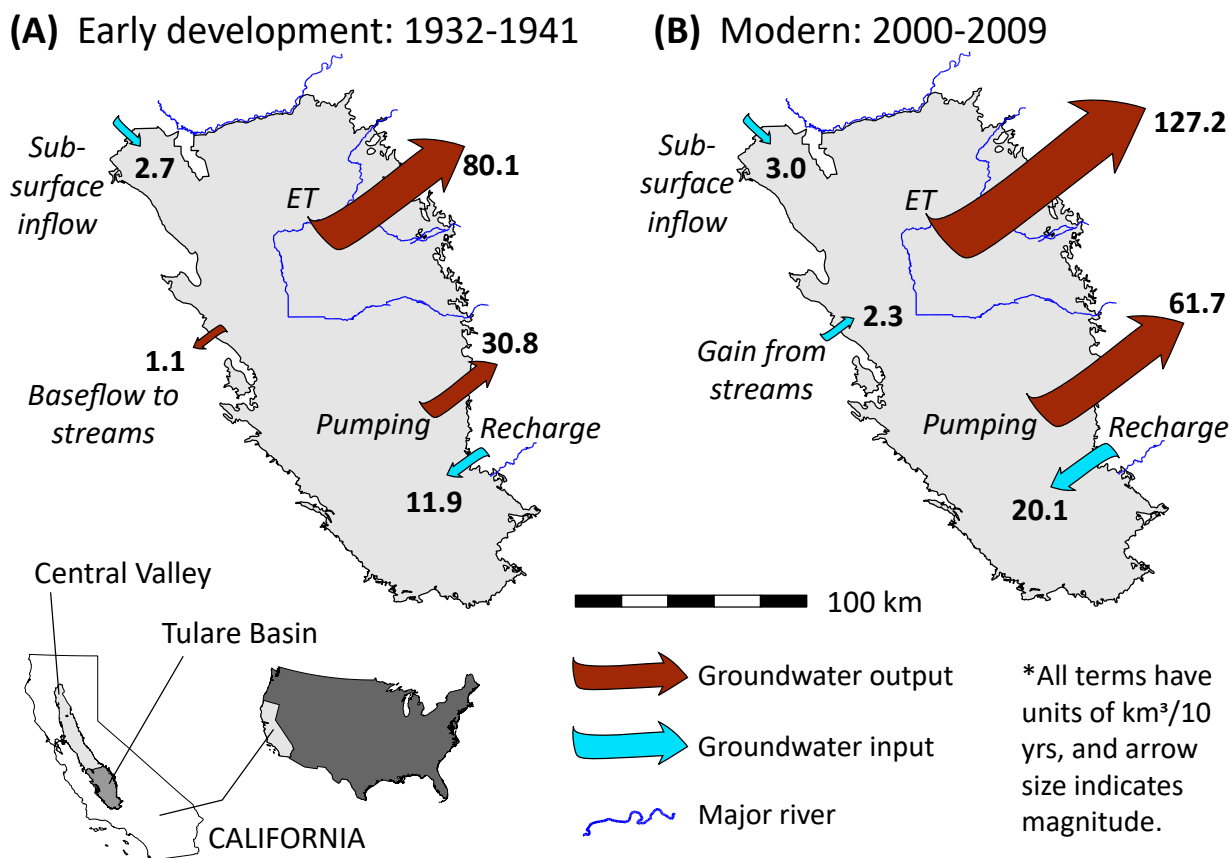


Figure 3.2: The TLB overlies an agriculturally intensive sedimentary aquifer in California's southern Central Valley. Significant changes are observed in selected decadal hydrologic year water budget terms derived from C2VSim at (A) early-groundwater-development (not to be confused with pre-groundwater-development) and (B) post-groundwater-development timescales in the TLB. Notably, gaining streams transition to losing streams, and increases are observed in pumping, evapotranspiration (ET), and recharge (from diversions and natural sources, like streams, lakes, and watersheds). All terms are aggregated at the scale of the TLB, except for subsurface inflow, which is calculated at the northern TLB boundary. Note that this is not the TLB groundwater budget (Table 3.1) nor the land surface and rootzone budget (SI Appendix Table 3.2), but rather, a combination of ground and surface water budget terms that illustrate hydrologic change and show the main inputs (recharge) and outputs (pumping and evapotranspiration). Major rivers (shown in blue) from north to south include the San Joaquin, Kings, Kaweah, Tule, and Kern. Minor streams and tributaries are not shown.

Table 3.1: Average annual groundwater and salt budget for the TLB (equation 3.5) from C2VSim (1961-10-31 to 2001-09-30), and the modified no-overdraft budget used in this analysis (equation 3.7).

	Source	Q (km^3/yr)	C (mg/L)	m (<i>Metric Mtons</i>)
Historical budget	R	2.451	32.5	8.027E-02
	B	0.236	32.5	7.475E-03
	C	0.572	32.5	1.852E-02
	I	0.011	32.5	3.250E-04
	P	-6.761	*	*
	N	1.883	*	*
	RWI	-	-	*
Alternate budget	ΔS	-1.608		
	R	2.451	32.5	8.027E-02
	B	0.236	32.5	7.475E-03
	C_{alt}	0	-	-
	M	0.678	32.5	2.204E-02
	I	0.011	32.5	3.250E-04
	P_{alt}	-5.259	*	*
	N	1.883	*	*
	RWI	-	-	*
	ΔS_{alt}	0	-	-

* non-constant term calculated at each time step

Q is the volumetric flow rate, C is the concentration of TDS, and m is the mass of salt. Groundwater budget terms are: R = recharge from streams, lakes, and watersheds, B = lateral mountain front recharge from streams and watersheds, C = subsidence flow, C_{alt} = subsidence flow to eliminate overdraft (along with M_{alt} and P_{alt}), M = managed aquifer recharge to eliminate overdraft (along with C_{alt} and P_{alt}), I = subsurface inflow from the north, P = groundwater pumping, P_{alt} = alternate groundwater pumping to eliminate overdraft (along with M and C_{alt}), N = net deep percolation (recharge from the land surface through vadose zone and into saturated groundwater), RWI are rock-water interactions. ΔS = change in groundwater storage. ΔS_{alt} = change in groundwater storage for the modified budget. The modified budget eliminates overdraft by reducing P to P_{alt} according to equation (3.12), and introducing recharge M .

Although a TLB water budget from pre-development times is not available, the surface

and subsurface hydrologic characteristics of the basin, which is a part of the larger Central Valley sedimentary basin (Figure 3.2), indicate that it was hydrologically open. We first discuss the surface hydrologic aspects. Despite the shallow topographic depression in which Tulare Lake used to exist, the freshwater lake periodically filled up and overflowed northward into the San Joaquin River (Grunsky, 1898; Davis, Green, Olmsted, & Brown, 1959), providing an outlet for any accumulated salts. Reconstructions of historical Tulare Lake level indicate that in 19 of the 29 years from 1850 to 1878, it filled up and flowed out of the basin to the north (USBR, 1970). This water and salt exit via intermittent surface inundation would be different than, say, baseflow to a stream, but would accomplish the same flushing function. No overflows are documented after 1878 due to the diversion of tributary waters for agricultural irrigation and municipal water use (ECORP, 2007).

The subsurface characteristics also indicate open hydrologic conditions. There is significant evidence that groundwater flowed northward into the adjacent San Joaquin Basin in pre-development times (circa early 1900s). This evidence includes (1) historical measurements of Central Valley groundwater TDS showing lowest TDS values in the TLB, with increasing TDS to the north into the San Joaquin Basin (Mendenhall, Dole, & Stabler, 1916, Table 23), consistent with northward groundwater flow and the accompanying down-hydraulic-gradient groundwater chemistry evolution that is routinely observed in sedimentary basins, e.g., (Palmer & Cherry, 1984); (2) the regional, south-to-north topographic gradient to provide the driving force for gravity-driven flow in the same direction, out of the TLB, even if there existed shallower, local groundwater flow components from north to south at the subtle depression that collected Tulare Lake (e.g., refer to classic work of Jozsef Tóth, 1970 on topographically controlled, gravity-driven flow systems); and (3) horizontal stratification of fine- and coarse-textured sediments in the Central Valley sedimentary basin that results in much lower effective hydraulic conductivities in the vertical direction than the horizontal e.g., (Weissmann, Zhang, LaBolle, & Fogg, 2002; Faunt et al., 2009), thereby minimizing influence of subtle topographic features like the Tulare Lake depression on all but the shallowest groundwater flow components (e.g., refer to Jozsef Tóth, 1970 and related work).

Summarizing, our conceptual model of the pre-development TLB hydrologic system is one in which the subtle topographic depression that collected the typically 12 m deep Tulare

Lake (Preston, 1990), together with the periodic overflow of the lake and discharge to the north, resulted in a partly open surface drainage system. Further, the larger topographic and geologic structure of the basin, together with groundwater chemistry evidence, indicates there was net-northward groundwater flow, making the TLB groundwater system an open hydrologic basin in pre-development times.

Parts of TLB may have been salinating to some degree before development due to shallow evaporation of groundwater and surface water (case (3) in Introduction), in contrast to the ABCSAL process that we describe in this paper. Portions of the TLB closed under pre-development conditions would lead to salt accumulation in and near its playas (e.g., Buena Vista Lake, Tulare Lake): an evaporative boundary of the basin and endpoint to all surface water discharge (case (2) above). This is consistent with observations of high salinity near and in these lakebeds (Hansen et al., 2018; Fujii & Swain, 1995). Although there exist local areas of shallow groundwater with elevated salinity on the west side of the TLB, these areas are typically associated with salt mobilization out of alluvial sediments originating from marine sedimentary source rocks in the Coast Ranges, and not from basin closure.

By the time regional groundwater levels were mapped in the early twentieth century, the TLB showed signs of closure: groundwater flow across the northern boundary was minimal, and flowed north to south, into the TLB (Mendenhall et al., 1916; Ingerson, 1941). Although pre-groundwater-development (pre-1850) water budgets are unavailable, two large-scale, regional groundwater flow models of the Central Valley (Brush et al., 2013; Faunt et al., 2009) provide decadal groundwater budgets for early- (1932-1941) and post-groundwater-development (2000-2009) timescales.

Relative to the decadal hydrologic water year budgets of early-groundwater-development, post-groundwater-development water budgets show much higher pumping, crop evapotranspiration, and recharge (Brush et al., 2013). As groundwater levels fell, gaining streams transitioned to losing streams, and subsurface inflow along the northern basin boundary slightly increased (Figure 3.2). Groundwater discharge to surface water almost entirely ceased. Surface water exits the basin in rare years when the Kings, Kaweah, and Kern rivers produce sufficiently large floods, mostly runoff

from the surrounding uplands. Evapotranspiration from irrigated crops has become the dominant water outflow, and this flow is much greater than it was during early-groundwater-development (Brush et al., 2013). Taken together, these hydrologic changes have transitioned the TLB into an anthropogenically closed groundwater system with commensurate onset of ABCSAL.

3.3.2 Mixing Cell Model Development

Given the large space and time scales of interest, and the large-scale effectively one-dimensional vertical flow conditions in the basin due to pumping and recharge, we used a lumped parameter approach based on upscaling water fluxes of a fully three-dimensional groundwater model. Although local hydrogeologic conditions vary and can lead to locally complex three-dimensional flow and transport, our focus here is on large scale salinization behavior and time scales, thus an upscaled model was appropriately parsimonious. Moreover, upscaling the advection dispersion equation to regional scales remains a scientific and computing challenge (Guo, Henri, Fogg, Zhang, & Zheng, 2020; Guo, Fogg, & Henri, 2019) beyond the scope of this study.

Mixing cell models, also called discrete-state compartment models, are computationally inexpensive and have successfully been used in place of complex flow models to provide rapid, first-order estimates of water budgets, mass flux, and contaminant concentrations (Michael Emerson Campana, 1975; M. Campana & Simpson, 1984; Michael E Campana, 1987; Carroll, Pohll, Earman, & Hershey, 2008; Kirk & Campana, 1990). A mixing cell approach segments the system into a set of control volumes. In each time step of the model, water and salt masses are passed between the cells, and new concentrations are calculated at each cell. Here, we represent the TLB groundwater system through a one-dimensional, vertical column of discrete control volumes (cells), given the predominance of vertical downward flow at the aquifer system scale. We assume that each cell consists of a fraction f of sediments participating in groundwater flow and salt transport with porosity η . We neglect flows and rock-water interactions in sediments not participating in transport, of proportion $1 - f$ (more details below). The thickness of each cell is chosen such that the advective travel time (Δt) of water and salt downward through each cell is exactly 50 years (synchronized tipping bucket model, see equation 3.4) below, thus full mixing occurs at each cell even

as the groundwater flow velocity decreases with depth. To determine the mixing cell parameters, water fluxes throughout the vertical domain (e.g., recharge, vertical flow rate, pumping) are obtained by averaging (i.e., mass-conservative upscaling) the TLB portion of a fully three-dimensional, heterogeneous groundwater flow model of the Central Valley (Brush et al., 2013).

The salt accumulation in a mixing cell at a discrete time k is a mass balance of the initial mass (m_k) [M], incoming mass (m_k^{in}) and exiting mass (m_k^{out}).

$$m_{k+1} = m_k + m_k^{in} - m_k^{out} \quad (3.1)$$

Input and output mass terms can be calculated for each term in the water and salt budget (Table 3.1), from their input and output concentration (C_k^{in}, C_k^{out} [ML^{-3}]) and input and output volumetric flow (Q_k^{in}, Q_k^{out} [L^3]):

$$m_k^{in} = C_k^{in} Q_k^{in} ; \quad m_k^{out} = C_k^{out} Q_k^{out} \quad (3.2)$$

Finally, the concentration in a mixing cell at time step k is:

$$C_{k+1} = \frac{m_k + m_k^{in} - m_k^{out} + \rho V}{V f \eta} \quad (3.3)$$

where V [L^3] is the total cell volume, f [–] is the fraction of sediments actively participating in groundwater flow and salt transport, η [–] is the porosity of those sediments, and ρ [ML^{-3}] is rock-water interaction coefficient. The fraction f is found to be 0.99 (Brush et al., 2013), which in the C2VSim model includes all textures but the Corcoran clay, a relatively impermeable clay layer comprising around 1% of the model volume. Porosity, η , is set to 0.40, the average for the TLB. Coarse and fine sediment porosities do not appreciably differ, averaging around 0.40 with an interquartile range of 0.39 - 0.41 for all textures, as demonstrated in abundant core analyses (Johnson, Moston, & Morris, 1968), and discussed further in SI Appendix Table 3.5 and Figure 3.9; hence, we did not consider varying η across aquifer layers.

To account for mass contribution from natural dissolution of geologic minerals, we define a zero order source term called the rock-water interaction coefficient ρ [ML^{-3}]. Rock dissolution

along groundwater flow paths is well documented in sedimentary aquifers (Palmer & Cherry, 1984; Oetting, Banner, & Sharp Jr, 1996; József Tóth, 1999; Mahlknecht, Schneider, Merkel, De León, & Bernasconi, 2004; Cloutier, Lefebvre, Therrien, & Savard, 2008). We obtain a representative mass dissolution rate from the slope of a representative TDS profile for the TLB from land surface to the base of fresh water (Williamson, Prudic, & Swain, 1989; Kang & Jackson, 2016). The product of the rock-water interaction coefficient ρ and the cell volume (V) is the additional mass accumulated from rock-water interactions in the cell. We also evaluate an alternative scenario with $\rho = 0$.

We solve (3.3) sequentially over the stacked mixing cells from top to bottom and across seven 50-year time steps from 1960 (initial condition) to 2310 (synchronized tipping bucket approach) to obtain the variation of salinity with depth and time.

The discretization, Δz_j , of the stacked series of mixing cells (Figure 3.3) is driven by the time step, $\Delta t = 50$ years, and the representative basin-scale vertical Darcy velocity, q_j , within the j^{th} mixing cell:

$$\Delta z_j = \frac{q_j}{f\eta} \cdot \Delta t \quad (3.4)$$

Since q_j is depth dependent, we solve (3.4) sequentially for $j = 1...m$, beginning at the water table to compute the vertical discretization of the stacked mixing cell model. Here, we assume that the inflow into a mixing cell, $q_{j-1,j}$ is representative of the flow rate q_j throughout the cell. Thus – to compute cell thicknesses with equation (3.4) – the pumping, P_j , lateral basin flow I_j , or subsidence flow C_j (Figure 3.3) conceptually flow into or out of the mixing cell bottom. The following sections provide further details on the parametrization of (3.3) and (3.4).

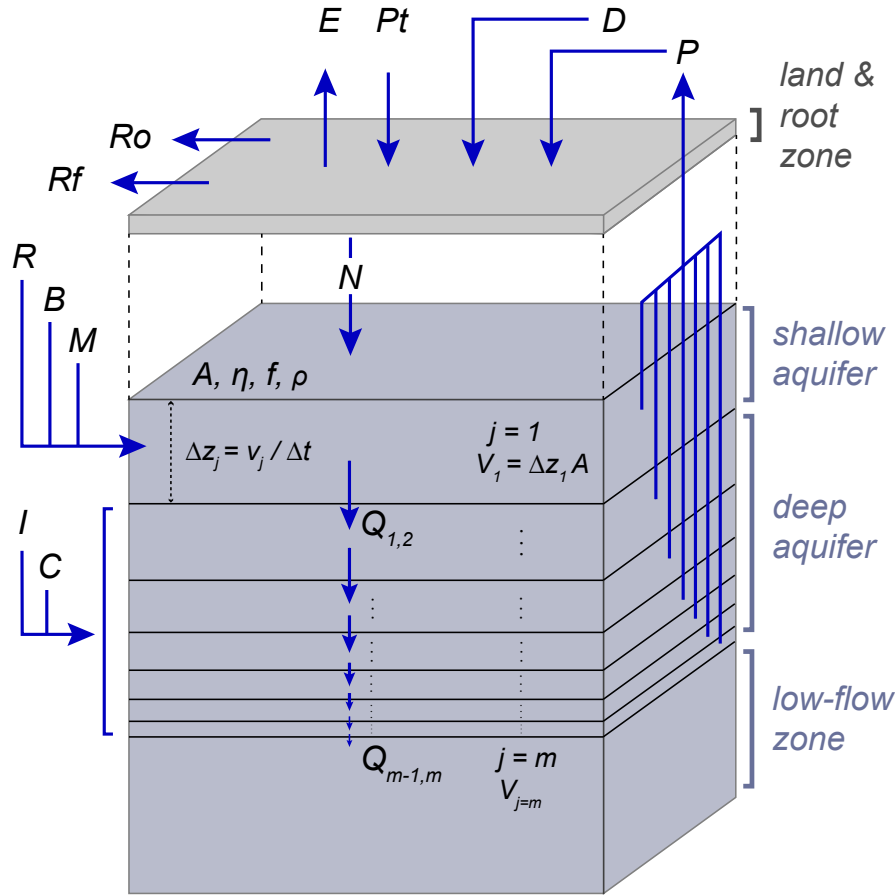


Figure 3.3: Conceptual land-rootzone model and groundwater mixing cell model with surface area A , porosity η , aquifer fraction f , rock-water interaction coefficient ρ , and m cells. The cell thickness Δz_j is given per equation (3.4), where average linear velocity $v_j = q_j/f\eta$. The cell volume V_j is the total bulk volume of the rock including aquifer and non-aquifer material. The TDS in cell j is calculated by equation (3.3). The land and root budget (SI Appendix Table 3.2) accounts for pumping (P), surface water diversions (D), precipitation (Pt), evapotranspiration (E), runoff (Ro), return flow (Rf), and net deep percolation (N). N enters the top of the groundwater mixing cell model along with recharge from streams, lakes, and watersheds (R), boundary inflow from mountain front recharge (B), and managed aquifer recharge (M). Internal flows from subsurface inflow from the north (I), subsidence flow (C), and pumping (P) are distributed proportional to cell volume, e.g., equation (3.12). The average annual groundwater and salt budget is reported in Table 3.1.

3.3.3 Boundary conditions, model parameters, and stochastic simulation

Initial conditions, boundary conditions, and model parameters are informed by the C2VSim groundwater flow model developed by the California Department of Water Resources (Brush et al., 2013), publicly available water quality data (CSWRBC, 2019c), and previous field studies of the TLB. The following describes methods used to determine (1) water and salt budgets, (2) salt fluxes from evaporative concentration and pumped groundwater, (3) the groundwater velocity-depth profile, (4) the initial TDS-depth profile, and (5) spatial parameters and aquifer properties. Lastly, we discuss the simulation timescale and the role of stochastic simulation.

3.3.3.1 Water and salt budgets

The water budget is based on C2VSim version 3.02, a 3 layer and 1,392 element, regional scale, finite-element groundwater flow model of California's Central Valley alluvial aquifer system (Brush et al., 2013). C2VSim is an application of the Integrated Water Flow Model (IWFM) (Dogruel, Nadir, & Brush, 2018), a water resources management and planning model that simulates surface water, stream-groundwater interaction, vadose zone flow, and groundwater flow. In the C2VSim model, California's Central Valley aquifer is separated into 21 subregions, and detailed land surface, root zone, and groundwater budgets for each subregion are calculated at monthly time steps from the 1923 to 2009 hydrologic years. The TLB is represented by subregions 14-21. Because of its detailed representation of surface-groundwater interaction, groundwater pumping, three-dimensional aquifer structure, and calibration, C2VSim was chosen as a reasonable representation of the TLB water budgets, groundwater velocities, and thus chosen to develop the mixing cell model.

The C2VSim model was run for the 40-year period from 1961-10-31 to 2001-09-30 to obtain an average annual TLB groundwater budget (an equivalent average annual landscape/root zone budget is provided in SI Appendix Table 3.2). This post-groundwater development water management time frame is characterized by pumping and overdraft, in addition to wet, dry, above normal, below normal, and critical water year types. The C2VSim change in groundwater storage

is defined as:

$$\Delta S = R + B + C + I + N - P \quad (3.5)$$

where ΔS is change in groundwater storage [L^3], R is basin recharge from streams, lakes, and watersheds [L^3], B is lateral mountain front recharge from streams and watersheds [L^3], C is subsidence based flow from clay compaction [L^3], I is subsurface inflow from the north [L^3], N is net deep percolation predominately from irrigation water [L^3], and P is groundwater pumping [L^3]. The dominant budget terms are P , R , and N (Table 3.1).

To demonstrate ABCSAL under long-term conditions that avoid further overdraft (but not basin closure), we solve the mixing cell model equations (3.3) - (3.4) alternatively for $\Delta S_{alt} = \Delta C_{alt} = 0$. Overdraft is eliminated with an alternate budget (Table 3.1), which adds managed aquifer recharge, M as inflow to the top mixing cell (Figure 3.3), and reduces pumping to an alternative pumping level, P_{alt} . We add $M = 0.68 \text{ km}^3$, which was determined by a prior study as the maximum theoretical recharge available to the San Joaquin Valley (which includes the TLB), assuming unlimited infrastructure and water transfer ability (Hanak et al., 2019). Eliminating overdraft in this way effectively maintains a steady-state, saturated model that remains closed to due to lack of baseflow and groundwater outflow. Hence, the water level is immobile, but the salt front can move, thus simulating salt migration without drying out cells due to overdraft.

Since M represents captured surface water flow, we assign it the same TDS as natural water (32.5 mg/L), discussed below. We also simulated M with a TDS of 0 mg/L (SI Appendix Table 3.9) and found that it had a negligible impact on resulting salt concentrations presented in this study (SI Appendix Table 3.8).

The alternate, reduced pumping P_{alt} , is computed by rearranging (3.5), adding M , and setting $\Delta S_{alt} = C_{alt} = 0$:

$$P_{alt} = R + B + M + I + N \quad (3.6)$$

Therefore, the modified no-overdraft alternate groundwater budget is:

$$\Delta S_{alt} = R + B + C_{alt} + M + I + N - P_{alt} = 0 \quad (3.7)$$

The salt budget is calculated by assigning a TDS concentration to each term in the groundwater budget (3.7). TDS for natural waters (e.g., stream, lake, and managed aquifer recharge budget terms) were determined to be 32.5 mg/L, by computing the median of the sampling distribution of sample TDS medians in TLB stream samples (USGS, 2016) from 1951 - 2019 (SI Appendix Figure 3.7 and Table 3.3). Similarly, the TDS of diverted surface water was calculated to be 264.5 mg/L, as the average annual water and salt budget from 1985 - 1994 of two major surface water conveyance structures, the California State Water Project and the State Water Project (Cismowski et al., 2006) (SI Appendix Table 3.3). Salt and water budgets are detailed in Table 3.1.

3.3.3.2 Velocity-depth profile

To explicitly solve for the mixing cell discretization (3.4), we fit a linear model to the C2VSim vertical Darcy velocities, reported for each finite element cell in the three layer C2VSim grid at the layer-to-layer boundaries. Due to increases in recharge and pumping caused by groundwater development and irrigation, the groundwater flow system is vertically dominant, and thus supports the application of a 1D, vertically oriented model. To account for groundwater velocity change in the alternate groundwater budget (3.7), groundwater velocity is scaled proportional to the decrease in vertical volumetric flow rate, $P_{alt}/(P + C) = 0.85$ (a 15 % reduction). This is equivalent to the ratio of net downward volumetric flow in the alternate budget to the net downward volumetric flow in the historical budget (Table 3.1).

$$q(z) = (\beta_0 + \beta_1 z) \cdot \frac{P_{alt}}{P + C} \quad (3.8)$$

where β_0 and β_1 are the regression coefficients (SI Appendix Table 3.4), and the overall change (reduction) in velocity is -15%. Mixing cell thickness (3.4) is determined by computing q_j from (3.8) for the depth, z , of the bottom of the mixing cell $j - 1$ (top of cell j). To ensure consistency between the water balance terms in (3.5) and the approximated vertical velocity profile

(3.8), we compute the water mass balance error, $MB_{error,j}$, for each mixing cell j :

$$MB_{error,j} = q_{j-1,j} + I_j - P_{alt,j} - q_{j,j+1} \quad (3.9)$$

For the uppermost mixing cell $j = 1$, we rearrange (3.9), replacing $q_{j-1,j}$ for the sum of N , R and B , and ignoring subsurface inflow I_j (Figure 3.3):

$$MB_{error,1} = N + R + B + M - P_{alt,1} - q_{1,2} \quad (3.10)$$

The cell by cell budget and mass balance errors (which are effectively zero, and equivalent to the cell-by-cell change in storage) are reported in SI Appendix Table 3.7.

3.3.3.3 Evapoconcentration and pumping

Evapotranspiration removes a majority of total applied water, leaving behind dissolved solids in the crop rootzone that eventually migrate into groundwater. We model the evapoconcentration of TDS in total applied water (a combination of pumped groundwater and imported surface water diversions) by accounting for the application efficiency (Burt et al., 1997), and thus the fraction of water that remains after evapotranspiration:

$$C_N = \left(\frac{m_D + m_P}{V_D + V_P} \cdot \frac{1}{1 - E_a} \right) = \frac{C_{D,P}}{1 - E_a} \quad (3.11)$$

C_N is the concentration of net deep percolation after accounting for evapotranspiration. m_D and m_P are the mass, and V_D and V_P are the volume of surface water diversions (D) and pumping (P), respectively. $C_{D,P}$ is the concentration of total applied water from surface water diversions and pumping (calculated by mixing diversions and pumped groundwater in their respective proportions, see SI Appendix Table 3.4), and E_a is the application efficiency, which has a measured regional average of 0.78 in the Tulare Basin (Sandoval-Solis et al., 2013), and agrees with measured values in hydrologically similar areas (Bob Hanson et al., 1995; Howell, 2003). Alternatively, the C2VSim landscape/soil water budget (SI Appendix Table 3.2) provides an application efficiency, E_a , of 0.88 when considering the amount of water infiltrating into the soil and deep percolation.

For sensitivity analysis, we run simulations for several E_a between 0.78 and 0.88 to further explore model outcome uncertainty.

For the stacked mixing cell model, we assume that P_{alt} in the no-overdraft groundwater budget (3.6) is distributed uniformly with depth, from the water table to the last mixing cell m . Similarly, we assume lateral inflow I is uniformly distributed across depth, from cell 2 to cell m . Therefore, pumping is proportional to mixing cell thickness, and the salt mass flux due to pumping during time step k in mixing cell j is:

$$m_{j,k} = \frac{V_j f\eta}{f\eta \sum_{i=1}^n V_i} PC_{j,k} \quad (3.12)$$

Noting that the $f\eta$ term drops out, and summing over all mixing cells at time k gives the total mass flux from groundwater pumping ($m_{P,k}$):

$$m_{P,k} = \sum_{j=1}^n \frac{V_j}{\sum_{i=1}^n V_i} PC_{j,k} \quad (3.13)$$

3.3.3.4 Initial TDS-depth profile

The initial TDS-depth profile is determined by fitting a linear model to the pre-1960 TDS-depth measurements (Figure 3.4) (CSWRBC, 2019c). Due to the influence of freshwater recharge at the land surface and rock-water interactions, pre-1960 TDS generally increases with depth, consistent with observations of increasing TDS with depth in the region (Kang & Jackson, 2016; Kharaka & Thordesen, 1992; DeSimone et al., 2010).

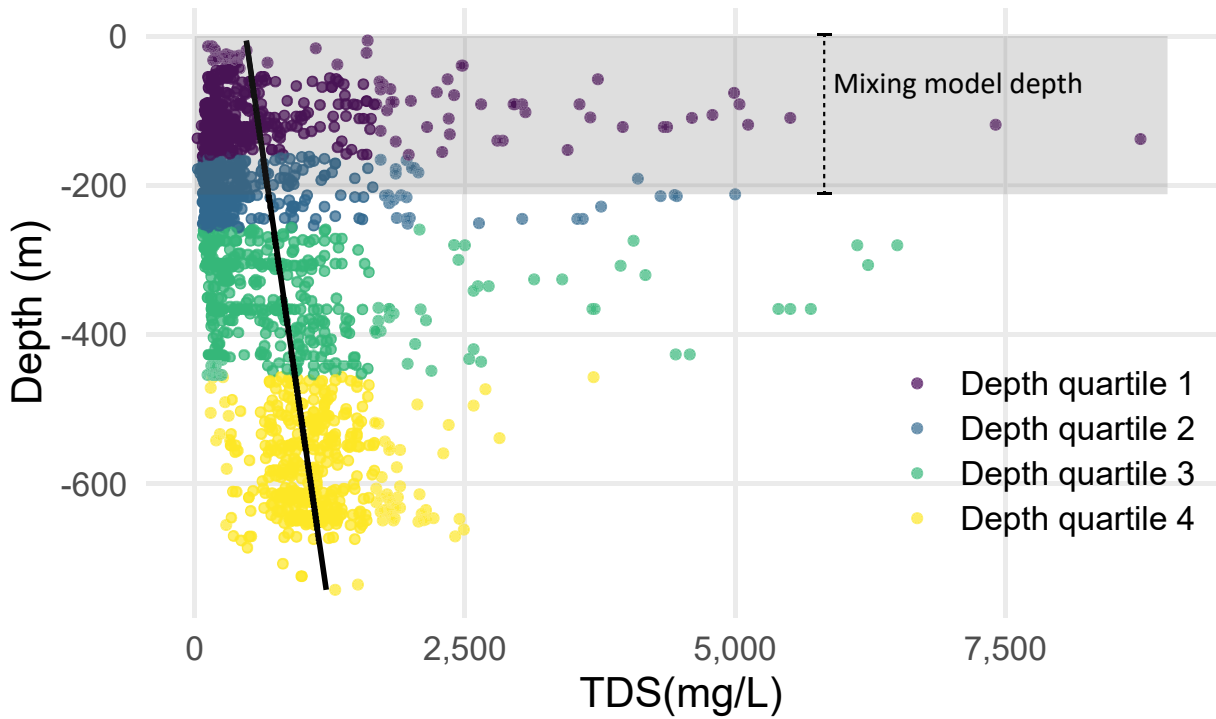


Figure 3.4: Pre-1960 groundwater quality generally decreases with depth, reaching an average concentration of 1,000 mg/L at 526 m deep. The initial TDS-depth concentration at $t = 0$ is approximated by a linear model, shown as a black line. The transparent, grey rectangle shows the depth of the mixing cell model (212 m).

3.3.3.5 Ensemble simulation

We assign a uniform probability distribution to the parameters of which we are least certain and discrete values to those that are measured (SI Appendix Table 3.6), then perform Monte Carlo simulation to generate an ensemble output. The mixing cell model is evaluated 1,000 times – which the computational simplicity of a lumped model permits; modeling uncertainty in this way with a distributed parameter, 3D flow and transport model would be computationally prohibitive. Parameter ranges are estimated from literature for rock-water interaction coefficient (Williamson et al., 1989; Kang & Jackson, 2016), detailed in section 4.3.3. As described in section 3.3.3.3, application efficiency is both measured (Sandoval-Solis et al., 2013), and calculated from

C2VSim (Brush et al., 2013).

To show the influence of rock-water interactions on the progression of closed basin salinization, we simulate two basic scenarios:

1. No rock-water interactions: mass accumulates from water budget inputs.
2. Rock-water interactions are present: mass accumulates from water budget inputs, but also internally via rock-water interactions (see section 4.3.3 for details).

3.4 Results

3.4.1 Groundwater and salt budget

The average historical C2VSim groundwater budget in the TLB from 1961-10-31 to 2001-09-30 (Table 3.1) reflects post-groundwater development conditions. Pumping removes an average of $-6.76 \text{ km}^3/\text{yr}$ from the groundwater system. Natural recharge from streams, lakes, and watersheds adds an average of $2.45 \text{ km}^3/\text{yr}$, and net deep percolation of agricultural irrigation adds an average of $1.89 \text{ km}^3/\text{yr}$. Smaller sources of water inflow include subsidence flow ($0.57 \text{ km}^3/\text{yr}$), lateral mountain front recharge from streams and watersheds ($0.24 \text{ km}^3/\text{yr}$), and subsurface inflow from the north ($0.01 \text{ km}^3/\text{yr}$).

The alternate budget (Table 3.1) used in this study eliminates overdraft ($\Delta S = 0$), and is identical to historical budget described above, except that pumping P_{alt} is reduced to $-5.26 \text{ km}^3/\text{yr}$, managed aquifer recharge M is added at a rate of $0.68 \text{ km}^3/\text{yr}$, and subsidence flow C_{alt} is reduced to 0. Importantly, in this alternative budget the basin remains closed.

Salt inputs to the system (Figure 3.5A) come from pumped groundwater, water budget terms, and rock-water interactions.

Groundwater pumping for agriculture is unlike other water budget terms (I, M, R, B) and rock-water interactions in that it does not *add* new salt into the system, but rather *recycles* existing salt from deeper layers to the land surface and back into shallow groundwater via irrigation (discussed in Section 3.4.2). In the no rock-water interactions scenario ($\rho = 0$), the median mass

recycled by pumped groundwater exceeds the mass input of all other water budget terms by a factor of 1.7 to 3.5 depending on the timeframe considered. When rock-water interactions are present ($\rho > 0$), they initially contribute a comparable mass to groundwater pumping (around 4 metric *Mtons*), but with time, salt accumulates in the aquifer, and the mass recycled by groundwater pumping exceeds the mass imparted by rock-water interactions (Figure 3.5A).

Annually, surface water diversions add 1.5 metric *Mtons* of salt to the study site. This is around 4 times the amount of all other non-pumping water budget terms combined (I, M, R, B), which add only 0.35 metric *Mtons*. We estimate that rock-water interactions add between 3.3 metric *Mtons* and 4.6 metric *Mtons* of salt annually. This exceeds the mass introduced by imported surface water and is comparable to the mass recycled by groundwater pumping.

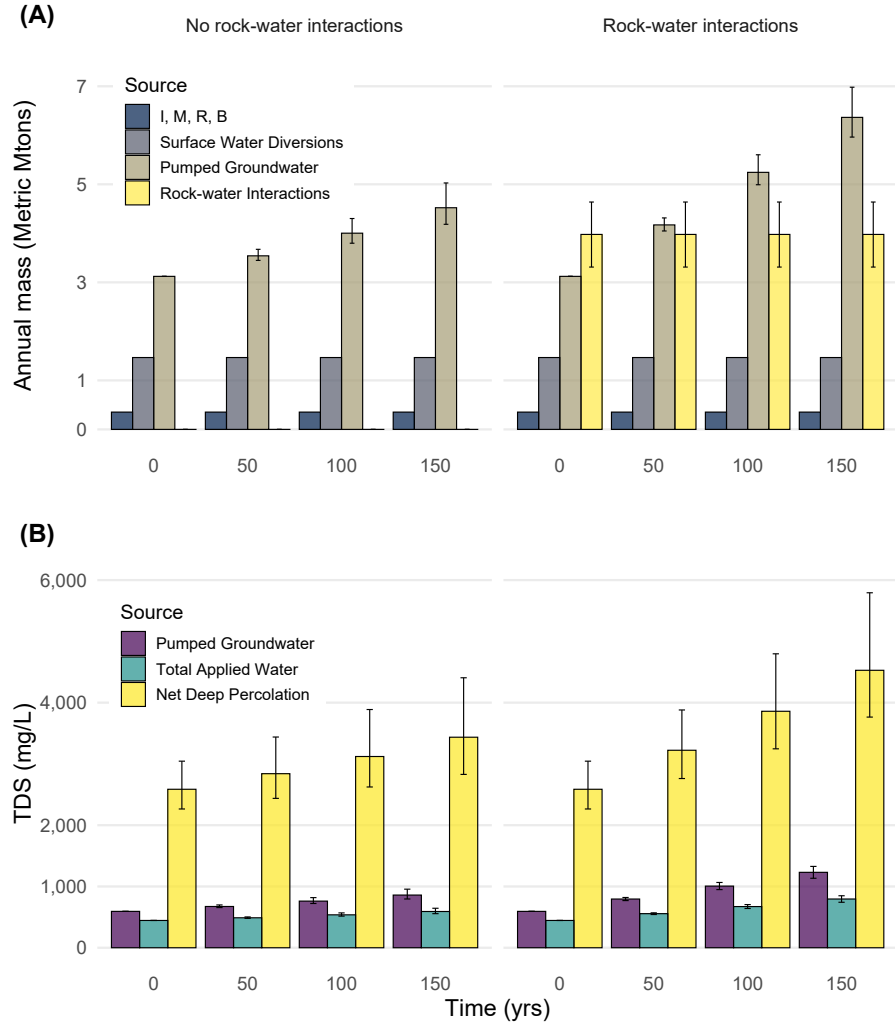


Figure 3.5: Annual mass flux and TDS of selected budget terms. The height of each column is the ensemble median result, and the width of error bars, if present, is the interquartile range of the ensemble distribution. (A) Pumped groundwater contributes more mass than surface water diversions and all other water budget terms combined (represented by their symbol: *I, W, R, B*). (B) TDS of *pumped groundwater* is diluted when mixed with imported surface water, which forms *total applied water*. However, evapotranspiration concentrates total applied water, which enters the groundwater system as *net deep percolation*. Over time in a closed basin system, the groundwater salinates, which in turn increases the concentration of total applied water and net deep percolation.

Due to the closed-basin hydrology of the study site, there are no exits for salt to leave

the system. Instead, pumping and irrigation recycle salts within the basin, and evapotranspiration by crops at the land surface increases the concentration of net deep percolation, which recharges groundwater (Figure 3.5B).

Evapoconcentration by crops at the land surface increases the average concentration of total applied water (pumped groundwater combined with surface water diversions) by 5.1 - 6.8 times its original amount, regardless of whether rock-water interactions are absent or present. As previously discussed, since pumped groundwater concentration increases with time, total applied water and thus net deep percolation also become increasingly saline over time.

3.4.2 Progression of groundwater salinization

The shallow aquifer (36 m) is heavily impacted by the recycling of salts via pumping and irrigation, and exceeds the freshwater concentration threshold (1,000 mg/L) within decadal timescales (Figure 3.6). Intermediate (132 m) and deep aquifers (187 m) exceed 1,000 mg/L within century-long timescales.

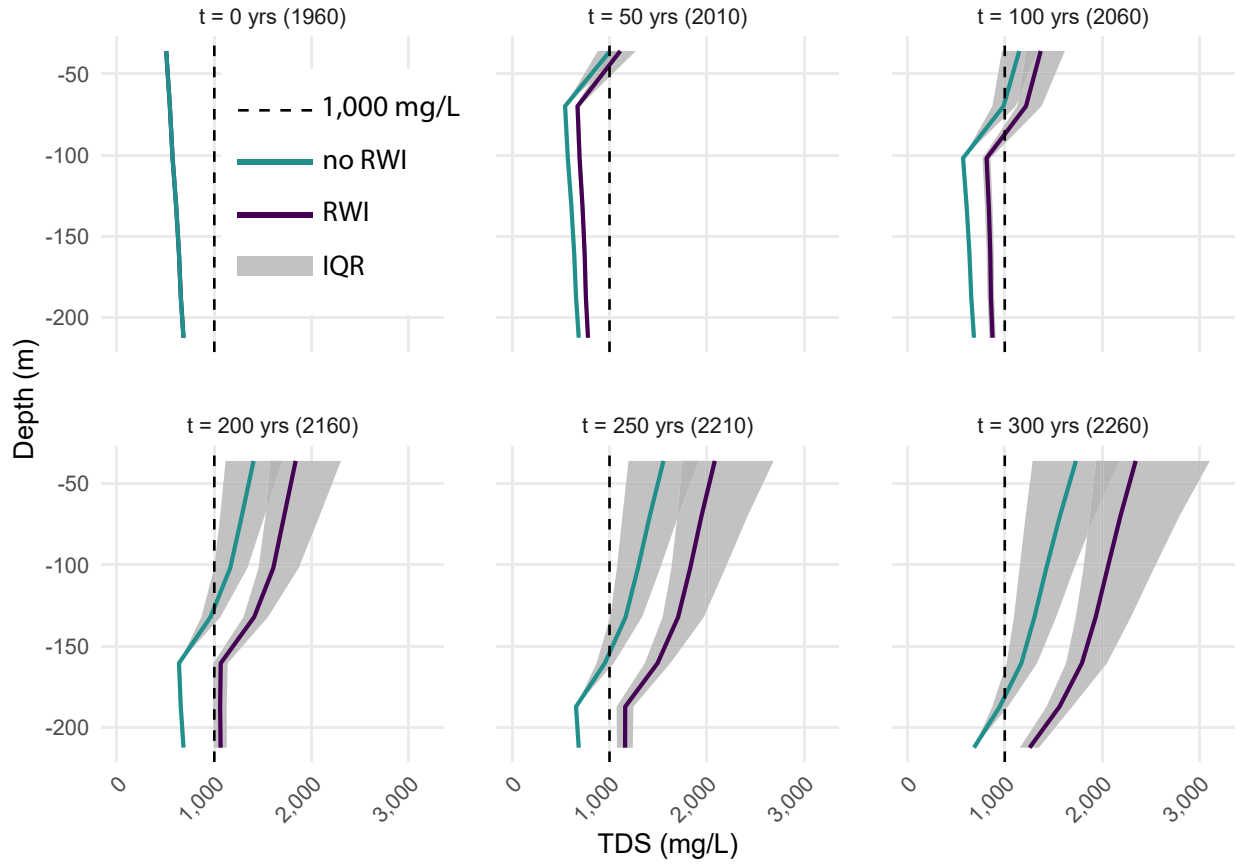


Figure 3.6: Progression of groundwater salinization ensemble results for two scenarios (with and without rock-water interactions). RWI stands for rock-water interactions. The blue and purple lines show the ensemble median concentration for the two scenarios, and the interquartile range (IQR) of the ensemble simulations is shown as a grey shaded area. Complete statistics are provided in SI Appendix Table 3.8.

Uncertainty in the salt balance results from parameter uncertainty expressed in the Monte Carlo simulation (section 3.3.3.5), which affects the distribution of calculated salt concentrations at the salt front. Deeper layer insensitivity results from being insulated from the salt front – a top down source. Accordingly, shallow layer uncertainty increases over time because salt is continuously added through top-down irrigation and recharge.

Let us first summarize the results with no rock-water interactions. At the beginning of the simulation (year 1960), initial TDS concentration increases gradually with depth (Figure 3.4 and

SI Appendix Table 3.8). Shallow aquifer salinity is 506 mg/L. After 50 yrs with $\rho = 0$, average shallow aquifer salinity reaches a median concentration of 975 mg/L with an interquartile range (IQR) of 871 - 1,124 mg/L. Thus, the TDS-depth profile at $t = 50$ begins to invert (i.e., shallow aquifer salinity exceeds deep aquifer salinity), consistent with modern-day observed TDS-depth relationships in the TLB (Hansen et al., 2018). After 200 yrs (year 2160), shallow aquifers reach brackish TDS levels with a median TDS of 1,314 mg/L (IQR: 1,100 - 1,654 mg/L). Finally, after 300 yrs (year 2310), median shallow aquifer TDS approaches nearly 1,574 mg/L (IQR: 1,264 - 2,103 mg/L).

Intermediate and deep aquifers are impacted much later than shallow systems, and exceed the freshwater TDS threshold on timescales of two to three centuries. After 200 yrs (year 2160), intermediate aquifer median TDS exceeds 1,000 mg/L (IQR: 861 - 1,048 mg/L). After 300 yrs (year 2260), deep aquifers (IQR: 867 - 1020 mg/L) experience the first arrival of the lumped salt front.

In the “rock-water interactions present” scenario ($\rho > 0$), the progression of groundwater salinization follows approximately the same trend and timescale as the scenario without rock-water interactions (described above), but the resulting concentrations are significantly greater, and deep groundwater salinates faster. In both scenarios, the greatest change in salinity occurs in the shallow aquifer within the first 50 yrs, which is due to the introduction of mass from total applied water (i.e., diversions and pumped groundwater), and the inability for that mass to exit because of basin closure. Moreover, regardless of whether rock-water interactions are included, the slope of the TDS-depth profile (Figure 3.6) gradually inverts and amplifies, and shallow groundwater becomes saltier than deep groundwater. Thus, even in the absence of rock-water interactions, moderate and constant salt inputs (mostly due to recycled groundwater and imported surface water) are sufficient to saline shallow aquifers within decades, and deep aquifers within centuries.

3.4.3 Additional perspective on the model

Lumped mixing cell models have a relatively small number of parameters, are computationally inexpensive, conceptually simple, and importantly, can represent the dominant hydrologic

features of a system. These strengths come with some tradeoffs. Mixing cell models simplify groundwater flow and contaminant transport by ignoring horizontal flow, geologic heterogeneity, dispersion, diffusion, sorption, and reactive transport. Strong vertical hydraulic gradients induced by pumping in agriculturally dominant systems (like the TLB), produce vertically dominated flow systems (Brush et al., 2013; Faunt et al., 2009). In upscaling these distributed models to the regional scale, the dominant role of vertical flux becomes apparent and explains why the mixing cell model captures the salient features of regional ABCSAL degradation. For more sub-regional or local applications, a fully three-dimensional distributed parameter model would be more appropriate (Zhang, Harter, & Sivakumar, 2006; Guo et al., 2019; Guo et al., 2020; Henri & Harter, 2019).

Additionally, we assume that the early-groundwater-development TDS-depth relationship is approximately equal to observed pre-1960 TDS data. Over the model domain (212 m deep), these measurements (SI Appendix Figure 3.8) are well distributed. We experimented with different values for the initial TDS-depth profile, and found that the results were relatively insensitive to the initial conditions, as the imported salt and the salt generated by rock-water interactions greatly exceeds the initial salt load.

3.5 Discussion

3.5.1 ABCSAL threatens regional groundwater quality and sustainable yield

In this study we show that ABCSAL is a hydrologic process where salts accumulate within an aquifer because basin closure eliminates exits for the salts. In the TLB, our calculated ABCSAL timescales have similar timescales to aquifer depletion, are consistent with 3D random walk salt transport simulations, and agree with observed decadal changes in shallow groundwater salinity in the TLB.

Our estimates of decadal timescales for shallow aquifer (36 m) salinization, and two to three centuries for intermediate (132 m) and deep aquifers (187 m) are similar to the estimated 390 year timescale of Central Valley aquifer depletion by Bridget R Scanlon et al., 2012, who assumed a remaining water storage of 860 km^3 in the year 2000, and a depletion rate of 2.2 km^3/yr . Bridget R

Scanlon et al., 2012 also noted that aquifer lifespan is likely shorter than 390 years in the TLB due to focused groundwater depletion in the area. Thus, ABCSAL, which constitutes a slow-moving form of regional groundwater quality degradation may significantly constrain groundwater sustainable yield on similar timescales to aquifer depletion in the TLB.

This study's predicted salinization time frames (i.e., decades for shallow systems, centuries for deep systems) are consistent with random walk salt and nitrate particle transport simulations in detailed 3D heterogeneous alluvial aquifers (Henri & Harter, 2019; Zhang et al., 2006), which suggests that the simple mixing cell model captures key transport dynamics. Thus, these results provide a useful benchmark for future research using more complex, distributed parameter, regional-scale transport models incorporating geologic heterogeneity and transient boundary conditions.

Morevoer, measured TDS change from historic (1910) to modern (1993-2015) time periods in the TLB (Hansen et al., 2018) agree with this study's modeled changes in TDS over similar timescales (1960 to 2010), especially given that groundwater development for agriculture in the TLB largely commenced around 1950. Hansen et al., 2018 measured a 110 - 850 mg/L increase in the interquartile range (IQR) of shallow aquifer TDS from historic to modern timescales, depending on the region considered in the TLB. Our results indicate an IQR increase in shallow aquifer TDS of 365 - 759 mg/L, depending on the inclusion of rock-water interactions (ρ in equation 3.3) in the model. This study's smaller IQR compared to Hansen et al., 2018 may suggest that our model parameters are over-constrained, and thus, do not reproduce the wider distribution of observed TDS IQR increase. However, it is also possible that the larger IQR from Hansen et al., 2018 indicates insufficient sampling (i.e., a perfectly random spatial sample with enough observations might yield a more constrained distribution of TDS measurements that more closely approximate the true population IQR). Nonetheless, given the broad aim of this study to estimate the approximate timescales of regionally downward salinization of the production aquifer under ABCSAL, the evolution of mass flux described by our model generally agrees with observations of shallow aquifer TDS increase in the TLB.

Unsustainable groundwater management eventually leads to undesirable effects (Giordano, 2009; “Sustainable Groundwater Management Act, California Water Code sec. 10720-10737.8,”

2014), such as: chronic groundwater level declines and depletion of groundwater storage; well failure (RA Pauloo et al., 2020); increased energy costs for pumping (Yoshihide Wada et al., 2010); land subsidence (Smith et al., 2017); sea water intrusion (Zektser, Loáiciga, & Wolf, 2005); desiccation of groundwater dependent ecosystems (TNC, 2014); and groundwater quality degradation (Smith et al., 2018; Foster, Chilton, Moeng, Cardy, & Schiffler, 2000). The negative externalities above are recognized consequences of unsustainable groundwater extraction. However, ABCSAL, which progressively deteriorates groundwater quality over decades to centuries, may be considered an additional, unrecognized threat to regional groundwater quality and sustainability in the TLB, and a constraint on groundwater sustainable yield in other food production regions of the world.

3.5.2 Key features of ABCSAL

ABCSAL arises from groundwater development, and is sustained by basin closure. Once a basin is closed, salinization does not depend on groundwater overdraft per se, but rather, on the closure itself, which prevents the basin from discharging salts.

Our findings indicate that the long-term fate of basins closed by groundwater pumping may be similar to that of naturally closed basins (Hardie & Eugster, 1970; Jones & Deocampo, 2003). However, unlike naturally-occurring closed basins, salt cycling in agriculturally intensive closed basins is driven by human-made water management decisions, and may progress more rapidly. Near the onset of the 21st century, average vertical groundwater movement in the Central Valley increased by about 6 times the rate from pre-development conditions, mainly as a result of agricultural recharge and withdrawal from public-supply and irrigation wells (Williamson et al., 1989). Strong vertical transport coupled in a closed basin drives TDS migration into deeper aquifers.

Although groundwater levels in the TLB are in chronic decline (Bridget R Scanlon et al., 2012), groundwater overdraft is not a necessary condition for ABCSAL to occur. To illustrate this point, we eliminated overdraft (equation 3.7) by increasing clean recharge M ($TDS = 32.5 \text{ mg/L}$) at $0.68 \text{ km}^3/\text{yr}$ following Hanak et al., 2019, and reducing pumping by 15 %. We still observed groundwater salinization, even though the water budget remained in steady state. We also applied completely clean recharge with $TDS = 0 \text{ mg/L}$ (SI Appendix Table 3.9), and found that it was

insufficient to stop or reverse ABCSAL because it did not fix the underlying basin closure. Thus, an area will accumulate salts if groundwater storage is stable or even increasing, as long as the basin remains closed and salts cannot exit.

Our study shows that ABCSAL is exacerbated by imported salts in surface water for irrigation, and by groundwater pumping. Although both surface water and groundwater irrigation are present in our study area, like overdraft, they are not necessary conditions for ABCSAL. However, basins with significant groundwater irrigation are particularly susceptible because pumping lowers groundwater levels and cuts off lateral outflow and subsurface baseflow exits, thus initiating ABCSAL.

The rate and magnitude of salinization depends on a variety of factors (e.g., concentration of total applied water, evapoconcentration, vertical groundwater velocity), but fundamentally depends on the severity of basin closure. Worldwide basins range from open (i.e., natural salt exits maintain freshwater conditions), to partially closed (i.e., some salts exit, but some remain and accumulate), to fully closed (e.g., salts have no exit and hence accumulate in deep groundwater). Groundwater salinization timescales in partially closed basins may be longer than those calculated in this study for the TLB, which is completely closed. Conversely, some basins may saline at faster rates than calculated for the TLB, depending on the hydrologic features represented in our mixing model.

3.5.3 Implications for groundwater management

This study demonstrates that if irrigated groundwater basins are operated in a way that hydrologically closes them, groundwater salinization (ABCSAL) is inevitable. It further demonstrates that the timescales of this phenomenon in the TLB are similar to those over which the groundwater in storage would be virtually exhausted according to classic concepts of overdraft. We know how to prevent overdraft by, for example, decreasing pumping or increasing recharge. This raises the parallel question: “How do we prevent ABCSAL?” In other words, how do we both develop groundwater resources, while also keeping groundwater basins hydrologically open?

Conceptually, one way to both pump abundant amounts of groundwater and to keep the

water table sufficiently shallow to produce groundwater discharge (via baseflow and lateral flow to adjacent basins) is to significantly increase groundwater recharge. In California this could in theory be accomplished by storing less water in surface reservoirs and storing more water in groundwater via managed aquifer recharge operations (Kocis & Dahlke, 2017; Ghasemizade et al., 2019; Gailey, Fogg, Lund, & Medellin-Azuara, 2019). Such an approach would be a radical shift from how our current civilization chooses to store water – mainly in surface reservoirs. In the discussion that follows we are not so much advocating such a paradigm shift in water resources management as we are suggesting the need for the beginnings of new conversations in water resources management about how to manage groundwater and surface water jointly in a way that better ensures the sustainability of both.

One challenge of filling up a groundwater basin enough to open it is to manage the water table sufficiently to prevent undesirable waterlogging effects. This would require changes in basin water resources management within a carefully managed scheme in which the pumping and recharge are optimized such that the basin opens up, while preventing the water table from getting so high that bare soil evaporation exacerbates salinization, as happened on the west side of the San Joaquin Valley (Schoups et al., 2005; K. Belitz & Phillips, 1995). The technology to monitor a groundwater basin and model it sufficiently to tightly manage it for optimal water table elevations does in fact exist, but would require levels of groundwater monitoring, modeling, and decision-making that are well beyond what is normally done. In the TLB, a further challenge would be that additional sources of clean recharge water within the TLB watersheds are not large enough to accomplish the requisite amounts of recharge, as rather drastic amounts of pumping reduction would likely be necessary, unless water for recharge could be imported from wetter northern Central Valley watersheds (Hanak et al., 2019). Moreover, the short- and long-term consequences on groundwater quality of increasing clean recharge and reducing pumping need investigation. This in turn would require the development of regional groundwater quality management models (Fogg & LaBolle, 2006; Kourakos & Harter, 2014).

If re-operation of the groundwater basin to increase groundwater storage and open the basin does not happen, water users in the TLB will ultimately be faced with desalinating pumped

groundwater for drinking water and irrigation, the ultimate costs of which remain unknown. If inland closed basin salinization proceeds at the historical rates projected in this study, the salinity of pumped groundwater may exceed thresholds safe for crop health within decades to a few centuries, depending on the depth of pumped groundwater. As prices for technology like reverse osmosis fall, and arid countries pioneer large-scale inland desalination plants for brackish groundwater (Nativ, 2004; Tal, 2006), desalination cost must be weighed against the cost of adaptive water management (e.g., fallowing fields, securing higher quality imported water, managed aquifer recharge) (Hanak et al., 2019).

In order to probe the full impact of ABCSAL in the TLB, particularly on shallow aquifers, which are critical to food and drinking water security worldwide, in this study we assumed no water management intervention as salinity accumulates. In reality, water users would adapt to increasingly saline aquifers by pumping from deeper, less saline aquifers, fallowing fields, mixing saline water with cleaner water, and desalinating pumped groundwater. Two and three centuries into the model, the assumption of no intervention is increasingly unrealistic as the concentration of total applied water approaches thresholds dangerous to crop health, and is likely to have prompted prior adaptive management. We deemed it necessary to evaluate the model at timescales upwards of two and three centuries in order to allow salinization to reach intermediate and deep aquifers. As our model assumes no intervention, results past 50 years of simulation (year 2010) should be interpreted as a worst case scenario.

Urban groundwater pumping might also close groundwater basins. However, there are two key differences between the hydrology of urban and agricultural areas. First, in urban areas, high evapotranspiration rates and subsequent salt concentration are unlikely unless large volumes of water are applied for landscape irrigation. Second, a substantial fraction of urban groundwater pumping (e.g., drinking water, household use, and industrial use) typically exits the basin via wastewater discharge, thus it is not returned to groundwater where it might saline shallow aquifers (as in the case of the TLB). Hence, the threat of ABCSAL in urban basins is likely to be much less than the threat in agriculturally intensive basins where groundwater is developed and recycled internally.

3.6 Conclusions

Irrigated agriculture in overdrafted aquifer systems supplies much of the world’s demand for food (Dalin, Wada, Kastner, & Puma, 2017). In this study, we demonstrate that intensive groundwater development can transform a fresh, open basin into an evaporation-dominated, closed-basin system. A closed basin is effectively a salt sink: aquifer salinization is inevitable because dissolved solids in groundwater cannot escape, and are recycled through pumpage, irrigation, and evapoconcentration by crops. This study provides a conceptual framework to understand this process, which we call “**Anthropogenic Basin Closure and groundwater SALinization**” (ABCSAL), and a mixing cell model to provide first-order estimates of ongoing aquifer salinization in the TLB, located in California’s Central Valley.

Our model indicates progressive salinization ($> 1,000 \text{ mg/L}$) of shallow aquifers (36 m) within decades. Intermediate (132 m) and deep aquifers (187 m) are impacted within two to three centuries. The TLB in California’s southern Central Valley is less than one century into this “experiment” and the first signs of shallow aquifer salinization have been observed (Hansen et al., 2018; CRWQCB, 2018). Estimated salinization timescales are similar to estimated aquifer depletion timescales in the area (Bridget R Scanlon et al., 2012), underscoring the urgency of regional-scale groundwater quality management.

This study is a first-order calculation of ABCSAL in an agriculturally intensive groundwater basin. Future research should emphasize a more comprehensive representation of subsurface transport processes through the development of groundwater quality management models. Key research questions that remain include investigating if managed aquifer recharge with relatively clean water may slow groundwater salinization. It also remains to be tested if it is possible to reverse groundwater salinization by increasing recharge until a basin “fills up” and discharges TDS into streams and lateral outflow which exit the basin. The practical likelihood of this mitigation strategy would require re-imagining integrated water resources management with a greater emphasis on subsurface storage. Ongoing ABCSAL without intervention may necessitate inland desalination to remediate saline groundwater resources, the costs of which remain presently unknown.

Traditionally, the concept of long-term sustainability of groundwater has hinged on the intuitive notion of not managing the basin in ways that result in eventual exhaustion of the groundwater stores. Herein we advance the less intuitive concept that long-term sustainability of groundwater also hinges on the salt balance, which in turn depends on how the groundwater quantity is managed. Fundamentally, ABCSAL can only be prevented by managing the basin groundwater quality in ways that open the basin.

3.7 Supporting Information Appendix

3.7.1 C2VSim average annual land surface and rootzone water budget (1961-10-31 to 2001-09-30)

Table 3.2: C2VSim average annual land surface and rootzone water budget (1961-10-31 to 2001-09-30).

Source	Q (km^3/yr)	C (mg/L)	m (<i>Metric Mtons</i>)
P	6.760	*	*
D	5.543	264.53	1.47
Pt	4.337	0	0
ET	-13.681	0	0
N	-1.883	*	*
Ro	-0.400	0	0
Rf	-0.670	0	0
ΔS	0.006		

* non-constant term calculated at each time step

Q is the volumetric flow rate, C is the concentration of TDS, and m is the mass of salt. Land and rootzone budget terms are: P = groundwater pumping, D = surface water diversions, Pt = precipitation, ET = evapotranspiration, N = net deep percolation from vadose zone into groundwater, Ro = runoff, Rf = return flow, ΔS = change in storage. The water balance equation is: $\Delta S = P + D + Pt - ET - N - Ro - Rf$.

3.7.2 TDS of natural waters measured at NWIS stations in Kern, Kings, Tulare, and Fresno counties

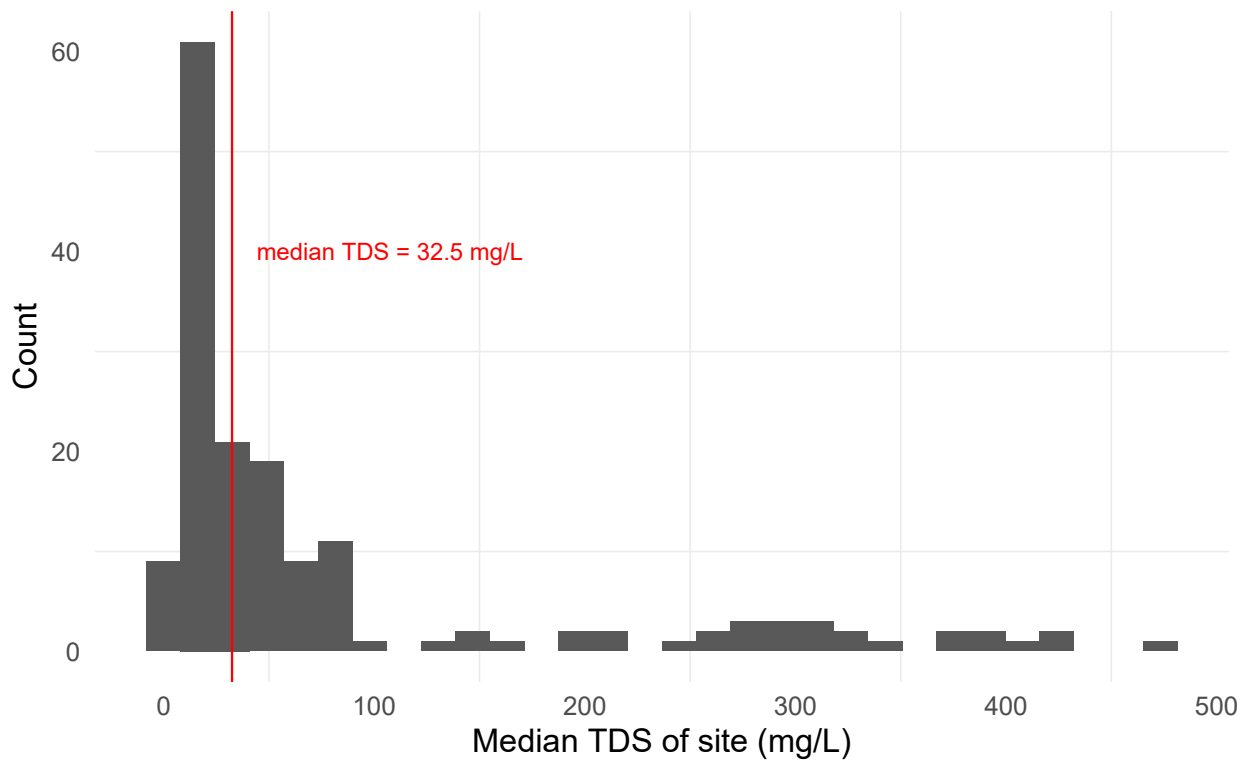


Figure 3.7: Median TDS of natural waters measured at NWIS stations in Kern, Kings, Tulare, and Fresno counties*.

*the following 162 NWIS station codes were analyzed: USGS-11186000, USGS-11187000, USGS-11191000, USGS-11194000, USGS-11203200, USGS-11203500, USGS-11204900, USGS-11206500, USGS-11206700, USGS-11206800, USGS-11206820, USGS-11208000, USGS-11208605, USGS-11208607, USGS-11208610, USGS-11208615, USGS-11208620, USGS-11208625, USGS-11208630, USGS-11208650, USGS-11208680, USGS-11208715, USGS-11208730, USGS-11209500, USGS-11210500, USGS-11210950, USGS-11212423, USGS-11213500, USGS-11218500, USGS-11220000, USGS-11221500, USGS-11221900, USGS-11222700, USGS-11230540, USGS-11247000, USGS-11250000, USGS-11251000, USGS-11253500, USGS-11254000, USGS-11256000, USGS-345002118424201, USGS-351355119194801, USGS-351745119203401, USGS-352641119404801, USGS-353328119395901, USGS-353933118274800, USGS-353953118234500,

USGS-354144118263400, USGS-354251119373101, USGS-354307119351401, USGS-355428119234901, USGS-355802116555201, USGS-360039119583101, USGS-361419119511801, USGS-362100118454001, USGS-362102118241501, USGS-362102118402801, USGS-362243119471001, USGS-362317118245201, USGS-362511118245201, USGS-362540118452901, USGS-362542118432701, USGS-362629118245301, USGS-362647118360801, USGS-362718118244101, USGS-362730118281401, USGS-362730118343001, USGS-362730118400001, USGS-362808118242101, USGS-362808118242102, USGS-362852118240901, USGS-362937118200801, USGS-362947118193801, USGS-363010118302801, USGS-363107118453501, USGS-363112118454601, USGS-363113118480101, USGS-363138118445801, USGS-363310118240101, USGS-363331118450701, USGS-363438118243901, USGS-363455118251301, USGS-363616118245801, USGS-363623118441401, USGS-363629118424201, USGS-363634118444901, USGS-363820118253101, USGS-363911118315501, USGS-363922119402001, USGS-364000118404500, USGS-364019120321101, USGS-364101118412400, USGS-364153118344701, USGS-364155119445000, USGS-364155119445002, USGS-364203118345000, USGS-364218118343401, USGS-364234118404401, USGS-364235118345200, USGS-364236118411301, USGS-364247118352200, USGS-364345118345901, USGS-364400120202600, USGS-364406118382200, USGS-364427118373900, USGS-364454118370100, USGS-364510118262301, USGS-364511118260901, USGS-364519120222001, USGS-364646118320301, USGS-364647118321701, USGS-364658118371801, USGS-364659118372100, USGS-364712120230400, USGS-364718120221800, USGS-364723118403401, USGS-364732118360601, USGS-364746119445400, USGS-364754118344801, USGS-364809118413901, USGS-364818119443800, USGS-364818119464700, USGS-365016120261300, USGS-365027120313401, USGS-365035118321501, USGS-365035119555300, USGS-365105120293001, USGS-365130119504200, USGS-365130120265200, USGS-365202118303701, USGS-365226118255801, USGS-365235119465800, USGS-365235119470700, USGS-365238118260101, USGS-365338118320901, USGS-365453118313301, USGS-365543118444001, USGS-365650118403001, USGS-365743118382501, USGS-365808118375901, USGS-365845118373601, USGS-365912120300000, USGS-365922118264801, USGS-365940120300000, USGS-365952118351001, USGS-370000119393000, USGS-370025119414500, USGS-370059118394101, USGS-370102118391901, USGS-370111118344601, USGS-370140119393000, USGS-370312118342201, USGS-370515120321600, USGS-370539118350701, USGS-370555118354601, USGS-370847118462601, USGS-371017118424601, USGS-371025118432101, USGS-371033118423501,

USGS-371123118473601, USGS-371127118454201, USGS-371212118480001

Table 3.3: TDS of natural waters (derived from NWIS samples, see Figure 3.7) and agricultural diversions (derived from Central Valley Project and State Water Project water and salt budgets). C is the concentration of TDS. From C2VSim, total applied water is 45.1% agricultural diversions and 54.9% groundwater pumping. Natural waters are the TDS of R , B , C , I , and M in Table 1. Agricultural diversions are D in Table 3.2.

Source	C (mg/L)
Natural waters	32.50
Agricultural diversions	264.53

3.7.3 Spatial distribution of pre-1960 groundwater quality in the TLB

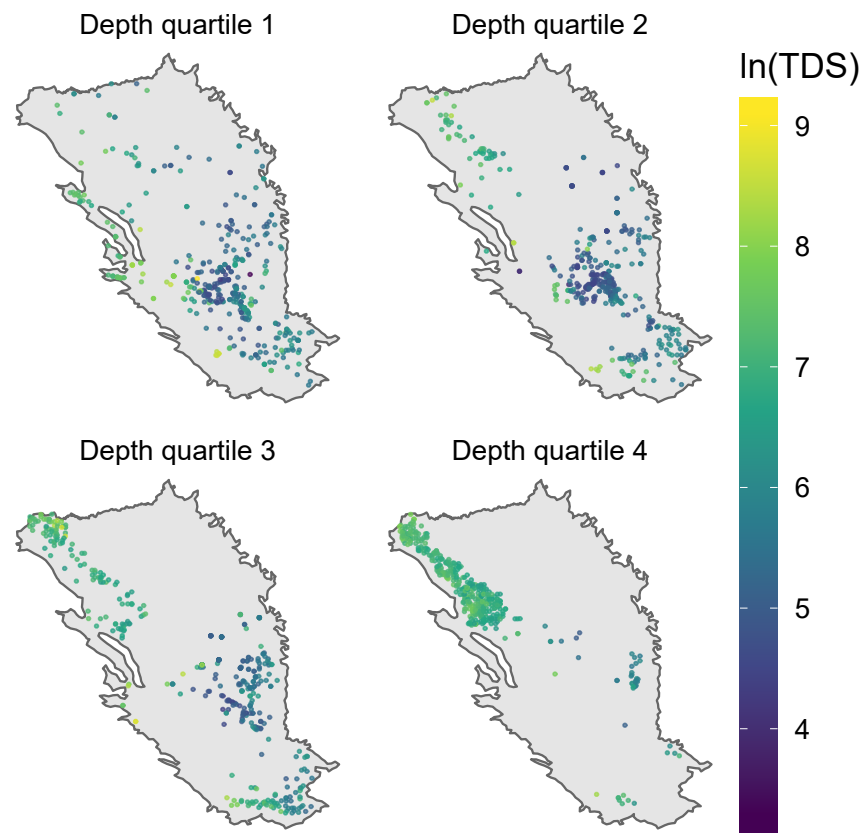


Figure 3.8: Spatial distribution of pre-1960 groundwater quality (Figure 3.4) at 4 depth quartiles from land surface to 762 m in depth (near the base of fresh water). The mixing model (depth = 212 m) is contained within depth quartiles 1 and 2. Quartile 1 = 0.00 to -160.93 m, Quartile 2 = -160.94 to -256.03 m, Quartile 3 = -256.04 m to -454.15, Quartile 4 = -454.16 to -762.00 m.

3.7.4 Vertical groundwater velocity in the TLB

Table 3.4: Linear model coefficients for Equation (3.8). The Darcy velocity (m/yr) at the top of cell $j = 1$ is β_0 , and decreases by β_1 with every vertical meter of depth. To account for groundwater velocity change in the alternate groundwater budget, groundwater velocity is scaled proportional to the decrease in vertical flow, $P_{alt}/(P - C)$, a 15 % reduction. This is equivalent to the ratio of net downward flow in the alternate budget to the historical budget (Table 1).

β_0	β_1	P_{alt}/P
0.34	-5.39E-4	0.85

3.7.5 Porosity of sediments in the TLB

Table 3.5: Sample mean porosities from Johnson (1968) Table 10.

η
0.436
0.327
0.422
0.406
0.401
0.446
0.401
0.423
0.390
0.423
0.442
0.407
0.406
0.391
0.393
0.375
0.405
0.397
0.396
0.369
0.427
0.438
0.389
0.440
0.365
0.395
0.331
0.356

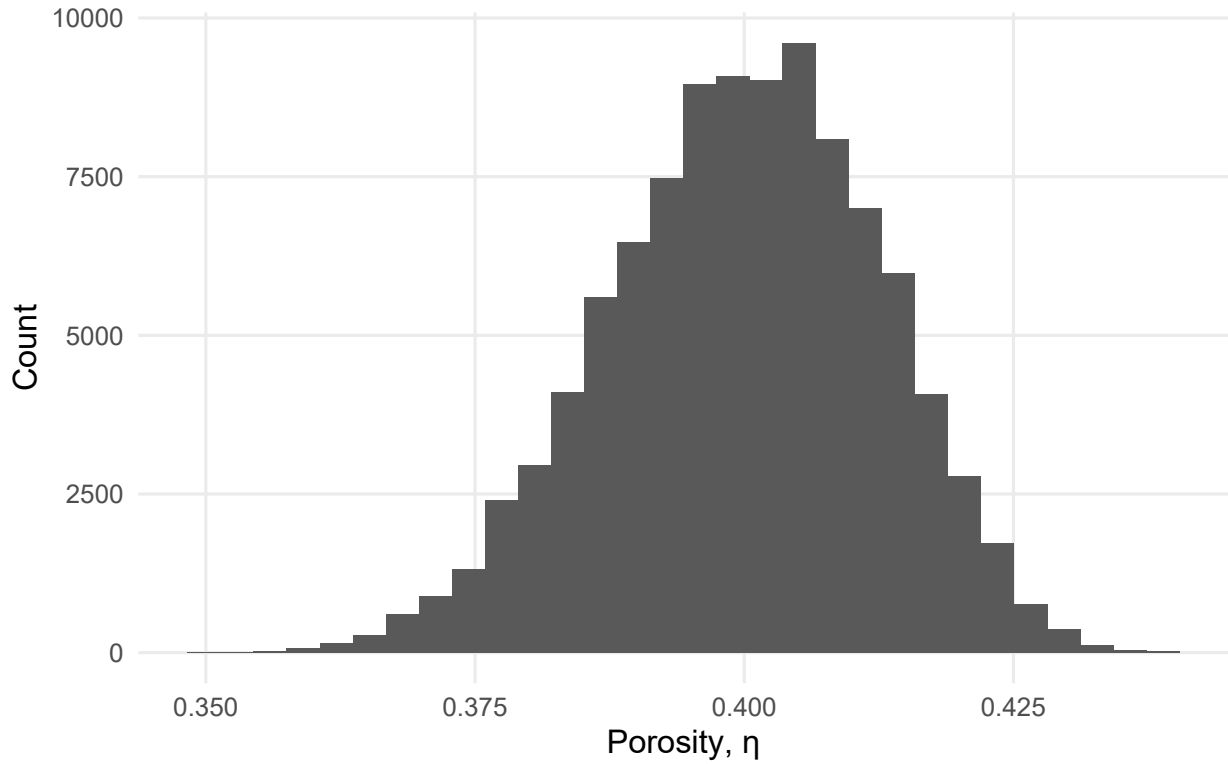


Figure 3.9: Sampling distribution of the porosity sample means from Johnson (1968), Table 3.5. The bootstrapped distribution of 100,000 samples of size $n = 5$ taken with replacement are approximately normal in distribution. Via the Central Limit Theorem, this indicates that the sampling distribution mean is approximately equal to the population mean. Thus, the sampling distribution mean (0.40) is used as the upscaled porosity in the mixing model. A single value is used because the interquartile range, bounded by 0.39 and 0.41, does not vary appreciably.

3.7.6 Mixing cell model geologic and hydrologic parameters and mass balance error

Table 3.6: Mixing cell model geologic and hydrologic parameters: η is the porosity, f is the aquifer fraction, ρ is the rock-water interaction coefficient, and E_a is the application efficiency. Ranges are provided for parameters used in the Monte Carlo simulation.

η [-]	f [-]	ρ [mg/km ³]	E_a [-]
0.40	0.99	0.09 - 0.17	0.78 - 0.88

Table 3.7: Cell by cell budget and mass balance error, per equations (9) and (10).

	Source	$Q \text{ (km}^3/\text{yr)}$
j = 1	N	1.883e+00
	R	2.451e+00
	B	2.355e-01
	M	6.784e-01
	$P_{alt,1}$	-3.040e-01
	$q_{1,2}$	-4.944e+00
j = 2	dS	8.327e-17
	$q_{1,2}$	4.944e+00
	I_2	6.194e-04
	$P_{alt,2}$	-2.864e-01
	$q_{2,3}$	-4.658e+00
j = 3	dS	-2.871e-16
	$q_{2,3}$	4.658e+00
	I_3	5.836e-04
	$P_{alt,3}$	-2.698e-01
	$q_{3,4}$	-4.389e+00
j = 4	dS	-1.717e-16
	$q_{3,4}$	4.389e+00
	I_4	5.499e-04
	$P_{alt,4}$	-2.542e-01
	$q_{4,5}$	-4.135e+00
j = 5	dS	8.587e-17
	$q_{4,5}$	4.135e+00
	I_5	5.181e-04
	$P_{alt,5}$	-2.395e-01
	$q_{5,6}$	-3.896e+00
j = 6	dS	2.676e-16
	$q_{5,6}$	3.896e+00
	I_6	4.882e-04
	$P_{alt,6}$	-2.257e-01
	$q_{6,7}$	-3.671e+00
j = 7	dS	-4.636e-16
	$q_{6,7}$	3.671e+00
	I_7	4.599e-04
	$P_{alt,7}$	-2.126e-01
	$q_{7,8}$	-3.459e+00
j = 8	dS	1.494e-16
	$q_{7,8}$	3.459e+00
	I_8	7.498e-03
	$P_{alt,8}$	-3.466e+00
	$q_{8,9}$	-6.250e-16
	dS	-3.691e-16

Cell by cell groundwater flows (Figure 3) are in steady state ($dS \approx MB_{error,j} \approx 0$). N enters the top of the groundwater mixing cell model along with recharge from streams, lakes, and watersheds (R), boundary inflow from mountain front recharge (B), and managed aquifer recharge (M). Subsidence flow $C_{alt} = 0$, per equation (3.6). Subsurface inflow from the north (I) and pumping (P) are distributed proportional to cell volume (V_j).

Table 3.8: Mixing model TDS-depth profile over time. Median and IQR refer to the median and interquartile range of TDS (mg/L) at the depth (d) of the cell bottom.

t (yrs)	d (m)	No RWI		RWI present	
		Median	IQR	Median	IQR
0	36	506	506-506	506	506-506
50	36	975	871-1124	1111	1007-1265
100	36	1101	961-1310	1369	1208-1603
150	36	1204	1029-1473	1600	1384-1922
200	36	1314	1100-1654	1836	1558-2264
250	36	1434	1176-1861	2081	1733-2638
300	36	1574	1264-2103	2345	1915-3057
0	70	543	543-543	543	543-543
50	70	543	543-543	672	650-693
100	70	960	865-1094	1218	1128-1361
150	70	1113	977-1315	1493	1346-1729
200	70	1218	1047-1480	1717	1518-2045
250	70	1326	1116-1659	1945	1688-2383
300	70	1449	1195-1867	2188	1864-2743
0	102	571	571-571	571	571-571
50	102	571	571-571	692	672-712
100	102	571	571-571	813	773-853
150	102	948	863-1070	1320	1231-1451
200	102	1120	988-1314	1606	1463-1830
250	102	1230	1063-1486	1829	1637-2144
300	102	1342	1136-1667	2056	1807-2485
0	132	609	609-609	609	609-609
50	132	609	609-609	723	704-742
100	132	609	609-609	837	798-874
150	132	609	609-609	950	893-1007
200	132	938	861-1048	1409	1317-1532
250	132	1124	997-1310	1705	1565-1923
300	132	1245	1082-1494	1934	1742-2243
0	160	637	637-637	637	637-637
50	160	637	637-637	744	726-762
100	160	637	637-637	851	816-887
150	160	637	637-637	959	905-1012
200	160	637	637-637	1066	994-1137
250	160	931	861-1030	1493	1388-1599
300	160	1131	1010-1308	1793	1650-2006
0	187	656	656-656	656	656-656
50	187	656	656-656	757	740-773
100	187	656	656-656	858	824-891
150	187	656	656-656	959	908-1009
200	187	656	656-656	1060	992-1127
250	187	656	656-656	1161	1076-1245
300	187	930	867-1020	1562	1450-1670
0	212	684	684-684	684	684-684
50	212	684	684-684	779	763-795
100	212	684	684-684	874	842-906
150	212	684	684-684	969	922-1017
200	212	684	684-684	1065	1001-1128
250	212	684	684-684	1160	1080-1239
300	212	684	684-684	1255	1159-1350

Table 3.9: Mixing model TDS-depth profile over time when the TDS of $M = 0 \text{ mg/L}$. Median and IQR refer to the median and interquartile range of TDS (mg/L) at the depth (d) of the cell bottom.

$t (\text{yrs})$	$d (\text{m})$	No RWI		RWI present	
		Median	IQR	Median	IQR
0	36	506	506-506	506	506-506
50	36	963	859-1112	1099	995-1252
100	36	1086	945-1294	1354	1193-1587
150	36	1186	1012-1454	1582	1367-1903
200	36	1292	1080-1631	1814	1538-2241
250	36	1410	1153-1833	2057	1710-2611
300	36	1546	1238-2071	2317	1889-3026
0	70	543	543-543	543	543-543
50	70	543	543-543	672	650-693
100	70	949	854-1083	1207	1117-1350
150	70	1098	962-1299	1478	1332-1713
200	70	1200	1030-1462	1699	1501-2026
250	70	1305	1096-1636	1923	1668-2361
300	70	1425	1173-1840	2163	1842-2717
0	102	571	571-571	571	571-571
50	102	571	571-571	692	672-712
100	102	571	571-571	813	773-853
150	102	938	853-1060	1310	1221-1441
200	102	1105	974-1299	1591	1449-1815
250	102	1212	1045-1467	1811	1620-2126
300	102	1321	1117-1645	2035	1788-2462
0	132	609	609-609	609	609-609
50	132	609	609-609	723	704-742
100	132	609	609-609	837	798-874
150	132	609	609-609	950	893-1007
200	132	929	852-1039	1400	1308-1523
250	132	1110	984-1295	1690	1551-1909
300	132	1228	1065-1476	1917	1725-2225
0	160	637	637-637	637	637-637
50	160	637	637-637	744	726-762
100	160	637	637-637	851	816-887
150	160	637	637-637	959	905-1012
200	160	637	637-637	1066	994-1137
250	160	922	853-1022	1485	1380-1591
300	160	1117	996-1294	1779	1637-1992
0	187	656	656-656	656	656-656
50	187	656	656-656	757	740-773
100	187	656	656-656	858	824-891
150	187	656	656-656	959	908-1009
200	187	656	656-656	1060	992-1127
250	187	656	656-656	1161	1076-1245
300	187	922	859-1013	1554	1442-1663
0	212	684	684-684	684	684-684
50	212	684	684-684	779	763-795
100	212	684	684-684	874	842-906
150	212	684	684-684	969	922-1017
200	212	684	684-684	1065	1001-1128
250	212	684	684-684	1160	1080-1239
300	212	684	684-684	1255	1159-1350

3.8 Acknowledgments

We gratefully thank Drs. Helen Dahlke, Jonathan Herman, Randy Dahlgren, Laura Foglia, and Yong Zhang for their feedback and modeling advice. Dr. Can Dogrul and the California Department of Water Resources Groundwater Modeling division offered instrumental C2VSim modeling guidance. Support for this research was provided by the University of California Agricultural and Natural Resources grant CA-D-LAW-6036-H, the National Science Foundation (NSF) Climate Change, Water, and Society (CCWAS) Integrated Graduate Education and Research Traineeship (IGERT) program at the University of California, Davis (<http://ccwas.ucdavis.edu>, DGE-10693333), the U.S./China Clean Energy Research Center for Water-Energy Technologies (CERC-WET), and the UC Office of the President's Multi-Campus Research Programs and Initiatives (MR-15-328473) through UC Water, the University of California Water Security and Sustainability Research Initiative. All data is accessible via Dryad at <https://datadryad.org/stash/dataset/doi:10.25338/B81P5K>, and procedures and models are accessible at <https://github.com/richpauloo/Monte-Carlo-Mixing-Model> (Richard Pauloo, 2020).

3.9 References

- Ayers, R. S., Westcot, & W, D. (1985). *Water quality for agriculture*. Food and Agriculture Organization of the United Nations Rome.
- Barlow, P. A. & Leake, S. A. (2015). *Streamflow Depletion by Wells—Understanding and Managing the Effects of Groundwater Pumping on Streamflow*. USGS.
- Barrett-Lennard, E. (2003). The interaction between waterlogging and salinity in higher plants: Causes, consequences and implications. *Plant and Soil*, 253(1), 35–54.
- Bear, J., Cheng, A. H.-D., Sorek, S., Ouazar, D., & Herrera, I. (1999). *Seawater intrusion in coastal aquifers: Concepts, methods and practices*. Springer Science & Business Media.
- Belitz, K. R. & Heimes, F. J. (1990). *Character and evolution of the ground-water flow system in the central part of the western San Joaquin Valley, California*. United States Geological Survey.
- Belitz, K. & Phillips, S. P. (1995). Alternative to agricultural drains in California's San Joaquin valley: Results of a regional-scale hydrogeologic approach. *Water Resources Research*, 31(8), 1845–1862.
- Bernstein, L. & Francois, L. (1973). Leaching requirement studies: Sensitivity of alfalfa to salinity of irrigation and drainage waters 1. *Soil Science Society of America Journal*, 37(6), 931–943.
- Brush, C. F., Dogrul, E. C., & Kadir, T. N. (2013). *Development and calibration of the California central valley groundwater-surface water simulation model (c2vsim), version 3.02-cg*. Sacramento, CA: Bay-Delta Office, California Department of Water Resources.
- Burow, K. R., Shelton, J. L., & Dubrovsky, N. M. (2008). Regional nitrate and pesticide trends in ground water in the eastern San Joaquin Valley, California. *Journal of Environmental Quality*, 37(5_Supplement), S-249.
- Burow, K. R., Stork, S. V., & Dubrovsky, N. M. (1998). *Nitrate and pesticides in ground water of the eastern San Joaquin Valley, California: Occurrence and trends*. USGS.
- Burt, C. M., Clemmens, A. J., Strelkoff, T. S., Solomon, K. H., Bliesner, R. D., Hardy, L. A., ... Eisenhauer, D. E. (1997). Irrigation performance measures: Efficiency and uniformity. *Journal of Irrigation and Drainage Engineering*, 123(6), 423–442.
- Campana, M. & Simpson, E. (1984). Groundwater residence times and recharge rates using a discrete-state compartment model and ¹⁴C data. *Journal of Hydrology*, 72(1-2), 171–185.
- Campana, M. E. [Michael E]. (1987). Generation of ground-water age distributions. *Groundwater*, 25(1), 51–58.
- Campana, M. E. [Michael Emerson]. (1975). *Finite-state Models of Transport Phenomena in Hydrologic Systems* (Doctoral dissertation, The University of Arizona, Tucson, Arizona, USA).
- Carroll, R. W., Pohll, G. M., Earman, S., & Hershey, R. L. (2008). A comparison of groundwater fluxes computed with MODFLOW and a mixing model using deuterium: Application to the eastern Nevada test site and vicinity. *Journal of Hydrology*, 361(3-4), 371–385.
- Chaudhuri, S. & Ale, S. (2014). Long term (1960–2010) trends in groundwater contamination and salinization in the Ogallala Aquifer in Texas. *Journal of Hydrology*, 513, 376–390.
- Cismowski, G., Cooley, W., Grober, L. S., Martin, J., McCarthy, M., Schnagl, R. S., & Toto, A. (2006). *Salinity in the Central Valley: An Overview*. Report of the Regional Water Quality Control Board, Central Valley Region, California Environmental Protection Agency (tech. rep. No. 206). Central Valley Regional Water Quality Control Board. Rancho Cordova, California.

- Cloutier, V., Lefebvre, R., Therrien, R., & Savard, M. M. (2008). Multivariate statistical analysis of geochemical data as indicative of the hydrogeochemical evolution of groundwater in a sedimentary rock aquifer system. *Journal of Hydrology*, 353(3-4), 294–313.
- CRWQCB. (2018). *Amendments to the Water Quality Control Plans for the Sacramento River and San Joaquin River Basins and Tulare Lake Basin To Incorporate a Central Valley-wide Salt and Nitrate Control Program*. California Environmental Protection Agency.
- CSWRBC. (2019a). A Compilation of Water Quality Goals. Retrieved February 7, 2019, from https://www.waterboards.ca.gov/water_issues/programs/water_quality_goals/
- CSWRBC. (2019b). California Regulations Related to Drinking Water, Title 22. Retrieved February 7, 2019, from https://www.waterboards.ca.gov/drinking_water/certlic/drinkingwater/Lawbook.html
- CSWRBC. (2019c). GAMA Groundwater Information System. Retrieved February 11, 2019, from <http://geotracker.waterboards.ca.gov/gamamap/public/>
- Dalin, C., Wada, Y., Kastner, T., & Puma, M. J. (2017). Groundwater depletion embedded in international food trade. *Nature*, 543(7647), 700–704.
- Datta, K. & De Jong, C. (2002). Adverse effect of waterlogging and soil salinity on crop and land productivity in northwest region of haryana, india. *Agricultural water management*, 57(3), 223–238.
- Davis, G. H., Green, J. H., Olmsted, F. H., & Brown, D. (1959). *Ground water conditions and storage capacity in the San Joaquin Valley, California*. USGS Water-Supply Paper 1469. Reston, Virginia: USGS.
- DeSimone, L. A., MacMahon, P. B., & Rosen, M. R. (2010). *Water Quality in Principal Aquifers of the United States , 1991 – 2010 Circular 1360*. USGS.
- Deverel, S. J. & Millard, S. P. (1988). Distribution and mobility of selenium and other trace elements in shallow groundwater of the western San Joaquin Valley, California. *Environmental science & technology*, 22(6), 697–702.
- Dogrul, E. C., Nadir, T., & Brush, C. F. (2018). *Integrated Water Flow Model IWFM-2015 Revision 706*. California Department of Water Resources.
- Döll, P., Hoffmann-Dobrev, H., Portmann, F. T., Siebert, S., Eicker, A., Rodell, M., ... Scanlon, B. R. (2012). Impact of water withdrawals from groundwater and surface water on continental water storage variations. *Journal of Geodynamics*, 59, 143–156.
- Domenico, P. A., Schwartz, F. W. et al. (1998). *Physical and chemical hydrogeology*. Wiley New York.
- ECORP. (2007). *Tulare lake basin hydrology and hydrography: A summary of the movement of water and aquatic species*. ECORP Consulting, Inc. U.S. Environmental Protection Agency.
- Eugster, H. P. [Hans P] & Hardie, L. A. [Lawrence A]. (1978). Saline lakes. In *Lakes* (pp. 237–293). Springer.
- Famiglietti, J. S. (2014). The global groundwater crisis. *Nature Climate Change*, 4(11), 945–948.
- Fankhauser, G. (2018). 2017 Kern County Agricultural Crop Report. Retrieved April 9, 2019, from http://www.kernag.com/caap/crop-reports/crop10_19/crop2017.pdf
- Faunt, C., Hanson, R. T., Belitz, K., Schmid, W., Predmore, S. P., Rewis, D. L., & McPherson, K. (2009). *Groundwater availability of the Central Valley Aquifer, California*, US Geological Survey Professional Paper (tech. rep. No. 1766). USGS. doi:[10.3133/pp1766](https://doi.org/10.3133/pp1766)
- Fetter, C. W. (2001). *Applied Hydrogeology* (4th). Upper Saddle River, NJ: Prentice Hall.

- Fogg, G. E. & LaBolle, E. M. (2006). Motivation of synthesis, with an example on groundwater quality sustainability. *Water Resources Research*, 42(3).
- Foster, S., Chilton, J., Moençg, M., Cardy, F., & Schiffler, M. (2000). *Groundwater in rural development: Facing the challenges of supply and resource sustainability*. The World Bank. doi:[10.1596/0-8213-4703-9](https://doi.org/10.1596/0-8213-4703-9)
- Fujii, R. & Swain, W. C. (1995). *Areal distribution of selected trace elements, salinity, and major ions in shallow ground water, Tulare Basin, southern San Joaquin Valley, California*. Water-Resour. Investig. Rep. 95-4048. USGS.
- Gailey, R. M., Fogg, G. E., Lund, J. R., & Medellin-Azuara, J. (2019). Maximizing on-farm groundwater recharge with surface reservoir releases: A planning approach and case study in California, USA. *Hydrogeology Journal*, 27(4), 1183–1206.
- Ghasemizade, M., Asante, K. O., Petersen, C., Kocis, T., Dahlke, H. E., & Harter, T. (2019). An integrated approach toward sustainability via groundwater banking in the southern central valley, California. *Water Resources Research*, 55(4), 2742–2759.
- Giordano, M. (2009). Global groundwater? Issues and solutions. *Annual review of Environment and Resources*, 34, 153–178.
- Gleeson, T., Wada, Y., Bierkens, M. F., & van Beek, L. P. (2012). Water balance of global aquifers revealed by groundwater footprint. *Nature*, 488(7410), 197–200.
- Greene, R., Timms, W., Rengasamy, P., Arshad, M., & Cresswell, R. (2016). *Soil and aquifer salinization: Toward an integrated approach for salinity management of groundwater* (A. J. Jakeman, O. Barreteau, R. J. Hunt, J.-D. Rinaudo, & A. Ross, Eds.). Cham: Springer International Publishing. doi:[10.1007/978-3-319-23576-9_15](https://doi.org/10.1007/978-3-319-23576-9_15)
- Grunsky, C. E. (1898). *Irrigation Near Bakersfield, California*. USGS. doi:[10.3133/wsp17](https://doi.org/10.3133/wsp17)
- Guo, Z., Fogg, G. E., & Henri, C. V. (2019). Upscaling of regional scale transport under transient conditions: Evaluation of the multirate mass transfer model. *Water Resources Research*, 55(7), 5301–5320.
- Guo, Z., Henri, C. V., Fogg, G. E., Zhang, Y., & Zheng, C. (2020). Adaptive multi-rate mass transfer (ammt) model: A new approach to upscale regional-scale transport under transient flow conditions. *Water Resources Research*.
- Hanak, E., Escrivá-Bou, A., Gray, B., Green, S., Harter, T., Jezdimirovic, J., ... Seavy, N. (2019). *PPIC: Water and the Future of the San Joaquin Valley* (tech. rep. No. February). Public Policy Institute of California.
- Hanak, E., Lund, J., Dinar, A., Gray, B., & Howitt, R. (2011). *Managing California's Water: From Conflict to Reconciliation*. San Francisco, CA: Public Policy Institute of California.
- Hansen, J. A., Jurgens, B. C., & Fram, M. S. (2018). Quantifying anthropogenic contributions to century-scale groundwater salinity changes, San Joaquin Valley, California, USA. *Science of the total environment*, 642, 125–136.
- Hanson, B. [Blaine], Grattan, S. R., & Fulton, A. (1999). *Agricultural salinity and drainage*. University of California Irrigation Program, University of California, Davis.
- Hanson, B. [Bob], Bowers, W., Davidoff, B., Kasapligil, D., Carvajal, A., & Bendixen, W. (1995). Field performance of microirrigation systems. In *Microirrigation for a changing world, proceedings of fifth international microirrigation congress, april 2–6* (pp. 769–774). American Society of Agricultural Engineers.

- Hardie, L. A. [Lawrence A.] & Eugster, H. P. [Hans P]. (1970). the Evolution of Closed-Basin Brines. *Mineral. Soc. Amer. Spec. Pap.* 3, 273–290.
- Harter, T. & Lund, J. R. (2012). *Addressing nitrate in California's drinking water: With a focus on Tulare Lake basin and Salinas Valley groundwater: Report for the state water resources control board report to the legislature.*
- Hem, J. D. (1985). *Study and interpretation of the chemical characteristics of natural water.* USGS.
- Henri, C. V. & Harter, T. (2019). Stochastic assessment of nonpoint source contamination: Joint impact of aquifer heterogeneity and well characteristics on management metrics. *Water Resources Research*, 55, 6773–6794.
- Hillel, D. (1992). *Out of the earth: Civilization and the life of the soil.* University of California Press.
- Hillel, D. (2000). *Salinity management for sustainable irrigation: Integrating science, environment, and economics.* The World Bank.
- Hook, J. (2018). 2017 Kings County Agricultural Crop Report. Retrieved April 9, 2019, from <https://www.countyofkings.com/home/showdocument?id=20426>
- Howell, T. A. (2003). Irrigation efficiency. *Encyclopedia of water science*, 467–472.
- Hunt, B. (1999). Unsteady stream depletion from ground water pumping. *Groundwater*, 37(1), 98–102.
- Ingerson, I. M. (1941). The hydrology of the Southern San Joaquin Valley, California, and its relation to imported water-supplies. *Eos, Transactions American Geophysical Union*, 22(1), 20–45.
- Johnson, A., Moston, R., & Morris, D. (1968). *Physical and hydrologic properties of water-bearing deposits in subsiding areas in central California, USGS Professional Paper 497-A*, 71.
- Jones, B. & Deocampo, D. (2003). Geochemistry of saline lakes. *Treatise on Geochemistry*, 5, 605.
- Jurgens, B. C., Burow, K. R., Dalgish, B. A., & Shelton, J. L. (2008). *Hydrogeology, water chemistry, and factors affecting the transport of contaminants in the zone of contribution of a public-supply well in Modesto, eastern San Joaquin Valley, California* (tech. rep. No. 2008–5156). USGS. doi:[10.3133/sir20085156](https://doi.org/10.3133/sir20085156)
- Jurgens, B. C., Fram, M. S., Belitz, K., Burow, K. R., & Landon, M. K. (2010). Effects of ground-water development on uranium: Central Valley, California, USA. *Groundwater*, 48(6), 913–928.
- Kang, M. & Jackson, R. B. (2016). Salinity of deep groundwater in California: Water quantity, quality, and protection. *Proceedings of the National Academy of Sciences*, 113(28), 7768–7773.
- Kaushal, S. S., McDowell, W. H., & Wollheim, W. M. (2014). Tracking evolution of urban biogeochemical cycles: Past, present, and future. *Biogeochemistry*, 121(1), 1–21.
- Kharaka, Y. K. & Thordesen, J. J. (1992). Stable isotope geochemistry and origin of waters in sedimentary basins. In *Isotopic signatures and sedimentary records* (pp. 411–466). Springer.
- Kirk, S. T. & Campana, M. E. [Michael E]. (1990). A deuterium-calibrated groundwater flow model of a regional carbonate-alluvial system. *Journal of Hydrology*, 119(1–4), 357–388.
- Kocis, T. N. & Dahlke, H. E. (2017). Availability of high-magnitude streamflow for groundwater banking in the central valley, California. *Environmental Research Letters*, 12(8), 084009.
- Kourakos, G. & Harter, T. (2014). Vectorized simulation of groundwater flow and streamline transport. *Environmental modelling & software*, 52, 207–221.

- Kreitler, C. W. (1993). *Geochemical techniques for identifying sources of ground-water salinization*. CRC press.
- Lindsey, B. & Johnson, T. (2018). Data from decadal change in groundwater quality web site, 1988-2014, version 2.0: U.s. geological survey. doi:[10.5066/F7N878ZS](https://doi.org/10.5066/F7N878ZS)
- Lopez-Berenguer, C., Martinez-Ballesta, M. d. C., Moreno, D. A., Carvajal, M., & Garcia-Viguera, C. (2009). Growing hardier crops for better health: Salinity tolerance and the nutritional value of broccoli. *Journal of agricultural and food chemistry*, 57(2), 572–578.
- Mahlknecht, J., Schneider, J. F., Merkel, B. J., De León, I. N., & Bernasconi, S. M. (2004). Groundwater recharge in a sedimentary basin in semi-arid mexico. *Hydrogeology Journal*, 12(5), 511–530.
- Mendenhall, W. C., Dole, R. B., & Stabler, H. (1916). *Ground water in San Joaquin Valley, California US Geological Survey Water-Supply Paper 398*, pp. 1–310.
- Munns, R. (2002). Comparative physiology of salt and water stress. *Plant, cell & environment*, 25(2), 239–250.
- Nativ, R. (2004). Can the desert bloom? Lessons learned from the Israeli case. *Groundwater*, 42(5), 651–657.
- Oetting, G. C., Banner, J. L., & Sharp Jr, J. M. (1996). Regional controls on the geochemical evolution of saline groundwaters in the edwards aquifer, central texas. *Journal of hydrology(Amsterdam)*, 181(1), 251–283.
- Palmer, C. D. & Cherry, J. A. (1984). Geochemical evolution of groundwater in sequences of sedimentary rocks. *Journal of hydrology*, 75(1-4), 27–65.
- Pauloo, R. [RA], Escriva-Bou, A., Dahlke, H., Fencl, A., Guillon, H., & Fogg, G. (2020). Domestic well vulnerability to drought duration and unsustainable groundwater management in california's central valley. *Environmental Research Letters*, 15(4), 044010.
- Pauloo, R. [Richard]. (2020). First release of ABCSAL mixing cell model accompanying the publication, "Anthropogenic Basin Closure and groundwater SALinization (ABCSAL)." . Github repository, <https://doi.org/10.5281/zenodo.3745508>.
- Pessarakli, M. (2016). *Handbook of plant and crop stress*. CRc press.
- Preston, W. L. (1990). *The tulare lake basin: An aboriginal cornucopia*. California Geographical Society.
- Richter, B. C. & Kreitler, C. W. (1986). Geochemistry of Salt Water Beneath the Rolling Plains, North-Central Texas. *Groundwater*, 24(6), 735–742.
- Russo, T. A. & Lall, U. (2017). Depletion and response of deep groundwater to climate-induced pumping variability. *Nature Geoscience*, 10(2), 105–108.
- Sandoval-Solis, S., Orang, M., Snyder, R., Orloff, S., Williams, K., & Rodriguez, J. (2013). *Spatial and temporal analysis of application efficiencies in irrigation systems for the state of california*. University of California Davis. Retrieved from http://watermanagement.ucdavis.edu/files/7913/7184/7743/Application_Efficiencies_-_UCDavis_-_Sandoval_Solis_et_al_2013_-_Conclusions.pdf
- Scanlon, B. R. [Bridget R.], Tyler, S. W., & Wierenga, P. J. (1997). Hydrologic issues in arid, unsaturated systems and implications for contaminant transport. *Reviews of Geophysics*, 35(4), 461–490. doi:[10.1029/97RG01172](https://doi.org/10.1029/97RG01172). eprint: <https://agupubs.onlinelibrary.wiley.com/doi/pdf/10.1029/97RG01172>

- Scanlon, B. R. [Bridget R], Faunt, C. C., Longuevergne, L., Reedy, R. C., Alley, W. M., McGuire, V. L., & McMahon, P. B. (2012). Groundwater depletion and sustainability of irrigation in the US High Plains and Central Valley. *Proceedings of the national academy of sciences*, 109(24), 9320–9325.
- Schmidt, K. D. (1975). Salt balance in groundwater of the tulare lake basin, california. In *Proceedings of the 1975 meetings of the arizona section* (pp. 177–184). Arizona-Nevada Academy of Science. Arizona-Nevada Academy of Science.
- Schoups, G., Hopmans, J. W., Young, C. A., Vrugt, J. A., Wallender, W. W., Tanji, K. K., & Panday, S. (2005). Sustainability of irrigated agriculture in the San Joaquin Valley, California. *Proceedings of the National Academy of Sciences*, 102(43), 15352–15356.
- Siebert, S., Burke, J., Faures, J.-M., Frenken, K., Hoogeveen, J., Döll, P., & Portmann, F. T. (2010). Groundwater use for irrigation—a global inventory. *Hydrology and earth system sciences*, 14(10), 1863–1880.
- Smith, R. G., Knight, R., Chen, J., Reeves, J., Zebker, H., Farr, T., & Liu, Z. (2017). Estimating the permanent loss of groundwater storage in the southern san joaquin valley, california. *Water Resources Research*, 53(3), 2133–2148.
- Smith, R. G., Knight, R., & Fendorf, S. (2018). Overpumping leads to california groundwater arsenic threat. *Nature communications*, 9(1), 2089.
- Sustainable Groundwater Management Act, California Water Code sec. 10720-10737.8. (2014). California State Water Resources Control Board.
- Tal, A. (2006). Seeking Sustainability: Israel's Evolving Water Management Strategy. *Science*, 313(August 2006), 1081–1085.
- TNC. (2014). *Groundwater and Stream Interaction in California's Central Valley: Insights for Sustainable Groundwater Management*. (tech. rep. No. February). The Nature Conservancy.
- Tóth, J. [Jozsef]. (1970). A conceptual model of the groundwater regime and the hydrogeologic environment. *Journal of Hydrology*, 10(2), 164–176.
- Tóth, J. [József]. (1999). Groundwater as a geologic agent: An overview of the causes, processes, and manifestations. *Hydrogeology journal*, 7(1), 1–14.
- USBR. (1970). *A Summary of Hydrologic Data for the Test Case on Acreage Limitation in Tulare Lake*. Hydrology Branch, Division of Project Development, Bureau of Reclamation.
- USGS. (2016). National water information system data available on the world wide web (usgs water data for the nation). doi:[10.5066/F7P55KJN](https://doi.org/10.5066/F7P55KJN)
- Vörösmarty, C. J., Green, P., Salisbury, J., & Lammers, R. B. (2000). Global water resources: Vulnerability from climate change and population growth. *Science*, 289(5477), 284–288.
- Wada, Y., Wisser, D., & Bierkens, M. F. (2014). Global modeling of withdrawal, allocation and consumptive use of surface water and groundwater resources. *Earth System Dynamics Discussions*, 5(1), 15–40.
- Wada, Y. [Yoshihide], Van Beek, L. P., Van Kempen, C. M., Reckman, J. W., Vasak, S., & Bierkens, M. F. (2010). Global depletion of groundwater resources. *Geophysical research letters*, 37(20).
- Weissmann, G. S., Zhang, Y., LaBolle, E. M., & Fogg, G. E. (2002). Dispersion of groundwater age in an alluvial aquifer system. *Water Resources Research*, 38(10), 16–1.
- Werner, A. D., Bakker, M., Post, V. E., Vandenbohede, A., Lu, C., Ataie-Ashtiani, B., ... Barry, D. A. (2013). Seawater intrusion processes, investigation and management: Recent advances and future challenges. *Advances in Water Resources*, 51, 3–26.

- Williamson, A. K., Prudic, D. E., & Swain, L. A. (1989). *Ground-water flow in the Central Valley, California, USGS Professional Paper 1401-D*. USGS. USGS.
- Winkel, L. H., Trang, P. T. K., Lan, V. M., Stengel, C., Amini, M., Ha, N. T., ... Berg, M. (2011). Arsenic pollution of groundwater in vietnam exacerbated by deep aquifer exploitation for more than a century. *Proceedings of the National Academy of Sciences*, 108(4), 1246–1251.
- Wooding, R., Tyler, S. W., & White, I. (1997). Convection in groundwater below an evaporating salt lake: 1. onset of instability. *Water Resources Research*, 33(6), 1199–1217.
- Wright, L. (2018). 2017 Fresno County Annual Crop & Livestock Report. Retrieved April 9, 2019, from <https://www.co.fresno.ca.us/Home>ShowDocument?id=30066>
- Wright, M. (2018). Tulare County Crop and Livestock Report 2017. Retrieved April 9, 2019, from <https://agcomm.co.tulare.ca.us/ag/index.cfm/standards-and-quarantine/crop-reports1/crop-reports-2011-2020/2017-crop-report/>
- Zektser, S., Loáiciga, H. A., & Wolf, J. (2005). Environmental impacts of groundwater overdraft: Selected case studies in the southwestern united states. *Environmental Geology*, 47(3), 396–404.
- Zhang, H., Harter, T., & Sivakumar, B. (2006). Nonpoint source solute transport normal to aquifer bedding in heterogeneous, markov chain random fields. *Water Resources Research*, 42(6).

Chapter 4

Mean flow direction modulates non-Fickian transport in a heterogeneous alluvial aquifer-aquitard system.¹

4.1 Abstract

Regional-scale groundwater quality degradation from nonpoint source pollution threatens the long-term sustainability of major alluvial aquifer-aquitard systems worldwide. Upscaled transport models can efficiently model regional nonpoint source transport, but fail to accurately characterize non-Fickian (anomalous) transport caused by transience in the mean flow direction. In this study we demonstrate that hydrogeologic factors explain this failure. Specifically, vertical anisotropy in K and seasonal pumping and recharge in typical alluvial aquifer systems can fundamentally change hydraulic gradients and shift the mean flow direction between mostly horizontal and mostly vertical flow. In order to understand the relationship between large shifts in mean flow direction

¹This chapter will be submitted to *Water Resources Research*: Pauloo, R. A., Fogg, G. E., Guo, Z. & Henri, C. V. “Mean flow direction modulates non-Fickian transport in a heterogeneous alluvial aquifer-aquitard system”.

and transport phenomena, we simulate 3D flow and transport of a conservative solute in a heterogeneous alluvial aquifer under varying mean flow directions representative of typical seasonal hydraulic gradient fluctuations. We examine tailing, plume spreading, and the spatial distribution of final particle positions. Results indicate that alterations to hydraulic gradients which control the mean flow direction can lead to increasingly non-Fickian transport. When flow is mostly horizontal, diffusion and slow advection dominant low-K facies slow mass transfer rates out of low-K material, and preferential flow along connected high-K networks cause increased spatial spreading along the mean flow direction. In contrast, predominantly vertical flow caused by spatially distributed pumping and recharge shifts mass transfer processes in low-K material from diffusion and slow advection dominant to advection dominant, which results in vertically oriented particle trajectories that compactly migrate through high and low K facies alike, and leads to increasingly Fickian transport. Thus, fluctuations in mean flow direction driven by vertical anisotropy of K and seasonal pumping and recharge in a typical alluvial aquifer-aquitard system create oscillating patterns of transport, ranging from persistently non-Fickian to more Fickian. Results illustrate the hydrogeologic factors that explain why upscaled transport models fail to capture non-Fickian transience in mean flow direction.

4.2 Introduction

Basin-scale groundwater quality in alluvial aquifer systems is threatened by nonpoint source contaminants including agricultural fertilizers (Burow, Shelton, & Dubrovsky, 2008), pesticides (Burow et al., 2008; Burow, Stork, & Dubrovsky, 1998), nitrates (Harter & Lund, 2012; Christopher Vincent Henri & Harter, 2019), and total dissolved solids (Hansen, Jurgens, & Fram, 2018a; Lindsey & Johnson, 2018) on large temporal (e.g., decades to centuries) and spatial scales (e.g., tens to hundreds of kilometers). Thus, regional groundwater quality management models (Fogg & LaBolle, 2006) are needed that can robustly represent non-Fickian (i.e., anomalous) transport under a range of geologic heterogeneity and transient flow boundary conditions encountered on large temporal and spatial scales. However, modeling regional nonpoint transport remains a

challenging task due to ubiquitous non-Fickian spreading which is difficult to model at regional scales with existing approaches, especially when the boundary conditions shift from steady state to transient flow (Guo, Henri, Fogg, Zhang, & Zheng, 2020; LaBolle & Fogg, 2001).

Transport modeling is challenged by non-Fickian transport across pore (Kang et al., 2014; Morales, Dentz, Willmann, & Holzner, 2017), field (Garabedian, LeBlanc, Gelhar, & Celia, 1991; Le Borgne & Gouze, 2008), and regional scales (Sivakumar, Harter, & Zhang, 2005; Christopher Vincent Henri & Harter, 2019), and in diverse heterogeneous geologic formations such as alluvial aquifers (G. S. Weissmann, Zhang, LaBolle, & Fogg, 2002; LaBolle & Fogg, 2001; Guo, Fogg, & Henri, 2019) and discrete fracture networks (Hyman, Painter, Viswanathan, Makedonska, & Karra, 2015; Edery, Geiger, & Berkowitz, 2016). Non-Fickian transport may be measured by features including nonlinear scaling of the second spatial moment (i.e., the mean squared displacement), early breakthrough, and late-time arrival (i.e., tailing) of solutes (Valocchi, 1985; Freyberg, 1986; Yong Zhang, Benson, & Baeumer, 2007; Haggerty, McKenna, & Meigs, 2000). The ubiquity of non-Fickian effects across disciplines and natural systems, and the inherent uncertainty in characterizing the scale and space-time dependencies of anomalous transport in heterogeneous media has led to multiple conceptualizations of how to mathematically model and upscale non-Fickian transport (Neuman & Tartakovsky, 2009).

Numerous studies show that anomalous transport in geologic media depends strongly on spatially heterogeneous hydraulic conductivity (Gelhar & Gelhar, 1993; Gedeon Dagan & Neuman, 2005; De Marsily et al., 2005), which gives rise to the velocity field (Brian Berkowitz, Cortis, Dentz, & Scher, 2006). In many alluvial aquifer-aquitard complexes, variability in the hydraulic conductivity (K) of sediments can range over 4-7 orders of magnitude (Fetter, 2001; Fogg & Zhang, 2016). The fluvial deposition processes that form alluvial aquifer-aquitard systems over millennia result in correlated fields (Galloway & Hobday, 2012), with interconnecting, high- K , coarse sand and gravel lenses (Fogg, 1986) that can percolate in all spatial dimensions (Fogg, Carle, & Green, 2000), even at substantially low volume fractions, such as 13% as noted in 3D percolation studies by Harter (2005). These high- K preferential flowpaths facilitate anomalous early time arrival, and are embedded within low- K , fine-grained clays and silts, which typically comprise the majority of

alluvial aquifer-aquitard volume fractions (Galloway & Hobday, 2012), and contribute to mass hold back and anomalous late-time solute tailing (LaBolle & Fogg, 2001; Brian Berkowitz et al., 2006; Haggerty et al., 2000; Benson, Wheatcraft, & Meerschaert, 2000).

The interaction between spatial heterogeneity and hydraulics determines transport processes. However, anomalous transport studies commonly investigate simple hydraulic boundary conditions characterized by a unidirectional gradient (Benson, Schumer, Meerschaert, & Wheatcraft, 2001; Edery, Guadagnini, Scher, & Berkowitz, 2014; Edery et al., 2016; Harvey & Gorelick, 2000; Pedretti, Fernández-Garcia, Sanchez-Vila, Bolster, & Benson, 2014; Willmann, Carrera, & Sánchez-Vila, 2008; LeBlanc et al., 1991; Julian, Boggs, Zheng, & Feehley, 2001; Z. Zhang & Brusseau, 1999; Christopher V Henri & Fernández-Garcia, 2015), which is typical of natural, ambient groundwater flow (e.g. a horizontal hydraulic gradient on the order of 10^{-3} Fetter, 2001). Many of these studies hold hydraulic boundary conditions constant in order to investigate how changing the spatial heterogeneity of the domain impacts solute transport. However, because of horizontal stratification of coarse- and fine-grained facies typical of many clastic sedimentary environments and hence significant vertical anisotropy of effective hydraulic conductivity (K), the vertical hydraulic gradients commonly exceed horizontal gradients by a factor of $10^1 - 10^2$ (e.g. Fogg, 1986; Belitz, Phillips, & Gronberg, 1993). In even moderately developed groundwater basins, and especially in agriculturally intensive ones, high rates of seasonal pumping and recharge from irrigation can further increase vertical hydraulic gradients (Styles & Burt, 1999; Gailey, 2018). Yet, only a few modeling studies investigate non-Fickian transport under such large shifts in regional hydraulic gradient, and these studies tend to emphasize local scale breakthrough measured at extraction wells or control planes. Matheron and De Marsily (1980) demonstrated in a 2D model with limited spatial heterogeneity that flow parallel to the bedding direction leads to preasymptotic anomalous transport, even at very long timescales because the solute travels along an increasingly non-stationary medium. Christopher Vincent Henri and Harter (2019) demonstrated that well design characteristics (e.g., well depth, pumping rate, and screen length) have a significant impact on the uncertainty of late arrival times generated by heterogeneity. Similarly, Libera, de Barros, and Guadagnini (2017) demonstrated that temporally variable pumping rates strongly affected contaminant breakthrough

curves at the pumping well. Guo et al. (2019) investigated anomalous transport arising from the transition from predominately horizontal to vertical flow, and found that internal hydraulic gradients between the high- and low-K materials strongly affect mass transfer between hydrofacies. Furthermore, (Guo et al., 2020) showed that an upscaled multirate mass transfer model failed to capture tailing effects when the mean flow direction changed. Thus, prior work suggests that hydraulic boundary condition transience can strongly impact non-Fickian transport, we still lack an understanding of how shifting hydraulic gradients (as opposed to the unidirectional gradient that most studies explore) may modulate the degree of anomalous transport observed in a heterogeneous aquifer-aquitard complex.



To the best of our knowledge, no studies have investigated the impact of mean flow direction on non-Fickian transport within a 3D, kilometer-scale, alluvial aquifer-aquitard system. Such a question bears importantly on modeling macroscopic nonpoint source transport in large alluvial groundwater systems, and may shed light on how to build better upscaled transport models that perform well across a range of transient hydraulic gradient conditions.

In this study, we simulate groundwater flow and random walk particle tracking in a detailed hydrofacies model of a typical alluvial aquifer-aquitard complex (with high vertical anisotropy in K) subject to an increasingly high vertical to horizontal hydraulic gradient ratio (VHGR), which is an indicator of the mean flow direction. In other words, if we increase the vertical hydraulic gradients in a system by a factor of 10, 100, or 1000 (e.g., due to natural geologic variation in vertical anisotropy of K, or during the transition from a fallow winter season to a summer growing season characterized by pumping and recharge), does this makes the transport more non-Fickian, and if so, by how much, and why? Changes in anomalous nonpoint source transport are compared between differing steady-state VHGR scenarios which collectively represent snapshots along a transition from predominantly horizontal (low VHGR) to vertical flow (high VHGR). We examine tailing, spatial variance of the nonpoint source plume, and the spatial distribution of final particle position to quantify and explain differences in non-Fickian spreading. Results are discussed in the context of the transition from advection to diffusion dominant systems, and related to the hydrogeology of the study site. We explore how our findings support a conceptualization of regional scale nonpoint source contaminant

migration characterized by oscillating patterns of non-Fickian transport, and how this perspective might inform the development of upscaled regional groundwater quality management models (Fogg & LaBolle, 2006).

4.3 Methods

First, a heterogeneous, hydrofacies-based geostatistical model of the Kings River alluvial fan in California's Central Valley was developed. Next, four VHGR scenarios of increasingly vertical groundwater flow were simulated, and used to solve the particle transport of a conservative solute. Lastly, the resulting 3D Lagrangian particle trajectories were analyzed in terms of their tailing, second spatial moment, and spatial distribution of final particle position.



4.3.1 Heterogeneous hydrofacies model and study site

The three-dimensional, spatially-correlated hydraulic conductivity domain (Figure 4.1) was simulated with Transition Probability Geostatistical Software (T-PROGS), which uses the transition probability approach described by Carle and Fogg (1996, 1997), Carle (1999). Details of the facies model are provided in G. S. Weissmann, Carle, and Fogg (1999), G. S. Weissmann and Fogg (1999), G. S. Weissmann, Mount, and Fogg (2002), G. S. Weissmann, Zhang, Fogg, and Mount (2004), and a brief summary is provided here.

A subsection of the Central Valley aquifer (California, USA) in the Kings River fan, was chosen as a study site representative of a typical alluvial aquifer for its high vertical anisotropy ($K_h/K_v = 238$), and its validated performance in simulating both flow (hydraulic head) and transport (groundwater age distribution) (G. S. Weissmann, Zhang, et al., 2002). The hydrofacies model was conditioned by analyzing more than 40 000 surface and shallow subsurface (< 2 m) features (e.g., borings, excavations, road cuts, and natural exposures) (Huntington, 1980), approximately 150 m of core and geophysical logs (Burow, Weissmann, Miller, & Placzek, 1997), approximately 1,000 m of continuous core (Harter et al., 2005), and numerous drillers' logs from water wells in the study area (G. S. Weissmann & Fogg, 1999). These analyses defined a conceptual geologic model

and the T-PROGS model parameters.

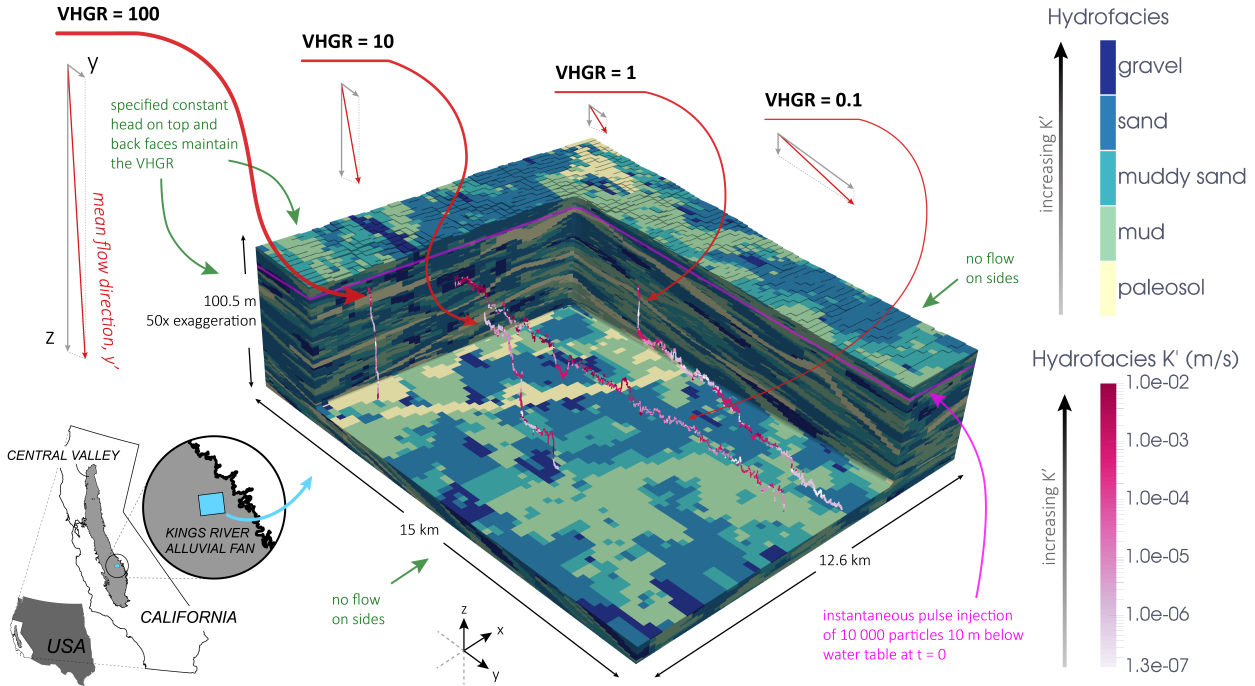


Figure 4.1: The Kings River alluvial fan hydrofacies model in California’s Central Valley (USA) with a section cut away to reveal the geologic heterogeneity and four representative particle trajectories from the four VHGR scenarios in this study (section 4.3.3). The location of the instantaneous nonpoint source term (10 000 particles, 10 m below the water table) is represented by a horizontal pink line. Particle trajectories are increasingly horizontal and non-Fickian with decreasing VHGR. Note that the vectors representing flow in z , y , (and their geometric sum in the mean flow direction, y') are illustrative, and not drawn to scale.

The Kings River alluvial fan is composed of four sequences created during Pleistocene glacial cycles and a fifth basal depositional unit prior to major glaciation events, each separated by laterally-extensive paleosols that formed during inter-glacial periods of pedogenesis (G. S. Weissmann, Mount, & Fogg, 2002), which, owing to their relatively low hydraulic conductivity, act as aquitards. Notably, one unit represents a incised valley fill of coarse-grained sediment, created by large glacial  wash in the east-west y direction of the domain. Key parameters derived from these analyses that constrained the T-PROGS model include the hydrofacies proportions, mean lengths

in xyz , and the embedded transition probabilities in xyz , which reflect the cross-correlation between facies and thus the probability that one facies contacts another in a given direction (Carle & Fogg, 1996). Next, Markov chain models corresponding to each unit were developed and combined to represent the highly heterogeneous stratigraphy: overlapping alluvial fans, interspersed with laterally-extensive paleosols, and a cross-cutting incised valley fill. G. S. Weissmann et al. (2004) provides a detailed overview of the development and combination of these models into a single conductivity field.

The model dimensions in xyz are 12.6 km x 15 km x 100.5 m, with discretization $\Delta x = \Delta y = 200$ m, and $\Delta z = 0.5$ m. Spatially variable K estimated from pumping tests, slug tests, core measurements, and literature values for similar lithologies (Burow, 1999; G. S. Weissmann et al., 1999) were assigned to each of the model cells by their simulated hydrofacies, which include gravel, sand, sandy mud, muddy sand, and paleosols (Table 4.1).

Hydrofacies	$l_x(m)$	$l_y(m)$	$l_z(m)$	$K(m/s)$	P_e^{100}	P_e^{10}	P_e^1	$P_e^{0.1}$
gravel	200	650	1.5	1.0E-02	2.05E+09	2.05E+08	2.05E+07	2.05E+06
sand	625	1500	3.3	1.0E-03	5.13E+08	5.13E+07	5.13E+06	5.13E+05
muddy sand	400	800	1.4	1.0E-05	2.90E+06	2.90E+05	2.90E+04	2.90E+03
mud	NA	NA	1.0	1.0E-06	289.86	28.99	2.9	0.29
paleosol	800	1500	1.9	1.3E-07	71.59	7.16	0.72	0.07

Table 4.1: Hydrofacies properties including mean lengths l in xyz directions (strike, dip, and vertical in Figure 4.1), hydraulic conductivity K (m/s), and average Peclet number across the VHGR scenarios.

We only use one realization of the hydrofacies model (Figure 4.1) because previous studies demonstrate that non-Fickian transport behavior does not appreciably differ between realizations due to good connectivity of aquifer facies (Guo et al., 2019; G. S. Weissmann, Zhang, et al., 2002).

4.3.2 Groundwater flow and transport simulation

Steady state, groundwater flow in the geostatistical model grid (Section 4.3.1) is simulated in MODFLOW (Harbaugh, Banta, Hill, & McDonald, 2000; McDonald & Harbaugh, 1988). The 3D groundwater flow equation used to compute long-term, average confined flow is:

$$\frac{\partial}{\partial x}(K_{xx}\frac{\partial h}{\partial x}) + \frac{\partial}{\partial y}(K_{yy}\frac{\partial h}{\partial y}) + \frac{\partial}{\partial z}(K_{zz}\frac{\partial h}{\partial z}) + W = S_s \frac{\partial h}{\partial t} \quad (4.1)$$

where K_{xx} , K_{yy} , and K_{zz} [LT^{-1}] are the hydraulic conductivities along the x , y , and z coordinate axes; h [L] is the potentiometric head; W [T^{-1}] is the volumetric flux per unit volume of sources ($W > 0$) or sinks ($W < 0$); S_s [L^{-1}] is the specific storage; and t [T] is time.

The water table is represented on the top of the domain with a constant head boundary condition, which is the same across all scenarios. Vertical flow out of the bottom of the model and into deeper groundwater, due to a combination of pumping at depth and recharge from above, is represented by another constant head boundary condition on the bottom of the domain, and is altered depending on the VHGR scenario in question (discussed in section 4.3.3). Two more constant head boundary conditions on the front and back faces of the model maintain a horizontal groundwater flow gradient of 0.001 along the y direction (Figure 4.1), and represent mountain front recharge along the eastern model boundary. Head values are spatially distributed across all active faces such that the mean flow direction is uniform across the entire domain (SI Appendix Figure 4.7). No flow boundaries are specified along the right and left faces of the domain (along the x direction).

Solute transport is simulated by the random-walk particle tracking method (LaBolle, Quastel, & Fogg, 1998; LaBolle, Quastel, Fogg, & Gravner, 2000) applied in the code RW3D (Fernández-Garcia, Illangasekare, & Rajaram, 2005; Christopher V Henri & Fernández-Garcia, 2014, 2015; Salamon, Fernández-Garcia, & Gómez-Hernández, 2006) that solves the advection-dispersion equation:

$$\theta \frac{\partial c}{\partial t} = \nabla \cdot (\theta D \nabla c) - \nabla \cdot (qc) \quad (4.2)$$

where c is the concentration of the dissolved solute [ML^{-3}], θ is the effective porosity [−], and \mathbf{D} is the dispersion tensor, defined as $\mathbf{D} = (\alpha_T |\mathbf{q}| + D^*) \mathbf{I} + (\alpha_L - \alpha_T) \mathbf{q} \mathbf{q}^t / |\mathbf{q}|$, where D^* is the molecular diffusion coefficient [$L^2 T^{-1}$], α_L and α_T are the longitudinal and transverse dispersivities [L], \mathbf{I} is the Dirac delta function, and $|\mathbf{q}|$ is the magnitude of the velocity vector [LT^{-1}].

The source term is a discrete, instantaneous pulse injection of 10 000 particles at 10 m below the water table (Figure 4.1). To simulate the spatial variability of contaminant mass arrival at the water table, flux-weighted injection is used to initialize particle motion. Simulations are run for a sufficient number of time steps such that all particles exit the domain (SI Appendix Table 4.4), and that the mean Lagrangian hydrofacies proportions (i.e., the proportion of particles in each hydrofacies) converge on the actual hydrofacies proportions over time (SI Appendix Figure 4.7). The Lagrangian particle tracking methods used in this study can be very computationally intensive, especially for the case of a regional-scale nonpoint source term, where the size of the domain (and hence the number of particles used to sample it) is large. Adding multiple injections of particles was computationally unrealistic, and moreover, under steady state flow, a continuous source injection and instantaneous pulse injection yield similar results.

LaBolle and Fogg (2001) demonstrated for a similar hydrofacies-based domain that solute transport results were insensitive to local-scale α , which was insignificant compared to the dispersion caused by the hydrofacies-scale heterogeneity of the conductivity domain. Moreover, G. S. Weissmann, Zhang, et al. (2002) investigated sensitivity analyses with α_L and $\alpha_T = 0.1$ m and = 0.01 m in the same Kings River Fan domain that we use in this study, and found that between geostatistical realizations, the simulation results did not differ appreciably in terms of the overall transport. Thus, we set longitudinal, transverse horizontal, and transverse vertical dispersivities to 0.01 times the cell discretization, $\alpha_L = \alpha_{TH} = 2.0$ m, and $\alpha_{TV} = 0.005$ m. These local-scale dispersivities were maintained across the VHGR scenarios in order to ensure comparability. We assume a conservative (non-reactive, non-sorbing) solute and set the molecular diffusion coefficient $D^* = 6.9\text{E-}10$ m²/s, based on G. S. Weissmann, Zhang, et al. (2002).

4.3.3 Hydraulic gradient scenarios

This aim of this study is to investigate the influence of mean flow direction on non-Fickian transport, thus we compare systems under different vertical to horizontal gradient ratio (**VHGR**):

$$VHGR = i_v/i_h \quad (4.3)$$

where i_v is the vertical gradient $\partial h/\partial z$, and i_h is the horizontal gradient $\partial h/\partial y$ (Figure 4.1). Increasing VHGR corresponds to increasingly vertical flow. Four scenarios are simulated, in which VHGR is varied over four orders of magnitude by fixing $i_h = 0.001$ (representing ambient horizontal groundwater flow from mountain front recharge), and adjusting i_v :

- VHGR = 0.1 ($i_v = 0.0001$): primarily horizontal flow with minimal recharge
- VHGR = 1 ($i_v = 0.001$): equal horizontal and vertical gradients
- VHGR = 10 ($i_v = 0.01$): substantial component of vertical groundwater flow
- VHGR = 100 ($i_v = 0.1$): dominantly vertical flow

 Because of the strong vertical anisotropy caused by the stratified interbedding of coarse and fine facies, the ratio between effective K_h and K_v in our study site is 238, which tends to produce natural values of VHGR > 1 in such systems (e.g. Fogg, 1986). Groundwater development by pumping can further increase VHGR, and the augmentation of recharge due to irrigation can still further increase it. For example, values of i_v in portions of the Central Valley can vary from order 10^{-3} in winter (non-pumping season) to 10^{-1} in summer (pumping season). Hence, taken independently, the four steady state VHGR flow fields represent stages along a transition from ambient, primarily horizontal groundwater flow to predominantly vertical flow induced by natural anisotropy in K and pumping and recharge, and permit an investigation of long-term plume evolution across these different hydraulic gradient conditions.

Across each VHGR, the Peclet number, P_e (i.e., the ratio of the characteristic time scales of advection to diffusion) was calculated for each hydrofacies (Table 4.1).

$$P_e = K i l / D^* \theta \quad (4.4)$$

where i is the vertical hydraulic gradient of the VHGR scenario and $D^* = 6.9\text{E-}10 \text{ m}^2/\text{s}$ (G. S. Weissmann et al., 2004; G. S. Weissmann, Labolle, Fogg, & Zhang, 2002), and θ is the hydrofacies porosity. Due to the influence of vertical gradients, P_e of gravel, sand, and muddy sand

were calculated using mean horizontal length scales (l_x , l_y), whereas the P_e of mud and paleosol were calculated using vertical length scales (l_z). For gravel, sand, and muddy sand, $\theta = 0.3$, and for mud and paleosol, $\theta = 0.5$. Mud was used as a background category, thus its lateral mean lengths (l_x and l_y) were already determined in the process of Markov chain modeling of the transition probability (G. S. Weissmann et al., 1999).

Generally, system-wide $P_e > 1$ is considered advection dominant, $P_e < 1$ indicates diffusion dominance, and slow advection (which may resemble a more diffusion-like process) may occur at relatively small P_e less than 1 (Guswa & Freyberg, 2000). In heterogeneous aquifer-aquitard systems, which vary in terms of the hydraulic conductivity field, porosity, and hydraulic gradient, P_e varies spatially. Importantly, the P_e of low-K mud and paleosol hydrofacies in this study can transition between advection and diffusion dominance due to changes in flow rates in these hydrofacies caused by different VHGR, with consequences for macroscopic transport behavior.

4.3.4 Metrics of non-Fickian transport

In order to compare the impact of various VHGR scenarios on anomalous transport, we measure tailing by fitting a tempered fractional advection-dispersion equation (TFADE) to breakthrough curves and comparing the tempering parameter. Tailing is the late-time arrival of solutes at a control plane, and indicates mass holdback in fines. We also compute the time and space evolution of the mean squared displacement (MSD), or second spatial moment, which measures the variance in plume displacement and represents how “spread out” all of the particles are from one another due to mass holdback and preferential flow. Lastly, we investigate the spatial distribution of final particle positions with respect to the site’s geologic heterogeneity, which illustrates preferential flow.

Between VHGR scenarios, travel times are re-scaled by $t_c = l_c/\bar{v}$, where t_c is the characteristic travel time to travel the average facies length, and l_c and \bar{v} are the characteristic length and mean velocity along the mean flow direction y' (details provided in SI Appendix Section 4.7.2 and Table 4.3).

4.3.4.1 Tailing

In order to quantify differences in tailing, a tempered fractional advection-dispersion equation (TFADE) model (Meerschaert, Zhang, & Baeumer, 2008) was fit to breakthrough at a control plane along the bottom face of the model:

$$\frac{\partial C(y', t)}{\partial t} + \beta e^{-\lambda t} \frac{\partial^\gamma [e^{\lambda t} C(y', t)]}{\partial t^\gamma} - \beta \lambda^\gamma C(y', t) = -V_L \frac{\partial C(y', t)}{\partial y'} + D_L \frac{\partial^2 C(y', t)}{\partial y'^2} \quad (4.5)$$

where t [T] is time; C [ML^{-3}] is the concentration; y' [L] is the position along the longitudinal direction; V_L [LT^{-1}] is the longitudinal velocity; D_L [L^2T^{-1}] is the molecular dispersion coefficient; β [$T^{\gamma-1}$] is the fractional capacity coefficient, which governs the mobile fraction; γ [-] is the time fractional order; λ [T^{-1}] is the tempering parameter. Importantly, λ represents the probability that the waiting times in the immobile phase transfer from a power-law to exponential distribution and thus, provides a quantitative measure of tailing: as λ approaches infinity, the TFADE reverts to the classic advection-dispersion equation, and a decreasing λ indicates longer tailing.

It was assumed that the sample of initial particles that exit the bottom face of the domain represented macroscopic breakthrough along this plane if the domain was infinitely wide in the x and y dimensions, and if simulation time was unlined. As VHGR decreases, horizontal flow causes more particles to exit the down-gradient face, yet a substantial fraction of 10 000 initial particles exit the bottom face in each simulation: 78.0, 74.7, 16.8, 7.7 % of particles break through the bottom of the domain after 1000 characteristic times in VHGR = 100, 10, 1, and 0.1 respectively.

4.3.4.2 Spatial variance

Next, the time evolution of the plume spatial variance is calculated. The mean squared displacement along a given direction x is:

$$\sigma_x^2 = \langle (x(t) - \langle x(t) \rangle)^2 \rangle \quad (4.6)$$

where $\langle \cdot \rangle$ denotes the average position in the x direction over all particles, and every particle is first initialized to an identical reference location (i.e., centered spatial moment). We calculate the spatial variance in the longitudinal, transverse vertical, and transverse horizontal directions using (4.6). Fickian diffusion occurs when the plume MSD varies as t^ϕ , where $\phi = 1$ (Berkowitz & Braester, 1991; Neuman, 1990). By contrast, non-Fickian transport occurs when ϕ does not equal unity. Super- and subdiffusion refer to $\phi > 1$ and $\phi < 1$ respectively. In order to ensure the MSD represented an accurate measure of macroscopic spatial variance of the plume (and not boundary effects created by early exiting particles), we restrict our analysis of the MSD results to before 32 characteristic time scales ($t/t_c \approx 10^{1.5}$). 

4.3.4.3 Final particle position

Lastly, we compare spatial distribution of final particle positions (i.e., the location at which particles exit the domain), and the geologic heterogeneity of the domain. The spatial patterns of particle exit points strongly illustrate preferential flow along high-K hydrofacies and lend insight into transport dynamics across VHGR scenarios.

4.4 Results

4.4.1 Tailing in breakthrough

Tailing  quantified in the vertical dimension, because downward contaminant migration is of practical concern to water quality in groundwater wells, and exacerbates site cleanup efforts.  We fit a TFADE model (Meerschaert et al., 2008) to breakthrough measured at a control plane along the bottom face of the model for each scenario, then compared fitted values of the tempering parameter λ (Section 4.3.4.1), which controls the immobile phase transfer from a power-law to exponential distribution (e.g., decreasing λ indicates more tailing) between scenarios. The fitted TFADE models agree well with the simulated breakthrough across all VHGR scenarios (Figures 4.2a-d). Importantly, as VHGR decreases, the fitted tempering parameter λ also decreases (Table 4.2), suggesting that between VHGR = 100 and VHGR = 0.1, the probability that particle waiting

times transfer from power-law to exponential distribution decrease by about a factor of 10^2 , roughly corresponding to the 10^3 change in vertical gradient across the scenarios (Table 4.1).

Late time slopes of the breakthrough curves were also measured, and are consistent with the TFADE results: as VHGR decreases and flow is increasingly horizontal, more tailing is observing, and consequently, late time slopes are increasingly positive (Figure 4.2e). Furthermore, the change in λ between between VHGR = 100 and 10 and between VHGR = 10 and 1 (about an order of magnitude difference) decreases to about a twofold difference of λ change between VHGR = 1 and 0.1 (Table 4.2). These differences in the change in λ are consistent with the change in the slope of the breakthrough curves (Figure 4.2e). Hence, results suggest that as VHGR decreases and the transport is increasingly dominated by diffusion limited trajectories, the late time tails reflect this limit.

VHGR	$\beta[T^{\gamma-1}]$	$\gamma[-]$	$\lambda[T^{-1}]$
100	0.50	0.88	6.0E-4
10	0.65	0.88	5.0E-5
1	0.80	0.85	7.5E-6
0.1	0.80	0.85	4.0E-6

Table 4.2: Fitted TFADE model parameters indicate an increasingly small tempering parameter as VHGR decreases, consistent with the observation of increased tailing in low VHGR scenarios.

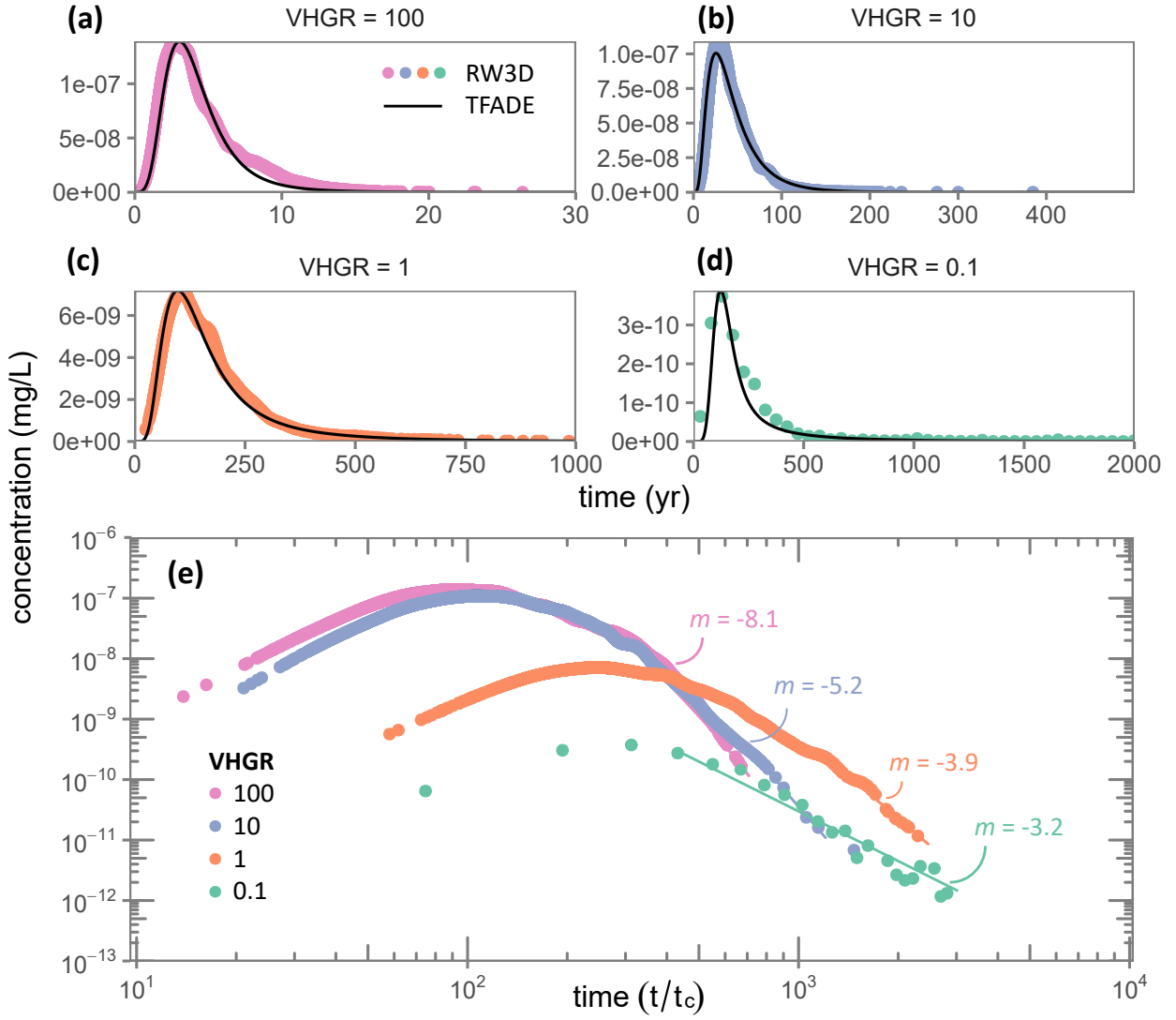


Figure 4.2: (a-d) RW3D breakthrough curves (colored points) and fitted TFADE models (black line) measured at the bottom face of the domain (Figure 4.1) for the four VHGR scenarios. Note the difference in x-axis travel times. (e) Breakthrough curves are normalized by the characteristic travel time (see SI Appendix Table 4.3 for details). Measured slopes of tails (denoted as m) increase as VHGR decreases, corresponding to increasingly anomalous transport.

4.4.2 Temporal evolution of the plume spatial variance

Temporal evolution of the centered second spatial moments (Equation 4.6) in the longitudinal and transverse directions are superdiffusive and non-Fickian at early times across all VHGR

scenarios; late time transitions either remain persistently preasymptotic, or revert to Fickian scaling, depending on the hydraulic gradient conditions (Figure 4.3). We now summarize spreading in the three directions:

4.4.2.1 Longitudinal spatial variance

The magnitude of longitudinal spatial variance (Figure 4.3a) increases with decreasing VHGR, and is preasymptotic and non-Fickian after 32 characteristic times for VHGR = 10, 1, and 0.1. In contrast, when VHGR = 100, late time longitudinal spreading is asymptotic and nearly Fickian ($\phi = 0.95$). Spatial plume variance is around 4 orders of magnitude greater for VHGR = 0.1 compared to VHGR = 100 at all times. This large difference in the scale of spreading results in a wider-ranging residence time distribution between the scenarios (Figure 4.5a). A strong vertical hydraulic gradient when VHGR = 100 forces particles through nearly all facies in the downward, longitudinal direction (perpendicular to bedding layers), effectively generating an ergodic sample of the system heterogeneity much more rapidly than in scenarios with lower VHGR, thus late time spreading becomes in more Fickian nature. By contrast, at low VHGR, some of the plume remains trapped in fines, and some spreads longitudinally along preferential pathways—both of which stretch the plume.

4.4.2.2 Transverse vertical spatial variance

Like longitudinal spreading, transverse vertical spreading (Figure 4.3b) in VHGR = 100 differs between the other three VHGR scenarios. VHGR = 100 is ballistic (i.e., $\phi > 2$) at early times ($\phi = 2.84$) due to entirely advection dominant facies (Table 4.1) and strong lateral connectivity of a high-K incised valley fill (Figure 4.4a) in the transverse vertical direction that facilitates preferential flow (discussed further in Sections 4.4.3 and 4.5.2). However this spatial variance slows to nearly Fickian spreading ($\phi = 0.95$) at late times. By contrast, VHGR = 10, 1, and 0.1 are super diffusive at early times ($1.77 \leq \phi \leq 1.91$) but remain persistently preasymptotic and superdiffusive ($1.34 \leq \phi \leq 1.36$) at late times rather than reverting to Fickian scaling as in VHGR = 100.

The smaller magnitude of transverse vertical spatial variance observed when VHGR =

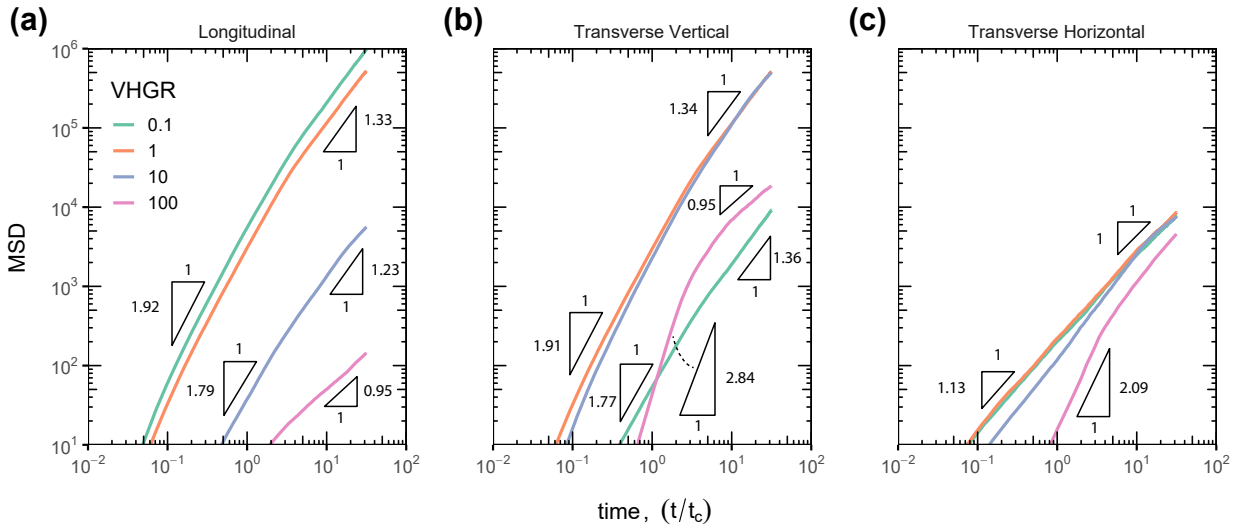


Figure 4.3: Temporal evolution of the centered second spatial moments (Equation 4.6) calculated from the distribution of particle trajectories along the (a) longitudinal, (b) transverse vertical, and (c) transverse horizontal directions indicate superdiffusive early time scaling that reduces to less superdiffusive or Fickian scaling in late times, depending on the VHGR and direction of scaling. Triangles at early and late times show the slope of MSD temporal scaling, ϕ (Section 4.3.4.2).

100 and 0.1 is explained by plume interactions with aquifer heterogeneity. When flow is vertical and downward (VHGR = 100), transverse transport is horizontal, tends to occur along extensive preferential pathways, and is driven toward these pathways by a powerful vertical gradient and all advection dominant facies. When flow is horizontal (VHGR = 0.1), transverse vertical transport is limited by diffusion dominant, laterally extensive paleosols and muds, which prevent spreading along this direction. The middle scenarios (VHGR = 1 and 10) by contrast have stronger vertical gradients to move particles past the first laterally extensive low-K layers, and then a combination of advection, slow advection, and diffusion dominant facies, which creates greater transverse vertical spreading.

The smaller magnitude of transverse vertical spatial variance observed when VHGR = 100 and 0.1 compared to VHGR = 10 and 1 is explained by plume interactions with aquifer heterogeneity. When flow is vertical and downward (VHGR = 100), transverse vertical transport

occurs along the y direction, which due to relatively high K'_y compared to K'_z should facilitate rapid spreading. However because all facies are advection dominant (Table 4.1) under the influence of powerful vertical gradients, particle trajectories tend to move relatively straight down along non-tortuous particle trajectories. For a different reason, when flow is horizontal ($\text{VHGR} = 0.1$), transverse vertical transport is limited by diffusion dominant, laterally extensive paleosols and muds, which prevent spreading along this direction. The middle scenarios ($\text{VHGR} = 1$ and 10) have a combination of advection, slow advection, and diffusion dominant facies, which simultaneously hold some mass back, and also move particles through laterally extensive low-K facies and layers, all of which results in relatively greater transverse vertical spreading.

4.4.2.3 Transverse horizontal spatial variance

The absence of a gradient in the transverse horizontal direction (Figure 4.3c) limits superdiffusive early time scaling ($1.13 \leq \phi \leq 2.09$), and leads to late time asymptotic Fickian scaling ($\phi = 1$) after 32 characteristic times across all VHGR scenarios. We suspect that transverse horizontal early time superdiffusive scaling when $\text{VHGR} = 100$ is related to the same processes that create early time superdiffusive transverse vertical spreading: migration into preferential pathways. However, since the mean lengths of gravels (and the incised valley fill) in the transverse horizontal x direction are less than in the transverse vertical y , the slope of early time superdiffusion is also less.

In all directions and across all VHGR scenarios tested in this study (except for the $\text{VHGR} = 100$ in the longitudinal direction), superdiffusive early time scaling becomes more Fickian in late times as particles explore more of the system space, and hence the transport is increasingly ergodic. When $\text{VHGR} = 100$, late time longitudinal and transverse second moments approach Fickian scaling (rather than remaining persistently asymptotic), which suggests that an advection dominant system with powerful vertical hydraulic gradients can have a homogenizing impact on the anomalous transport created by system-scale heterogeneity. Furthermore, it illustrates how the degree of non-Fickian effects created when the mean flow direction changes (e.g., persistent superdiffusive scaling) may challenge upscaled approaches that currently fail to capture non-Fickian

effects under similar boundary condition transience (Guo et al., 2020).

4.4.3 Influence of geology on preferential flow and tailing

Non-Fickian transport is influenced by geologic heterogeneity in the hydrofacies model, including a high-K, interconnected incised valley fill, laterally extensive low-K paleosols, and the large volume fraction of low-K mud that plays an important role in diffusion and slow advection dominant transport.

The incised valley fill runs ~~the~~ laterally along the y direction, and interconnects to an exit on the down-gradient side of the domain (Figures 4.4a-b). As VHGR decreases, particles take increasingly horizontal trajectories, and the incised valley fill and other interconnecting sand and gravel lenses act as a conduit for preferential flow that cause more particles exit the down-gradient side of the domain (Figures 4.4d,f,h,j), where they form clusters around gravel and sand facies (Figure 4.4b). Across all VHGR scenarios, particle trajectories that exit via the incised valley fill on the down-gradient side tend to exit at earlier timescales compared to other particles that exit the down-gradient side (lighter colored dots in the black oval compared to darker colored dots without outlines in Figures 4.4c,e,g,i), and compared to particles that take longer flowpaths and exit the bottom of the model at late times (darker colored dots in Figures 4.5c,e,g,i).

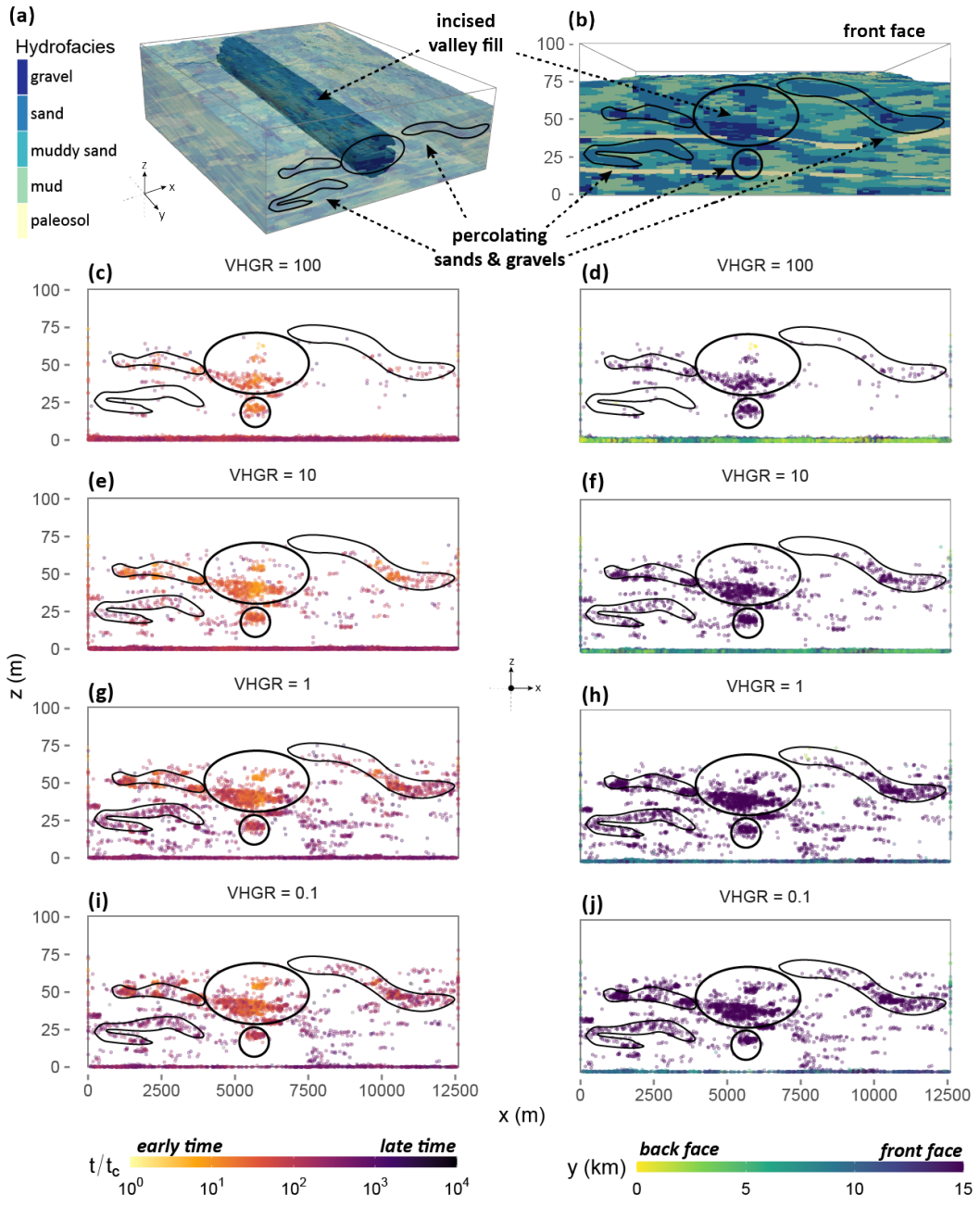


Figure 4.4: (a) Transparent hydrofacies domain highlighting a lateral, interconnected sand and gravel incised valley fill; (b) The down-gradient side of the domain. A black oval marks the incised valley fill exit, and black outlines mark prominent interconnecting sands and gravel bodies that promote preferential flow. These same regions are marked in black in all other subplots; (c,e,g,i) The final z and x position of particles, colored by the time they exit the domain (residence time); (d,f,h,j) the final z and x position of particles, colored by the length (y) into the page, where yellow is the up-gradient side and purple is the down-gradient side. Particle clusters at $z = 0$ m indicate trajectories that exit the bottom face (Figure 4.5).

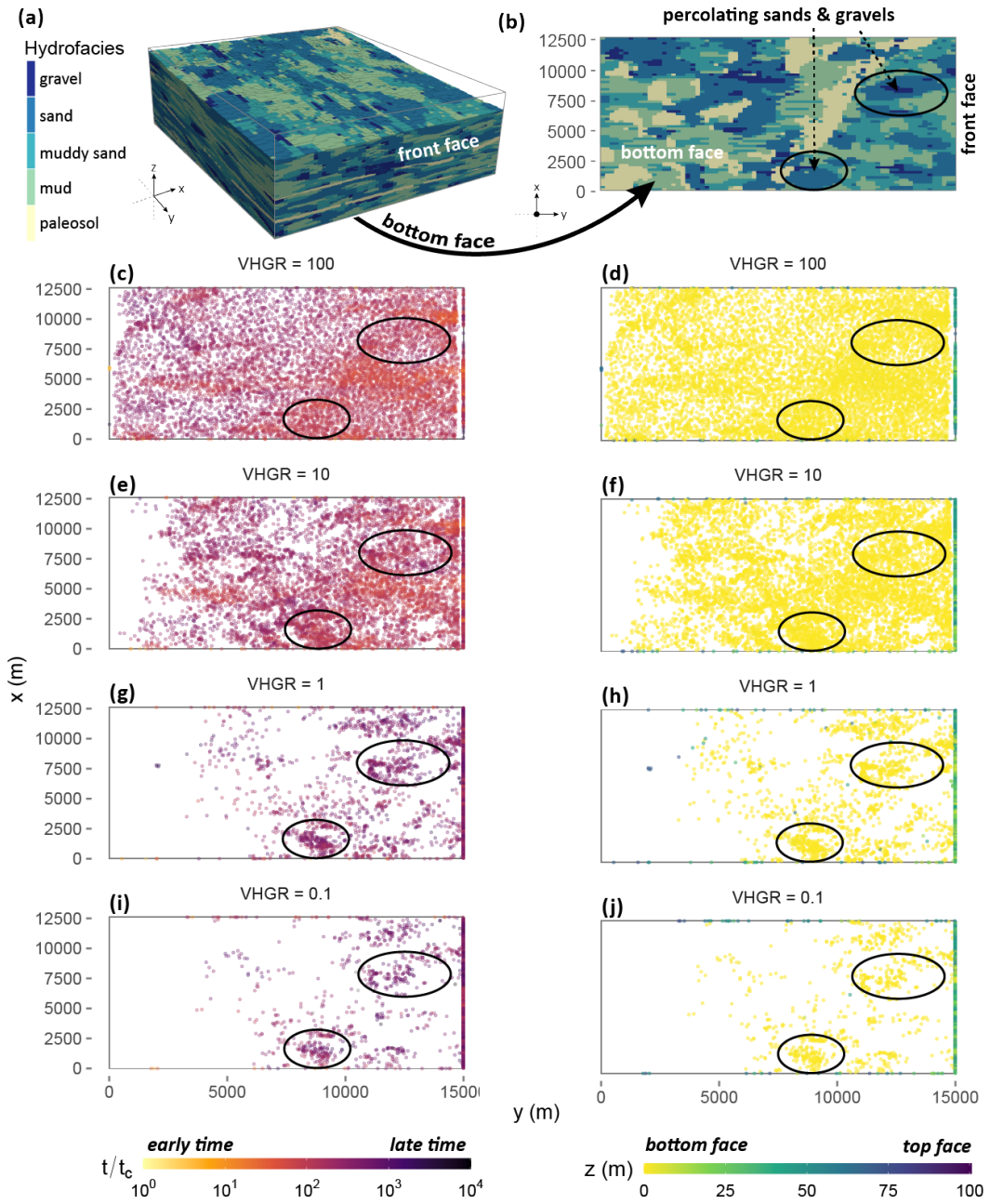


Figure 4.5: (a) The 3D hydrofacies domain; (b) the bottom of the domain with prominent sand and gravel bodies outlined in black; (c,e,g,i) the final x and y position of particles, colored by the time they exit the domain (residence time); (d,f,h,j) the final x and y position of particles, colored by the length (z) into the page, where yellow is the bottom face and purple is the top face. Particle clusters at $y = 15\,000\, m$ indicate trajectories that exit the down-gradient side of the domain (Figure 4.4).

Notably, even at VHGR = 100 when most particle trajectories take vertical paths and exit the bottom face of the domain (yellow points in Figure 4.5d), some particles rapidly migrate in the transverse vertical direction along the incised valley fill to exit the down-gradient side (purple dots in the black oval in Figure 4.4d). Moreover, early time arrival through the incised valley fill when VHGR = 100 (Figure 4.4c) suggests that transverse horizontal preferential flow still occurs along interconnected coarse facies even under strong vertical gradients, and explains the ballistic early time transverse vertical scaling ($\phi = 2.84$) in this scenario (Figure 4.3b).

Laterally extensive low-K paleosols limit (Figure 4.4b) the vertical migration of particles, and create segmented breakthrough along the down-gradient side of the domain where particles tend to exit above or below paleosol layers, but rarely through them (Figures 4.4d,f,h,j).

4.5 Discussion

4.5.1 Mean flow direction modulates the degree of non-Fickian transport

In clastic sedimentary environments, significant vertical anisotropy in K and seasonal pumping and recharge can create strong vertical hydraulic gradients that in turn cause oscillations in mean flow direction. This study aimed to assess impacts of these shifting flow directions on the regional-scale, non-Fickian transport of nonpoint source contaminants in a typical alluvial aquifer-aquitard complex. Results demonstrate that shifting VHGR can *modify the degree* of non-Fickian transport. Decreasing VHGR led to increasingly non-Fickian transport, measured by tailing at a control plane along the bottom face of the model, increased and persistent non-Fickian scaling of the second spatial moment, and increased preferential flow along interconnected high-K facies.

Our results are consistent with previous studies which demonstrate that non-Fickian spreading measured (at a target well) can accompany the change from plume migration along an ambient groundwater gradient, to transient pump-and-treat conditions (LaBolle & Fogg, 2001; Guo et al., 2019; Guswa & Freyberg, 2000), which facilitates the release of mass stored in fine-grained material. Results illustrate that non-Fickian spreading of a nonpoint source plume depends on the mean flow direction, modified in many aquifer systems worldwide by ubiquitous pumping

wells (Famiglietti, 2014; Gleeson, Wada, Bierkens, & van Beek, 2012; Wada et al., 2010) that increase vertical head gradients and drive flow downward.



Together, the increasingly non-Fickian effects (e.g., increased tailing, greater spatial spreading) that result as the mean flow direction shifts from horizontal to vertical suggest a conceptual model of nonpoint source transport in agriculturally intensive alluvial groundwater basins characterized by oscillating patterns of more Fickian vertical migration during periods of intense pumping and recharge, interspersed by periods of persistently non-Fickian lateral plume stretching under ambient groundwater flow when pumps are off and fields are not irrigated, except perhaps in areas with significant natural vertical anisotropy in K. These insights into the dependence of non-Fickian transport on mean flow direction bear importantly on efforts to model and manage nonpoint source contamination like salts (Hansen, Jurgens, & Fram, 2018b) and nitrates (Pastén-Zapata, Ledesma-Ruiz, Harter, Ramirez, & Mahlknecht, 2014) in large irrigated basins where the flow boundary conditions (and hence VHGR) are inherently transient. Thus, an unresolved challenge for existing methods that upscale the advection-dispersion equation (Neuman & Tartakovsky, 2009) is the ability to capture the varying non-Fickian behavior of regional, nonpoint source transport resulting from changes in the mean flow direction (Guo et al., 2020). This study advances a hydrogeologic perspective towards understanding the physical genesis of this challenge.

4.5.2 Hydrogeologic heterogeneity underpins non-Fickian transport

Differing degrees of non-Fickian transport and plume spreading arise from hydrogeologic heterogeneity in the study site, which can be understood in terms of high ln-K variance, the transition from diffusion to advection dominant transport, and persistently non-Fickian transport caused by preferential flow and mass holdback.

4.5.2.1 The role of high ln-K variance

The geologically-based conductivity field in this study represents multi-scale heterogeneity, by which we mean multiple geologic sequences with large variance in K (G. S. Weissmann & Fogg, 1999), in contrast to stochastic Gaussian models with typical ln-K variances, $\sigma_{lnK}^2 < 1$

or 2 (Gelhar & Gelhar, 1993; Rubin, 2003). For our study site, $\sigma_{lnK}^2 = 8.3$, approximated by $\sigma_{lnK}^2 \approx R^2/3$ (Fogg & Zhang, 2016), where R is the range between the minimum and maximum values of K in orders of base 10 magnitude (i.e., 5 in this study). Results suggest that non-Fickian transport is strongly affected by the transition of low-K facies along diffusion, slow advection, and advection dominated system states (Section 4.5.2.2); and by the presence of an incised valley fill and laterally extensive, low-K paleosols (Section 4.5.2.3). Furthermore, the persistently preasymptotic MSD scaling observed in some VHGR scenarios reinforce the notion suggested by other researchers (e.g. Matheron & De Marsily, 1980; Neuman, 1990; X. Zhang & Lv, 2007) that the late-time transition from non-Fickian to Fickian transport may never occur in natural geologic formations under certain gradient conditions. Thus, a key component to capturing non-Fickian effects is proper parameterization of the ln-K variance of the spatial heterogeneity.

4.5.2.2 Transitions between diffusion and advection dominant transport

In a spatial model with ln-K variance, transience in the hydraulic gradients can create systems that range from fully advection dominant, to systems of mixed advection and diffusion dominance, the latter of which will have greater non-Fickian effects.

As VHGR increases and flow is increasingly vertical, the hydrofacies Peclet number (Table 4.1) and hence advection dominant transport also increases. Importantly, in our study site, as VHGR increases from 0.1 to 100, the mud and paleosol facies shift from diffusion dominant ($P_e < 1$) to slow advection and advection dominant ($P_e > 1$). Consequently, high VHGR causes mass to migrate nearly straight through fines, consistent with the findings of Guswa and Freyberg (2000), who observed accelerated solute release from low permeability zones under the influence of pumping in a slow-advection mass transfer system. In contrast to a diffusion dominant system, pumping would have little to no effect on the mass release from fines. Slow-advection is thus more related to the groundwater velocity, as opposed to a mass transfer model that strictly assumes diffusive controls on mass release from low permeability lenses. In this study, the decrease in non-Fickian transport observed at increasing VHGR and hence P_e leads us to speculate that hydraulic forcings may exert a similar effect on transport as aquifer-aquitard spatial properties (e.g. H.-Zhang, Harter,

& Sivakumar, 2006; Yong Zhang et al., 2007; Yin et al., 2020; Zhang, Green, & Fogg, 2013). For instance, Zhang et al. (2013) found that in domains containing hydrofacies with relatively short mean lengths, particles moved more rapidly between hydrofacies, which increased the likelihood for solutes to sample the full range of flow velocities, and thus more rapidly reach ergodicity. Similarly, we find that strong vertical flow (e.g., VHGR = 100) can push particles through all facies alike, thus accelerating mass transport between hydrofacies and rapidly reaching ergodicity. Furthermore, Yong Zhang et al. (2007), Zhang et al. (2013) observed that diffusion limited vertical floodplain layer thicknesses controlled late time non-Fickian solute tailing. Similarly, our results suggest that higher VHGR can shift facies from diffusion to advection dominance and diminish non-Fickian tailing. Hence, non-Fickian transport imparted by spatial heterogeneity should not be viewed as constant, but rather, as continually modified by hydraulic transience.

4.5.2.3 Persistent non-Fickian transport

Describing persistent, late time, non-Fickian transport observed in this study (Section 4.4.2) remains a modeling challenge. We now discuss the factors that control persistently preasymptotic non-Fickian transport, specifically how it relates to hydrofacies heterogeneity, preferential flow, and the transition from diffusion to advection dominant transport.

First, the super-linear growth of early time plume spatial variance observed in this study (i.e., superdiffusion, $\phi > 1$) is consistent with other simulations in heterogeneous porous media (Zhang et al., 2013; Kang et al., 2014; Hunt, Skinner, Ewing, & Ghanbarian-Alavijeh, 2011). The conventional understanding of this phenomenon is that preferential flow in highly permeable facies stretches the plume front downstream, while the trailing plume tail remains trapped by low-permeability facies near the source (Fiori, Janković, & Dagan, 2003; Dagan, Fiori, & Janković, 2003; Yong Zhang, Green, & Baeumer, 2014; LaBolle & Fogg, 2001). As ergodicity is reached in late times, plume spatial variance approaches Fickian scaling, which has been observed in numerous experiments (e.g. Kang et al., 2014; Le Borgne et al., 2010; Cortis, Gallo, Scher, & Berkowitz, 2004) and is relatively easier to model. However, persistently asymptotic behavior may never arise because the time needed to reach asymptotic behavior in natural geologic systems may be sufficiently large

that the solute will encounter new spatial nonstationarities along the displacement distance before Fickian scaling is reached, and is thus always in a state of transition, never reaching asymptotic behavior (Matheron & De Marsily, 1980; Gillham, Sudicky, Cherry, & Frind, 1984; Neuman, 1990).

We speculate that the multiple-scale geologic heterogeneity in our study area causes persistently non-Fickian superdiffusion at late times in longitudinal and transverse directions for all $VHGR \leq 10$. This persistent late time non-Fickian transport is supported by LaBolle and Fogg (2001), who noted persistent preasymptotic ambient transport in a similar well-connected, hydrofacies-based alluvial fan model. Moreover, X. Zhang and Lv (2007) found that transition times in simple, 2D uniform media were so large, that the authors speculated that in natural geologic media with multiple-scale heterogeneity, the transition from anomalous to Fickian transport may never complete. Complimentary to these observations, our results indicate that sufficiently high $VHGR$ can reduce the impact of mass sequestration in fines, lead to a more compact plume in all directions, and hence, promote asymptotic late time Fickian scaling in all dimensions, thus lending itself towards being more appropriately described by an upscaled model.

The important role of preferential flow on persistent non-Fickian transport is illustrated by the impact of a lateral, connected, incised valley fill and other prominent interconnecting sand and gravel bodies (Figure 4.4a). When $VHGR = 100$, rapid particle migration into the incised valley fill transverse vertical to the mean flow direction resulted in early time hyper-ballistic scaling ($\phi = 2.84$) of transverse vertical MSD that slowed to nearly Fickian scaling ($\phi = 0.95$) at late times as ergodicity was reached. In contrast, when $VHGR = 10, 1$, and 0.1 , preferential flow along high-K networks stretched some of the plume at the same time that fines sequestered other parts of it, leading to persistent and oftentimes a greater magnitude of late-time spreading ($\phi = 1.34 - 1.36$). Across all scenarios, particles traveled laterally through the incised valley and exited the down-gradient side at relatively earlier times (Figure 4.4c). Observations of faster transport along highly-permeable, interconnected sand and gravel lenses are consistent with numerous studies of preferential flow (Winograd & Pearson Jr, 1976; Jussel, Stauffer, & Dracos, 1994; Moreno & Tsang, 1994; Tsang & Neretnieks, 1998; Fogg, 1986; Heeren et al., 2010; Maxwell, Carle, & Tompson, 2008; Zheng & Gorelick, 2003; G. S. Weissmann et al., 2004; LaBolle & Fogg, 2001).

Final particle positions and the hydrofacies they occupy at that time further illustrate the importance of advection and diffusion dominant transport and preferential flow. When VHGR = 100 and advection dominates transport, particles are nearly indiscriminate in terms of the facies they occupy upon exiting the bottom face of the domain (i.e., even spatial distribution of yellow dots in Figure 4.5d). By contrast, when VHGR = 0.1, spatial patterns of particles that exit the bottom face of the domain (yellow dots in Figure 4.5j)) and the down-gradient side (purple dots in Figure 4.4j) correlate with more conductive, high K facies (blue and dark blue sand and gravel in Figures 4.5b and 4.4b). This indicates preferential flow along interconnecting sand and gravel lenses, and partly explains the increased non-Fickian transport with decreasing VHGR as a result of relatively rapid plume stretching along these fast flowpaths.

4.5.3 Implications for upscaled transport models

The varying degrees of non-Fickian transport that arise from the interaction of hydraulics and geologic heterogeneity challenge the application of the advection-dispersion equation towards subsurface transport problems in natural geologic media. At regional scales (e.g., tens to hundreds of kilometers), subsurface characterization may be intractable or cost-prohibitive, and even if reliable subsurface models were available, the computational complexity of solving transport over these scales would be enormous. Hence, regional upscaled transport models are needed. These upscaled models must be able to represent non-Fickian effects created by preferential flow in connected high-conductivity facies, mass transfer processes between high- and low-conductivity media, and as we show in this study, the different degrees of non-Fickian transport introduced by changes in the mean flow direction due to varying VHGR (e.g., in the case of significant pumping and recharge).

In a previous study, Guo et al. (2020) demonstrated an adaptive multirate mass transfer (aMMT) model which improved breakthrough curve estimation for diffusion dominant transient flow by incorporating time-dependent mass transfer coefficients based on the equivalent flow velocity. However, the aMMT approach failed to capture tailing in breakthrough curves when the mean flow direction changed, as in the case of shifting VHGR. In this study, we extend the work of Guo et al. (2020) and illustrate that as VHGR changes, the transition from diffusion to slow advection and

advection dominance in the discrete hydrofacies of a system can fundamentally change the mass transfer processes. Specifically, high VHGR (provided it creates system-wide advection dominance) can cause solutes to move nearly straight through facies (e.g., Figures 4.1 4.5d even though the vertical effective K is much less than the horizontal effective K, whereas low VHGR (diffusion to slow advection dominance some facies) can lead to mass holdback in fines (Figure 4.2) and strong preferential flow (Figures 4.4h,j and 4.5h,j). Thus, a future promising direction towards the goal of improving estimation of late time tailing under transient flow is to quantify changes in VHGR, P_e , mean flow direction, and characteristic length scales along the mean flow direction, and relate these to mass transfer processes parameters in a upscaled model (e.g., aMMT).

4.5.4 Study limitations and additional considerations

We explore highly detailed nonpoint source plume evolution across a series of steady state flow simulations in order to observe regional-scale, long term transport under conditions that represent the transition from relatively ambient groundwater flow to predominantly vertical flow. However, these steady state simulations do not capture mass transfer effects that occur when hydraulic boundary conditions rapidly change, as in the case of a pumping well being turned on. For example, Bastani and Harter (2020) found that transport models based on steady state flow did not capture short-term oscillations of nitrate concentrations in pumping wells at the local scale. Similarly Guo et al. (2020) showed that the aMMT model failed to reproduce transport when the flow direction changed, and (LaBolle & Fogg, 2001) observed the release of mass stored in fine-grained material when boundary conditions changed from plume migration along an ambient groundwater gradient, to transient pump-and-treat conditions. Thus a future challenge is to explore nonpoint source plume evolution in a transient simulation that incorporates transitions between each VHGR scenario, and which represents the hydraulic conditions observed in natural irrigated basins with extensive pumping.

Heterogeneous porous media affects reactive solute transport by controlling solute mixing and residence times (Perez-Fodich & Derry, 2019), which may be more important for certain solutes and depth zones. In this study, we simulate a nonreactive solute, which may not be suitable for

some nonpoint source contaminants in fully saturated groundwater. More research needed on how reaction rates may alter the non-Fickian effects explored in this study, for instance, by mineral dissolution of the domain which adds a source term (Schoups et al., 2005), or in the case of nitrates, by denitrification in the soil zone (Lee, Lee, Hyun, Clement, & Hamilton, 2006).

It is well known that hydrofacies geometry influences contaminant transport, and hence, our study is best interpreted with respect to the characteristic geology of the domain. For example, Yin et al. (2020) found that larger hydrofacies width increased high-permeability connectivity, and thus superdiffusion; conversely, larger mean hydrofacies thickness slowed solute migration and reduced plume scaling. Any extrapolation the results presented herein to other areas should be accompanied by a careful consideration of the hydrogeology of the new study site.

4.6 Conclusions

We simulated 3D steady state groundwater flow and nonpoint source contaminant transport in a regional scale ($15 \text{ km} \times 12.6 \text{ km} \times 100 \text{ m}$) geostatistical representation of a heterogeneous alluvial aquifer-aquitard system. In horizontally stratified clastic sedimentary aquifer systems it is common for the strong vertical anisotropy of hydraulic conductivity to produce spatially and temporally varying vertical and horizontal components of the hydraulic gradient, in turn producing a complex interplay between the stratified heterogeneity and physical transport processes. These effects can be augmented and made highly transient by the effects of pumping and recharge in, for example an agricultural system where oscillations between primarily horizontal and primarily vertical flow are caused by seasonal fluctuations in pumping as well as the recharge produced by irrigation. Thus we tested the impact of these varying mean flow directions on non-Fickian transport, and observed increasingly non-Fickian transport as flow was increasingly horizontal (i.e., when the VHGR decreased). Importantly, when VHGR was large (e.g., 100), the plume was more compact: particle trajectories exhibited late time asymptotic Fickian scaling of spatial variance, and moved perpendicular to the direction of aquifer bedding (even though the vertical effective K is much less than the horizontal effective K), and nearly straight through high- and low-conductivity facies alike.

As VHGR decreased (e.g., 10 and 1) flow became more horizontal and transport was more non-Fickian – particle trajectories increasingly moved along laterally extensive facies, took preferential flowpaths, and exhibited greater (and preasymptotic) spatial spreading and tailing in breakthrough measured along a control plane at the bottom face of the model. Hence, the non-Fickian transport imparted by spatial heterogeneity should not be viewed as constant, but rather, as continually modified by hydraulic transience that may transition facies from diffusion to advection dominance and thus alter non-Fickian mass transfer dynamics. These results illustrate why conventional methods to upscale anomalous transport under transient flow conditions remains a challenge, and indicates that future efforts to upscale regional-scale, transient nonpoint source transport may benefit by incorporating information on the time-dependent changes in VHGR, P_e , mean flow direction, and characteristic length scales along the direction of mean flow.

4.7 Supporting Information Appendix

4.7.1 Simulated groundwater head for VHGR scenarios

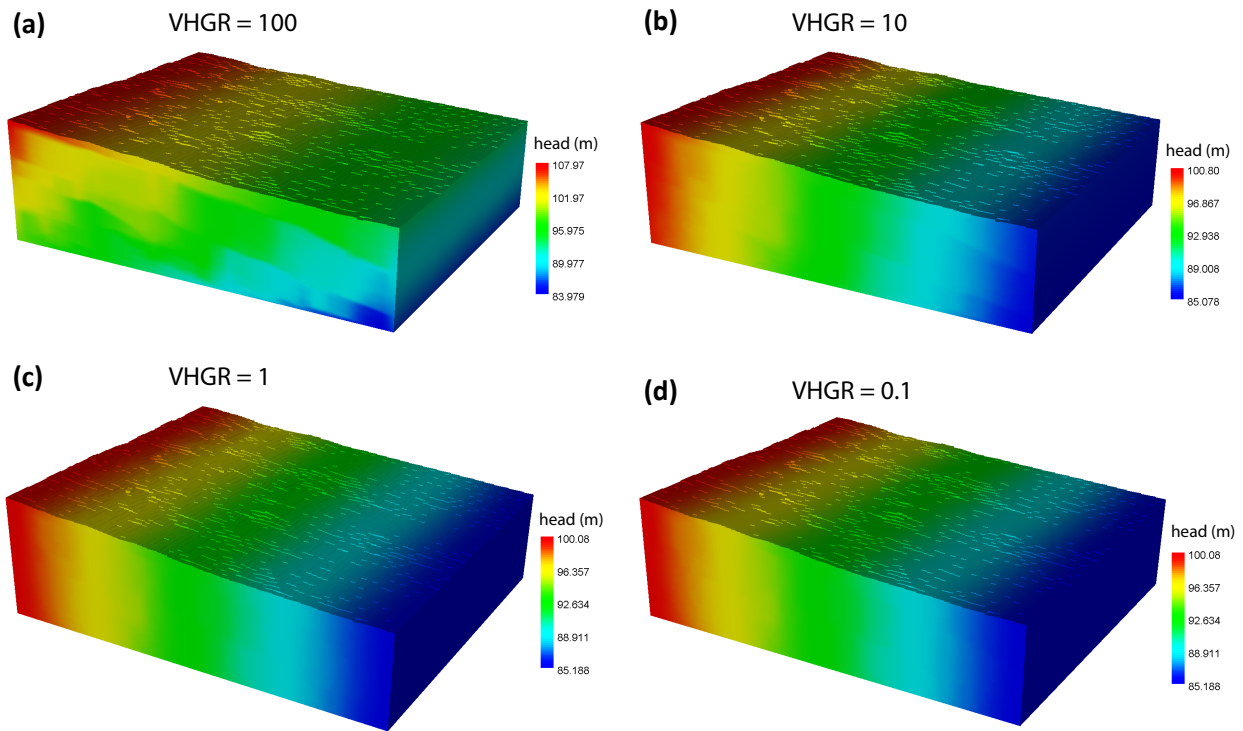


Figure 4.6: (a-d) Simulated steady state groundwater head across the 4 VHGR scenarios tested in this study.

4.7.2 Particle trajectory coordinate rotation and travel time normalization via the characteristic travel time

In order to ensure comparability across the range of VHGR scenarios of differing travel times and mean flow direction, we perform coordinate rotations and normalize travel times by a characteristic travel time to travel the average facies length, t_c .

First, we compute the mean Lagrangian velocity across all trajectories, \bar{v} and use the characteristic time to travel the average facies length, t_c , to normalize time across VHGR scenarios (SI Appendix Table S1). The mean velocity and facies length are calculated along the direction

of mean flow. Since this direction varies across VHGR, by an angle Φ relative to the horizontal direction, and the model outputs trajectories in a regular 3D Cartesian grid, we rotate the particle trajectory coordinates about the x axis by Φ to recover the transformed y and z components along the longitudinal and transverse vertical directions respectively (y' and z'):

$$\begin{aligned} y' &= z \cdot \sin(\Phi) + y \cdot \cos(\Phi) \\ z' &= z \cdot \cos(\Phi) - y \cdot \sin(\Phi) \end{aligned} \quad (4.7)$$

Flow occurs along zy , thus the x coordinates (transverse horizontal) remain unchanged. After transforming coordinates according to (4.7), we calculate longitudinal displacement along y' , transverse vertical displacement along z' , and transverse horizontal displacement along x .

Table 4.3: Mean velocity \bar{v} along the longitudinal direction (y'), the angle of mean flow, relative to the horizontal direction in the un-rotated Cartesian coordinate system Φ , the characteristic hydrofacies length l_c along the longitudinal direction, and the characteristic time t_c along the longitudinal direction ($t_c = l_c/\bar{v}$).

VHGR	$\Phi(^{\circ})$	l_c (m)	\bar{v} (m/yr)	t_c (yr)
100	89.43	2.19	73.33	0.046
10	84.29	2.20	8.40	0.252
1	45.00	3.09	7.20	0.093
0.1	5.71	21.97	53.01	0.319

4.7.3 RW3D parameters

Table 4.4: RW3D parameters for each VHGR scenario including the number of injected particles (particle count), the maximum simulation time (max time), and the number of snapshots saved (snapshot count). Note that the snapshot count = max time · 10 000, meaning that for each scenario, 100 snapshots were taken per year of simulation time.

VHGR	particle count	max time (yrs)	snapshot count
100	10 000	100	10 000
10	10 000	500	50 000
1	10 000	1000	100 000
0.1	10 000	5000	500 000

4.7.4 Hydrofacies proportions over time

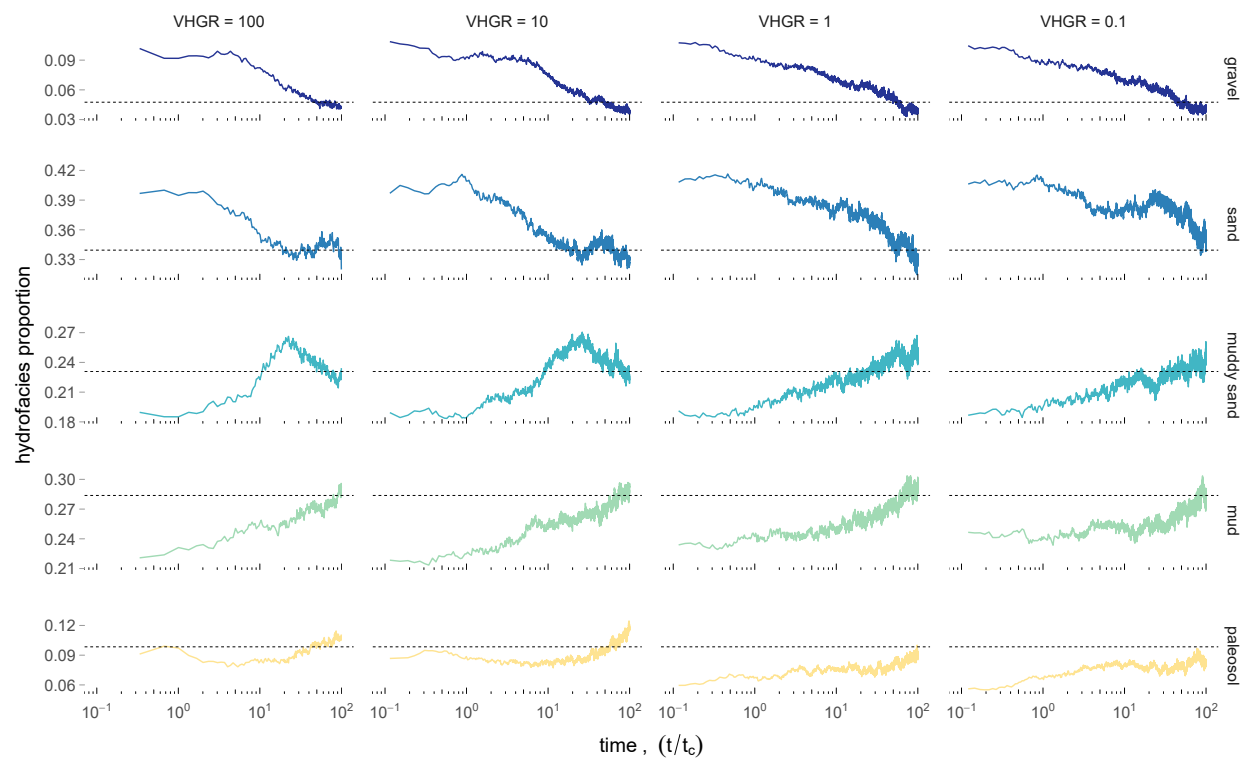


Figure 4.7: Proportion of hydrofacies occupied by the particles as a function of time across the 4 VHGR scenarios indicate mixing: over about 32 characteristic times, proportions converge onto the hydrofacies proportions shown as black, dashed horizontal lines. Note the difference in y axis between the rows, each of which correspond to a distinct hydrofacies..

4.8 Acknowledgments

We gratefully thank Drs. Yong Zhang, Marco Dentz, and Song Wei for their feedback and modeling advice. Support for this research was provided by the National Science Foundation (NSF) Climate Change, Water, and Society (CCWAS) Integrated Graduate Education and Research Traineeship (IGERT) program at the University of California, Davis (<http://ccwas.ucdavis.edu>, DGE-10693333), and by the U.S./China Clean Energy Research Center for Water-Energy Technologies (CERC-WET).

4.9 References

- Bastani, M. & Harter, T. (2020). Effects of upscaling temporal resolution of groundwater flow and transport boundary conditions on the performance of nitrate-transport models at the regional management scale. *Hydrogeology Journal*, 1–24.
- Belitz, K., Phillips, S. P., & Gronberg, J. A. M. (1993). *Numerical simulation of ground-water flow in the central part of the western san joaquin valley, California*. USGPO; For sale by the Books and Open-File Reports Section, US Geological ...
- Benson, D. A., Schumer, R., Meerschaert, M. M., & Wheatcraft, S. W. (2001). Fractional dispersion, lévy motion, and the made tracer tests. *Transport in porous media*, 42(1-2), 211–240.
- Benson, D. A., Wheatcraft, S. W., & Meerschaert, M. M. (2000). Application of a fractional advection-dispersion equation. *Water resources research*, 36(6), 1403–1412.
- Berkowitz, B. & Braester, C. (1991). Dispersion in sub-representative elementary volume fracture networks: Percolation theory and random walk approaches. *Water resources research*, 27(12), 3159–3164.
- Berkowitz, B. [Brian], Cortis, A., Dentz, M., & Scher, H. (2006). Modeling non-fickian transport in geological formations as a continuous time random walk. *Reviews of Geophysics*, 44(2).
- Burow, K. R. (1999). *Evaluation of processes affecting 1, 2-dibromo-3-chloropropane (dbcp) concentrations in ground water in the eastern San Joaquin Valley, California: Analysis of chemical data and ground-water flow and transport simulations*. US Department of the Interior, US Geological Survey.
- Burow, K. R., Shelton, J. L., & Dubrovsky, N. M. (2008). Regional nitrate and pesticide trends in ground water in the eastern San Joaquin Valley, California. *Journal of Environmental Quality*, 37(5_Supplement), S–249.
- Burow, K. R., Stork, S. V., & Dubrovsky, N. M. (1998). *Nitrate and pesticides in ground water of the eastern San Joaquin Valley, California: Occurrence and trends*. USGS.
- Burow, K. R., Weissmann, G., Miller, R., & Placzek, G. (1997). Hydrogeologic facies characterization of an alluvial fan near Fresno, California, using geophysical techniques. *US Geol. Surv. Open File Rep.*, 97, 46, 15.
- Carle, S. F. (1999). T-progs: Transition probability geostatistical software. *University of California, Davis, CA*, 84.
- Carle, S. F. & Fogg, G. E. (1996). Transition probability-based indicator geostatistics. *Mathematical Geology*, 28(4), 453–476.
- Carle, S. F. & Fogg, G. E. (1997). Modeling spatial variability with one and multidimensional continuous-lag markov chains. *Mathematical Geology*, 29(7), 891–918.
- Cortis, A., Gallo, C., Scher, H., & Berkowitz, B. (2004). Numerical simulation of non-fickian transport in geological formations with multiple-scale heterogeneities. *Water Resources Research*, 40(4).
- Dagan, G., Fiori, A., & Janković, I. (2003). Flow and transport in highly heterogeneous formations: 1. conceptual framework and validity of first-order approximations. *Water Resources Research*, 39(9).
- Dagan, G. [Gedeon] & Neuman, S. P. (2005). *Subsurface flow and transport: A stochastic approach*. Cambridge University Press.
- De Marsily, G. [Gh], Delay, F., Gonçalvès, J., Renard, P., Teles, V., & Violette, S. (2005). Dealing with spatial heterogeneity. *Hydrogeology Journal*, 13(1), 161–183.

- Edery, Y., Geiger, S., & Berkowitz, B. (2016). Structural controls on anomalous transport in fractured porous rock. *Water Resources Research*, 52(7), 5634–5643.
- Edery, Y., Guadagnini, A., Scher, H., & Berkowitz, B. (2014). Origins of anomalous transport in heterogeneous media: Structural and dynamic controls. *Water Resources Research*, 50(2), 1490–1505.
- Famiglietti, J. S. (2014). The global groundwater crisis. *Nature Climate Change*, 4(11), 945–948.
- Fernàndez-Garcia, D., Illangasekare, T. H., & Rajaram, H. (2005). Differences in the scale-dependence of dispersivity estimated from temporal and spatial moments in chemically and physically heterogeneous porous media. *Advances in water resources*, 28(7), 745–759.
- Fetter, C. W. (2001). *Applied Hydrogeology* (4th). Upper Saddle River, NJ: Prentice Hall.
- Fiori, A., Janković, I., & Dagan, G. (2003). Flow and transport in highly heterogeneous formations: 2. semianalytical results for isotropic media. *Water resources research*, 39(9).
- Fogg, G. E. (1986). Groundwater flow and sand body interconnectedness in a thick, multiple-aquifer system. *Water Resources Research*, 22(5), 679–694.
- Fogg, G. E., Carle, S. F., & Green, C. (2000). Connected-network paradigm for the alluvial aquifer system. *Special Papers-Geological Society of America*, 25–42.
- Fogg, G. E. & LaBolle, E. M. (2006). Motivation of synthesis, with an example on groundwater quality sustainability. *Water Resources Research*, 42(3).
- Fogg, G. E. & Zhang, Y. [Yong]. (2016). Debates—stochastic subsurface hydrology from theory to practice: A geologic perspective. *Water Resources Research*, 52(12), 9235–9245.
- Freyberg, D. L. (1986). A natural gradient experiment on solute transport in a sand aquifer: 2. spatial moments and the advection and dispersion of nonreactive tracers. *Water Resources Research*, 22(13), 2031–2046.
- Gailey, R. M. (2018). Using geographic distribution of well-screen depths and hydrogeologic conditions to identify areas of concern for contaminant migration through inactive supply wells. *Hydrogeology Journal*, 26(6), 2071–2088.
- Galloway, W. E. & Hobday, D. K. (2012). *Terrigenous clastic depositional systems: Applications to fossil fuel and groundwater resources*. Springer Science & Business Media.
- Garabedian, S. P., LeBlanc, D. R., Gelhar, L. W., & Celia, M. A. (1991). Large-scale natural gradient tracer test in sand and gravel, cape cod, massachusetts: 2. analysis of spatial moments for a nonreactive tracer. *Water Resources Research*, 27(5), 911–924.
- Gelhar, L. W. [Lynn W] & Gelhar, L. (1993). *Stochastic subsurface hydrology*. Prentice-Hall Englewood Cliffs, NJ.
- Gillham, R., Sudicky, E., Cherry, J., & Frind, E. (1984). An advection-diffusion concept for solute transport in heterogeneous unconsolidated geological deposits. *Water Resources Research*, 20(3), 369–378.
- Gleeson, T., Wada, Y., Bierkens, M. F., & van Beek, L. P. (2012). Water balance of global aquifers revealed by groundwater footprint. *Nature*, 488(7410), 197–200.
- Guo, Z., Fogg, G. E., & Henri, C. V. (2019). Upscaling of regional scale transport under transient conditions: Evaluation of the multirate mass transfer model. *Water Resources Research*, 55(7), 5301–5320.
- Guo, Z., Henri, C. V., Fogg, G. E., Zhang, Y., & Zheng, C. (2020). Adaptive multirate mass transfer (ammt) model: A new approach to upscale regional-scale transport under transient flow conditions. *Water Resources Research*, 56(2), e2019WR026000.

- Guswa, A. J. & Freyberg, D. L. (2000). Slow advection and diffusion through low permeability inclusions. *Journal of contaminant hydrology*, 46(3-4), 205–232.
- Haggerty, R., McKenna, S. A., & Meigs, L. C. (2000). On the late-time behavior of tracer test breakthrough curves. *Water Resources Research*, 36(12), 3467–3479.
- Hansen, J. A., Jurgens, B. C., & Fram, M. S. (2018a). Quantifying anthropogenic contributions to century-scale groundwater salinity changes, San Joaquin Valley, California, USA. *Science of the total environment*, 642, 125–136.
- Hansen, J. A., Jurgens, B. C., & Fram, M. S. (2018b). Quantifying anthropogenic contributions to century-scale groundwater salinity changes, san joaquin valley, california, usa. *Science of the total environment*, 642, 125–136.
- Harbaugh, A. W. [Arlen W], Banta, E. R., Hill, M. C., & McDonald, M. G. (2000). *Modflow-2000, the u. s. geological survey modular ground-water model-user guide to modularization concepts and the ground-water flow process*. United States Geologic Survey.
- Harter, T. (2005). Finite-size scaling analysis of percolation in three-dimensional correlated binary markov chain random fields. *Physical Review E*, 72(2), 026120.
- Harter, T. & Lund, J. R. (2012). *Addressing nitrate in california's drinking water: With a focus on tulare lake basin and salinas valley groundwater: Report for the state water resources control board report to the legislature*.
- Harter, T., Onsoy, Y., Heeren, K., Denton, M., Weissmann, G., Hopmans, J., Horwath, W., et al. (2005). Deep vadose zone hydrology demonstrates fate of nitrate in eastern san joaquin valley. *California agriculture*, 59(2), 124–132.
- Harvey, C. & Gorelick, S. M. (2000). Rate-limited mass transfer or macrodispersion: Which dominates plume evolution at the macrodispersion experiment (made) site? *Water Resources Research*, 36(3), 637–650.
- Heeren, D. M., Miller, R. B., Fox, G. A., Storm, D. E., Halihan, T., & Penn, C. J. (2010). Preferential flow effects on subsurface contaminant transport in alluvial floodplains. *Transactions of the ASABE*, 53(1), 127–136.
- Henri, C. V. [Christopher V] & Fernàndez-Garcia, D. (2014). Toward efficiency in heterogeneous multispecies reactive transport modeling: A particle-tracking solution for first-order network reactions. *Water Resources Research*, 50(9), 7206–7230.
- Henri, C. V. [Christopher V] & Fernàndez-Garcia, D. (2015). A random walk solution for modeling solute transport with network reactions and multi-rate mass transfer in heterogeneous systems: Impact of biofilms. *Advances in water resources*, 86, 119–132.
- Henri, C. V. [Christopher Vincent] & Harter, T. (2019). Stochastic assessment of non-point source contamination: Joint impact of aquifer heterogeneity and well characteristics on management metrics. *Water Resources Research*.
- Hunt, A., Skinner, T., Ewing, R., & Ghanbarian-Alavijeh, B. (2011). Dispersion of solutes in porous media. *The European Physical Journal B*, 80(4), 411–432.
- Huntington, G. L. (1980). Soil-land form relationships of portions of the san joaquin river and kings river alluvial depositional systems in the great valley of california.
- Hyman, J., Painter, S. L., Viswanathan, H., Makedonska, N., & Karra, S. (2015). Influence of injection mode on transport properties in kilometer-scale three-dimensional discrete fracture networks. *Water Resources Research*, 51(9), 7289–7308.

- Julian, H. E., Boggs, J. M., Zheng, C., & Feehley, C. E. (2001). Numerical simulation of a natural gradient tracer experiment for the natural attenuation study: Flow and physical transport. *Groundwater*, 39(4), 534–545.
- Jussel, P., Stauffer, F., & Dracos, T. (1994). Transport modeling in heterogeneous aquifers: 1. statistical description and numerical generation of gravel deposits. *Water Resources Research*, 30(6), 1803–1817.
- Kang, P. K., de Anna, P., Nunes, J. P., Bijeljic, B., Blunt, M. J., & Juanes, R. (2014). Pore-scale intermittent velocity structure underpinning anomalous transport through 3-d porous media. *Geophysical Research Letters*, 41(17), 6184–6190.
- LaBolle, E. M. & Fogg, G. E. (2001). Role of molecular diffusion in contaminant migration and recovery in an alluvial aquifer system. In *Dispersion in heterogeneous geological formations* (pp. 155–179). Springer.
- LaBolle, E. M., Quastel, J., & Fogg, G. E. (1998). Diffusion theory for transport in porous media: Transition-probability densities of diffusion processes corresponding to advection-dispersion equations. *Water Resources Research*, 34(7), 1685–1693.
- LaBolle, E. M., Quastel, J., Fogg, G. E., & Gravner, J. (2000). Diffusion processes in composite porous media and their numerical integration by random walks: Generalized stochastic differential equations with discontinuous coefficients. *Water Resources Research*, 36(3), 651–662.
- Le Borgne, T., Dentz, M., Bolster, D., Carrera, J., de Dreuzy, J.-R., & Davy, P. (2010). Non-fickian mixing: Temporal evolution of the scalar dissipation rate in heterogeneous porous media. *Advances in Water Resources*, 33(12), 1468–1475.
- Le Borgne, T. & Gouze, P. (2008). Non-fickian dispersion in porous media: 2. model validation from measurements at different scales. *Water Resources Research*, 44(6).
- LeBlanc, D. R., Garabedian, S. P., Hess, K. M., Gelhar, L. W., Quadri, R. D., Stollenwerk, K. G., & Wood, W. W. (1991). Large-scale natural gradient tracer test in sand and gravel, cape cod, massachusetts: 1. experimental design and observed tracer movement. *Water Resources Research*, 27(5), 895–910.
- Lee, M.-S., Lee, K.-K., Hyun, Y., Clement, T. P., & Hamilton, D. (2006). Nitrogen transformation and transport modeling in groundwater aquifers. *Ecological modelling*, 192(1-2), 143–159.
- Libera, A., de Barros, F. P., & Guadagnini, A. (2017). Influence of pumping operational schedule on solute concentrations at a well in randomly heterogeneous aquifers. *Journal of hydrology*, 546, 490–502.
- Lindsey, B. & Johnson, T. (2018). Data from decadal change in groundwater quality web site, 1988-2014, version 2.0: U.s. geological survey. doi:[10.5066/F7N878ZS](https://doi.org/10.5066/F7N878ZS)
- Matheron, G. & De Marsily, G. (1980). Is transport in porous media always diffusive? a counterexample. *Water Resources Research*, 16(5), 901–917.
- Maxwell, R. M., Carle, S. F., & Tompson, A. F. (2008). Contamination, risk, and heterogeneity: On the effectiveness of aquifer remediation. *Environmental Geology*, 54(8), 1771–1786.
- McDonald, M. & Harbaugh, A. (1988). *Modflow, a modular three-dimensional finite difference groundwater flow model, open-file report 83-875, chapter a1*. United States Geologic Survey. Washington, DC.
- Meerschaert, M. M., Zhang, Y., & Baeumer, B. (2008). Tempered anomalous diffusion in heterogeneous systems. *Geophysical Research Letters*, 35(17).

- Morales, V. L., Dentz, M., Willmann, M., & Holzner, M. (2017). Stochastic dynamics of intermittent pore-scale particle motion in three-dimensional porous media: Experiments and theory. *Geophysical Research Letters*, 44(18), 9361–9371.
- Moreno, L. & Tsang, C.-F. (1994). Flow channeling in strongly heterogeneous porous media: A numerical study. *Water Resources Research*, 30(5), 1421–1430.
- Neuman, S. P. (1990). Universal scaling of hydraulic conductivities and dispersivities in geologic media. *Water resources research*, 26(8), 1749–1758.
- Neuman, S. P. & Tartakovsky, D. M. (2009). Perspective on theories of non-fickian transport in heterogeneous media. *Advances in Water Resources*, 32(5), 670–680.
- Pastén-Zapata, E., Ledesma-Ruiz, R., Harter, T., Ramirez, A. I., & Mahlknecht, J. (2014). Assessment of sources and fate of nitrate in shallow groundwater of an agricultural area by using a multi-tracer approach. *Science of the Total Environment*, 470, 855–864.
- Pedretti, D., Fernàndez-Garcia, D., Sanchez-Vila, X., Bolster, D., & Benson, D. (2014). Apparent directional mass-transfer capacity coefficients in three-dimensional anisotropic heterogeneous aquifers under radial convergent transport. *Water Resources Research*, 50(2), 1205–1224.
- Perez-Fodich, A. & Derry, L. A. (2019). Organic acids and high soil co₂ drive intense chemical weathering of hawaiian basalts: Insights from reactive transport models. *Geochimica et Cosmochimica Acta*, 249, 173–198.
- Rubin, Y. (2003). *Applied stochastic hydrogeology*. Oxford University Press.
- Salamon, P., Fernàndez-Garcia, D., & Gómez-Hernández, J. (2006). Modeling mass transfer processes using random walk particle tracking. *Water resources research*, 42(11).
- Schoups, G., Hopmans, J. W., Young, C. A., Vrugt, J. A., Wallender, W. W., Tanji, K. K., & Panday, S. (2005). Sustainability of irrigated agriculture in the san joaquin valley, california. *Proceedings of the National Academy of Sciences*, 102(43), 15352–15356.
- Sivakumar, B., Harter, T., & Zhang, H. (2005). A fractal investigation of solute travel time in a heterogeneous aquifer: Transition probability/markov chain representation. *Ecological Modelling*, 182(3-4), 355–370.
- Styles, S. W. & Burt, C. M. (1999). Subsurface flows water balance components for irrigation districts in the san joaquin valley. *Bioresource and Agricultural Engineering*, 39.
- Tsang, C.-F. & Neretnieks, I. (1998). Flow channeling in heterogeneous fractured rocks. *Reviews of Geophysics*, 36(2), 275–298.
- Valocchi, A. J. (1985). Validity of the local equilibrium assumption for modeling sorbing solute transport through homogeneous soils. *Water Resources Research*, 21(6), 808–820.
- Wada, Y., Van Beek, L. P., Van Kempen, C. M., Reckman, J. W., Vasak, S., & Bierkens, M. F. (2010). Global depletion of groundwater resources. *Geophysical research letters*, 37(20).
- Weissmann, G. S., Carle, S. F., & Fogg, G. E. (1999). Three-dimensional hydrofacies modeling based on soil surveys and transition probability geostatistics. *Water Resources Research*, 35(6), 1761–1770.
- Weissmann, G. S. & Fogg, G. E. (1999). Multi-scale alluvial fan heterogeneity modeled with transition probability geostatistics in a sequence stratigraphic framework. *Journal of Hydrology*, 226(1-2), 48–65.
- Weissmann, G. S., Labolle, E. M., Fogg, G. E., & Zhang, Y. (2002). Modeling environmental tracer-based groundwater ages in heterogeneous aquifers. *Water Resources Research*, 38, 1198–1211.

- Weissmann, G. S., Mount, J. F., & Fogg, G. E. (2002). Glacially driven cycles in accumulation space and sequence stratigraphy of a stream-dominated alluvial fan, san joaquin valley, california, usa. *Journal of Sedimentary Research*, 72(2), 240–251.
- Weissmann, G. S., Zhang, Y., Fogg, G. E., & Mount, J. F. (2004). Influence of incised-valley-fill deposits on hydrogeology of a stream-dominated alluvial fan.
- Weissmann, G. S., Zhang, Y. [Yong], LaBolle, E. M., & Fogg, G. E. (2002). Dispersion of ground-water age in an alluvial aquifer system. *Water Resources Research*, 38(10), 16–1.
- Willmann, M., Carrera, J., & Sánchez-Vila, X. (2008). Transport upscaling in heterogeneous aquifers: What physical parameters control memory functions? *Water Resources Research*, 44(12).
- Winograd, I. J. & Pearson Jr, F. (1976). Major carbon 14 anomaly in a regional carbonate aquifer: Possible evidence for megascale channeling, south central great basin. *Water Resources Research*, 12(6), 1125–1143.
- Yin, M., Zhang, Y., Ma, R., Tick, G. R., Bianchi, M., Zheng, C., ... Liu, X. (2020). Super-diffusion affected by hydrofacies mean length and source geometry in alluvial settings. *Journal of Hydrology*, 582, 124515.
- Zhang, H., Harter, T., & Sivakumar, B. (2006). Nonpoint source solute transport normal to aquifer bedding in heterogeneous, markov chain random fields. *Water Resources Research*, 42(6).
- Zhang, X. & Lv, M. (2007). Persistence of anomalous dispersion in uniform porous media demonstrated by pore-scale simulations. *Water Resources Research*, 43(7).
- Zhang, Y., Green, C., & Fogg, G. (2013). The impact of medium architecture of alluvial settings on non-fickian transport. *Advances in Water Resources*, 54, 78–99.
- Zhang, Y. [Yong], Benson, D. A., & Baeumer, B. (2007). Predicting the tails of breakthrough curves in regional-scale alluvial systems. *Groundwater*, 45(4), 473–484.
- Zhang, Y. [Yong], Green, C. T., & Baeumer, B. (2014). Linking aquifer spatial properties and non-fickian transport in mobile-immobile like alluvial settings. *Journal of hydrology*, 512, 315–331.
- Zhang, Z. & Brusseau, M. L. (1999). Nonideal transport of reactive solutes in heterogeneous porous media: 5. simulating regional-scale behavior of a trichloroethene plume during pump-and-treat remediation. *Water Resources Research*, 35(10), 2921–935.
- Zheng, C. & Gorelick, S. M. (2003). Analysis of solute transport in flow fields influenced by preferential flowpaths at the decimeter scale. *Groundwater*, 41(2), 142–155.

Chapter 5

Concluding Remarks

Writing near the turn of the 21st century, Dr. Norman Borlaug, a Nobel Laureate and key figure in the Green Revolution credited with pivotal advancements in plant genetics, noted that the continued success of the Green Revolution depended on fresh water availability, and called for a “Blue Revolution” to secure reliable water resources. Civilization’s reliance on unsustainable groundwater pumping, especially in clastic sedimentary groundwater basins found in arid and semi-arid regions worldwide, limits the lifespan of these freshwater stores (Scanlon et al., 2012; Wada et al., 2010; Gleeson, Wada, Bierkens, & van Beek, 2012). For example, in California’s Central Valley, aquifer lifespan has been estimated at 390 years or less depending on the exact location and depletion rate (Scanlon et al., 2012). Although aquifer depletion poses a long-term existential threat, a range of negative consequences (e.g., land subsidence, surface water depletion, destruction of groundwater-dependent ecosystems) will impact surface and groundwater systems long before aquifer stores run dangerously low, and these impacts will be exacerbated by surface water shortages in a warming climate (Rhoades, Jones, & Ullrich, 2018; Swain, Langenbrunner, Neelin, & Hall, 2018; Cook, Ault, & Smerdon, 2015), which has historically increased groundwater pumping to augment lost surface water supply (Hanak, Lund, Dinar, Gray, & Howitt, 2011; Medellin-Azuara et al., 2016). Thus, by addressing the short term consequences of aquifer depletion, the larger and slower-moving existential threat of aquifer depletion is also mitigated.

This dissertation focuses on the development of models to address two understudied con-

sequences of aquifer depletion: well failure and closed basin salinization. Chapter 2 demonstrates how data assimilation from monitoring well networks and open data from state agencies can be combined into a physical model of well failure that forecasts the impact of extended drought duration, groundwater management regimes, and wet winter recharge events in California's Central Valley. Chapter 4 advances a conceptual model of Anthropogenic Basin Closure and groundwater SALinization (ABCSAL), and first-order estimates of salinization in California's Tulare Basin. Chapter 3 uses 3D numerical flow and transport modeling in a complex hydrofacies model to show that transience in the mean flow direction caused by naturally-occurring (due to natural anisotropy in K) and induced hydraulic gradient transience (from pumping and recharge) can change the governing mass transfer processes in hyrdofacies, leading to differing degrees of non-Fickian transport.

Chapter 2 demonstrates the vulnerability of domestic wells to both naturally-occurring hydrologic events (e.g., drought and wet winter recharge) and human-made water management decisions (e.g., sustainable and business as usual management regimes). Results indicate that extended drought durations (e.g., 5 to 8 years) can lead to a greater annual rate of well failure than observed during historic droughts (e.g., 2012-2016) as groundwater levels intersect an increasingly dense portion of the distribution of domestic well pump depths. Moreover, human water management decisons matter. Four times as many wells failed—even when controlling for hydrologic uncertainty—between a strict sustainability scenario in which groundwater levels were not allowed to fall after 2020, compared to a business as usual scenario that projected current groundwater level decline trends into 2040. Wet winter recharge events, and hence reduced pumping (Hanak et al., 2019) and flood-based managed aquifer recharge (Kocis & Dahlke, 2017) show potential to lessen the degree of domestic well failure. Looking forward, as Internet-of-things technologies mature and remote sensor networks are increasingly cost-effective and easy to maintain, the real-time monitoring of groundwater (Calderwood, Pauloo, Yoder, & Fogg, 2020) will permit data-driven models like the one presented in this study to automatically assimilate real-time groundwater level data and provide on-the-fly well failure risk estimates. Thus, it is conceivable that an early warning system for domestic well failure—not unlike existing early warning systems for drought (Pozzi et al., 2013; Huang & Yuan, 2004)—may be a future possibility enabled by sensor technology and cloud

computing.

Similarly to Chapter 2, the topic of Chapter 3 remains understudied due to its relatively new emergence. Chapter 3 explores a mechanism by which groundwater pumping eliminates hydrologic exits for naturally-occurring salts in a basin (e.g., via baseflow and lateral subsurface outflow), after which those entrained salts accumulate in shallow aquifers due recycling from pumping and irrigation, before they are driven into deeper aquifer over century-long timescales. We call this process Anthropogenic Basin Closure and groundwater SALinization (ABCSAL). Importantly, results from a first-order mixing cell model indicate that shallow aquifers reach drinking water minimum thresholds for total dissolved solids (TDS) within decades, a result consistent with measurements of shallow aquifer TDS increase in the past century in the study site (Hansen, Jurgens, & Fram, 2018). These results suggest that one mechanism to reverse or slow ongoing ABCSAL may include “filling the basin up” with significant recharge to restore baseflow and lateral subsurface outflow. Although the practical reality of such a management action may be cost-prohibitive or physically limited by available surface water in the Tulare Basin, it remains a viable solution in other basins worldwide experiencing ABCSAL. Moreover, a greater emphasis on subsurface water storage will require tightly monitoring and managing the ground and surface water interactions with distributed sensor networks, in order to prevent capillary rise and salinization from bare soil evaporation (Belitz & Phillips, 1995). Without these mitigative management actions, ongoing and long-term ABCSAL may require inland desalination of pumped groundwater.

Building on the work presented in Chapter 3, Chapter 4 uses 3D numerical groundwater flow and transport simulations in a detailed hydrofacies model with large variance in K (Weissmann & Fogg, 1999) to better understand how hydraulic transience in the mean flow direction influences the degree of non-Fickian transport observed in hydrogeologic systems (e.g., nonpoint source salts discussed in Chapter 2). In California’s Central Valley and other typical clastic sedimentary alluvial aquifer-aquitard systems worldwide, high vertical anisotropy in K naturally created by the interbedding of high and low K sediments, combined with pumping and recharge, can create flow systems that oscillate between predominately vertical and horizontal flow. Although other studies have noted that classical methods to upscale transport fail to represent tailing when the mean

flow direction changes (Guo, Fogg, & Henri, 2019; Guo, Henri, Fogg, Zhang, & Zheng, 2020), the hydrogeologic underpinnings of this phenomenon remain poorly understood. Results indicate that relatively higher vertical to horizontal gradient ratio (VHGR) coincident with increasingly vertical mean flow direction can transition low-K facies from diffusion- to advection-dominant, and cause vertical groundwater flow to move directly through facies that typically act as aquitards at lower VHGR (e.g., paleosols, clays, and silts). In other words, when systems transition from diffusion- to advection-dominant, non-Fickian behavior (e.g., tailing, spatial variance, preferential flow) all decrease. These results imply a conceptual model of oscillating patterns in the degree of non-Fickian transport that correspond to seasonal patterns of pumping and recharge. Hence, non-Fickian transport models will better characterize flow systems under higher VHGR, depending on the gradients, characteristic facies length scales, and the Peclet number (P_e) of the distinct hydrofacies which describes the ratio of advection to diffusion time scales. These results also suggest a physical mechanism for arsenic leaching from low-K clays observed in the Central Valley during periods of land subsidence (Smith, Knight, & Fendorf, 2018), driven by advective flushing as strong vertical gradients “force” groundwater through clays. Lastly, the strong dependence of mass transfer on hydrogeologic features illustrated in this study suggests that future efforts to upscale regional-scale, transient nonpoint source transport may benefit by incorporating information on the time-dependent changes in VHGR, P_e , mean flow direction, and characteristic length scales along the direction of mean flow.

Securing sustainable groundwater resources in the 21st century and beyond will require the further development and refinement of hydrogeologic science, and numerical and data-driven models to assimilate that understanding and provide critical insights. Although this dissertation focuses on groundwater problems in California, the themes explored herein are extensible to other heavily pumped groundwater systems worldwide. Indeed, it is only through enhanced understand of aquifers that civilization may bring about a Blue Revolution in groundwater resources monitoring, modeling, and management.

5.1 References

- Belitz, K. & Phillips, S. P. (1995). Alternative to agricultural drains in California's San Joaquin Valley: Results of a regional-scale hydrogeologic approach. *Water Resources Research*, 31(8), 1845–1862.
- Calderwood, A. J., Pauloo, R. A., Yoder, A. M., & Fogg, G. E. (2020). Low-cost, open source wireless sensor network for real-time, scalable groundwater monitoring. *Water*, 12(4), 1066.
- Cook, B. I., Ault, T. R., & Smerdon, J. E. (2015). Unprecedented 21st century drought risk in the American Southwest and Central Plains. *Science Advances*, 1(1), e1400082.
- Gleeson, T., Wada, Y., Bierkens, M. F., & van Beek, L. P. (2012). Water balance of global aquifers revealed by groundwater footprint. *Nature*, 488(7410), 197–200.
- Guo, Z., Fogg, G. E., & Henri, C. V. (2019). Upscaling of regional scale transport under transient conditions: Evaluation of the multirate mass transfer model. *Water Resources Research*, 55(7), 5301–5320.
- Guo, Z., Henri, C. V., Fogg, G. E., Zhang, Y., & Zheng, C. (2020). Adaptive multirate mass transfer (ammt) model: A new approach to upscale regional-scale transport under transient flow conditions. *Water Resources Research*, 56(2), e2019WR026000.
- Hanak, E., Escrivá-Bou, A., Gray, B., Green, S., Harter, T., Jezdimirovic, J., ... Seavy, N. (2019). *PPIC: Water and the Future of the San Joaquin Valley* (tech. rep. No. February). Public Policy Institute of California.
- Hanak, E., Lund, J., Dinar, A., Gray, B., & Howitt, R. (2011). *Managing California's Water: From Conflict to Reconciliation*. San Francisco, CA: Public Policy Institute of California.
- Hansen, J. A., Jurgens, B. C., & Fram, M. S. (2018). Quantifying anthropogenic contributions to century-scale groundwater salinity changes, San Joaquin Valley, California, USA. *Science of the Total Environment*, 642, 125–136.
- Huang, W.-C. & Yuan, L.-C. (2004). A drought early warning system on real-time multireservoir operations. *Water resources research*, 40(6).
- Kocis, T. N. & Dahlke, H. E. (2017). Availability of high-magnitude streamflow for groundwater banking in the central valley, California. *Environmental Research Letters*, 12(8), 084009.
- Medellin-Azuara, J., MacEwan, D., Howitt, R. E., Sumner, D. A., Lund, J. R., Scheer, J., ... Arnold, B. (2016). *Economic Analysis of the 2016 California Drought on Agriculture: A report for the California Department of Food and Agriculture*. Center for Watershed Sciences, University of California Davis, CA.
- Pozzi, W., Sheffield, J., Stefanski, R., Cripe, D., Pulwarty, R., Vogt, J. V., ... Westerhoff, R., et al. (2013). Toward global drought early warning capability: Expanding international cooperation for the development of a framework for monitoring and forecasting. *Bulletin of the American Meteorological Society*, 94(6), 776–785.
- Rhoades, A. M., Jones, A. D., & Ullrich, P. A. (2018). The Changing Character of the California Sierra Nevada as a Natural Reservoir. *Geophysical Research Letters*, 45(23), 13–008.
- Scanlon, B. R., Faunt, C. C., Longuevergne, L., Reedy, R. C., Alley, W. M., McGuire, V. L., & McMahon, P. B. (2012). Groundwater depletion and sustainability of irrigation in the US High Plains and Central Valley. *Proceedings of the National Academy of Sciences*, 109(24), 9320–9325.
- Smith, R. G., Knight, R., & Fendorf, S. (2018). Overpumping leads to California groundwater arsenic threat. *Nature Communications*, 9(1), 2089.

- Swain, D. L., Langenbrunner, B., Neelin, J. D., & Hall, A. (2018). Increasing precipitation volatility in twenty-first-century California. *Nature Climate Change*, 8(5), 427.
- Wada, Y., Van Beek, L. P., Van Kempen, C. M., Reckman, J. W., Vasak, S., & Bierkens, M. F. (2010). Global depletion of groundwater resources. *Geophysical research letters*, 37(20).
- Weissmann, G. S. & Fogg, G. E. (1999). Multi-scale alluvial fan heterogeneity modeled with transition probability geostatistics in a sequence stratigraphic framework. *Journal of Hydrology*, 226(1-2), 48–65.